SEMMELWEIS EGYETEM

DOKTORI ISKOLA

Ph.D. értekezések

3299.

BARABÁS BENCE

Funkcionális Idegtudományok

című program

Programvezető: Dr. Sperlágh Beáta, egyetemi tanár

Témavezető: Dr. Hájos Norbert, tudományos tanácsadó

Neuronal Circuits in the Cholinergic Basal Forebrain, Amygdala, and Medial Prefrontal Cortex Contributing to Noxious Stimulus Processing

PhD thesis

Barabás Bence

Molecular Medicine Doctoral School

Semmelweis University

Supervisor: Hájos Norbert, D.Sc, Ph.D

Official reviewers: Dávid Csaba, Ph.D
Tóth Attila, Ph.D

Head of the Complex Examination Committee:
Dr. Alpár Alán, Ph.D, Habil, D.Sc

Members of the Complex Examination Committee:
Dr. Zelles Tibor, MD, Ph.D
Dr. Wittner Lucia, Ph.D, D.Sc

Budapest
2025

Table of Contents

List of abbreviations

Aca – anterior commissure, anterior part

ACh – acetylcholine

ACo – anterior cortical amygdaloid nucleus

Acp – anterior commissure, posterior part

AAC– axo-axonic cell

AI – agranular insular cortex

AHi – amygdalohippocampal area

AHiAL – amygdalohippocampal area, anterolateral part

AHiPM – amygdalohippocampal area, posteromedial part

AIS – axon initial segment

APir – amygdalopiriform transition area

BA – basal amygdala

BAa – basal amygdala, anterior part

BAp – basal amygdala, posterior part

BFCNs – basal forebrain cholinergic neurons

BLA – basolateral amygdala

BMA – basomedial amygdala

BC – basket cell

CB1– cannabinoid receptor type 1

CCK – cholecystokinin

CCKBC – cholecystokinin-expressing basket cell

Calb – calbindin

CeL – central amygdala, lateral division

CeM – central amygdala, medial division

ChAT – choline acetyltransferase

ChC – chandelier cell

Cg1 – cingulate cortex, area 1

Cg2 – cingulate cortex, area 2

CTB – choleratoxin B subunit

dPFC – dorsal prefrontal cortex

DEn – dorsal endopiriform nucleus

DI – dysgranular insular cortex

DP – dorsal peduncular cortex

FB – FastBlue

FG – Fluorogold

Flpo – Mouse codon-optimized flippase recombinase

GABA – gamma-amino butyric acid

GAD-67 – glutamate decarboxylase 67

IL – infralimbic cortex

IN – interneuron

IPSC – inhibitory postsynaptic current

IPACL – interstitial nucleus of the posterior limb of the anterior commissure, lateral part

IPACM – interstitial nucleus of the posterior limb of the anterior commissure, medial part

ISI– interneuron-selective interneuron

LEnt – lateral entorhinal cortex

LH – lateral hypothalamic area

LO – lateral orbital cortex

LPO – lateral preoptic area

M1 – primary motor cortex

M2 – secondary motor cortex

MCPO – magnocellular preoptic nucleus

MeA – medial amygdala, anterior part

MeP – medial amygdala, posterior part

MO – medial orbital cortex

mPFC – medial prefrontal cortex

MS – medial septal nucleus

NDS – normal donkey serum

NGS – normal goat serum

NGFC- neurogliaform cell

NPY – neuropeptide Y

PAG – periaqueductal gray

PB – phosphate buffer

PC – pyramidal cell

PFA – paraformaldehyde

PFC – prefrontal cortex

PIR – piriform cortex

PMCo – posteromedial cortical amygdaloid nucleus

PL – prelimbic cortex

PV – parvalbumin

PVBC – parvalbumin-expressing basket cell

PS – parastrial nucleus

PTI – perisomatic-region targeting inhibitory neurons

SST – somatostatin

VAChT – vesicular acetylcholine transporter

VGAT – vesicular gamma-amino butyric acid transporter

VGLUT3 – vesicular glutamate transporter type 3

VIP – vasoactive intestinal polypeptide

VTA – ventral tegmental area

VO – ventral orbital cortex

VP/SI – ventral pallidum/substantia innominata

vPFC – ventral prefrontal cortex

1.Introduction

1.1 Overview

Recognizing threats is essential for animal survival. Therefore, it is not surprising that many brain circuits contribute to the detection of dangerous situations, leading to the elevation of attention and promoting affective brain state linked to the threat (Davis, 1997; Izquierdo et al., 2016; Ledoux, 2000; Tovote et al., 2015). This danger-triggered mental state helps generate the most appropriate behavioral responses, aiming to avoid, or at least, reduce any potential harm as well as forming memory that can guide future avoidance of similar threats. The complex brain processes involved in recognizing and responding to threat are regulated at different levels in the nervous system. Top-down control is provided by cortical circuits located in the basolateral amygdala (BLA) and medial prefrontal cortex (mPFC) (Burgos-Robles et al., 2009; Herry et al., 2008; Little and Carter, 2013; Mcdonald et al., 1996; Sotres-Bayon et al., 2012; Weiskrantz, 1956). These two structures can be parceled based on their connectivity and role playing e.g., in the control of fear and negative emotional states (Lacroix et al., 2000; Ledoux, 2000).

As a general principle, cortical function is efficiently and rapidly affected by subcortical inputs in a brain state-dependent manner. One of the subcortical afferent systems contributing critically to cortical network operation originates from the basal forebrain (BF), a heterogeneous structure located in the medial-ventral part of the brain (Hasselmo and Sarter, 2011; Mesulam et al., 1983; Solari and Hangya, 2018; Zaborszky, 2002). In this brain region, there are three neuron types: cholinergic, GABAergic, and glutamatergic cells that are known to project to cortical areas (Farr et al., 1999; Goldbach et al., 1998; Pascual et al., 2004).

Interestingly, cholinergic cells in the nucleus basalis of Meynert of the BF have been proposed to project to cortical regions, e.g., to frontal and posterior cortical areas, that are functionally interconnected with each other (Gombkoto et al., 2021; Zaborszky et al., 1997; 2015). These results suggest that BF cholinergic inputs may orchestrate activity in functionally related cortical areas, promoting interaction between regions and ultimately, enhancing neural computation. However, this attractive hypothesis has not been fully verified.

Previous studies have revealed that the BLA and mPFC receive cholinergic inputs

primarily from the two main parts of the BF, the horizontal limb of the diagonal band (HDB) and ventral pallidum/ substantia innominata (VP/SI), respectively (Bloem et al., 2014; Carlsen et al., 1985; Mayo et al., 1984; Nagai et al., 1982). Whether the mPFC and BLA networks can be simultaneously or differentially regulated by cholinergic afferents conveying salient information has yet to be determined. It is a particularly important question as several studies have shown a role for the cholinergic system in fear related processes, including acquisition and memory recall (Crimmins et al., 2023; Jiang et al., 2016; Knox, 2016; Mineur et al., 2022; Power et al., 2003).

Furthermore, the cholinergic system also plays a pivotal role in shaping cortical network operation in various conditions, including salient information transmission and processing. By modulating neuronal excitability, acetylcholine (ACh) influences arousal, attention, and sensory computation (Hasselmo and Starter, 2011). Acting on nicotinic and muscarinic receptors found on both excitatory pyramidal cells and inhibitory interneurons, it enhances signal-to-noise ratios, sharpens sensory discrimination, and supports synchronous neuronal activities, including theta (Vandecasteele et al., 2014; Lee et al., 1994) and gamma oscillations (Betterton et al., 2017; Hasselmo, 2006; Yu and Dayan, 2005). Its ability to facilitate disinhibition and plasticity further proves its importance in adapting cortical activity to environmental cues, suggesting that cholinergic afferents could dynamically regulate cortical network operations across different behavioral states (Letzkus et al., 2011; Knox, 2016; Sarter et al., 2009). Importantly, cholinergic neurons in the BF have been shown to rapidly convey salient information, including noxious signals to the cortical structures (Hangya et al., 2015), showing their critical contribution to painful stimulus processing.

In this thesis we aimed to reveal the structural basis of BF cholinergic control over the interconnected BLA-mPFC fear state -regulation circuits. In addition, we studied the effects of salient/ noxious stimulation on the activity in BF cholinergic cells and spiking dynamics in frontal cortical neurons with a focus on interneuron firing. Using retrograde and anterograde tracing techniques, together with immunocytochemistry, we mapped the projection areas of BF cholinergic neurons located in the HDB and VP/SI, first within the entire amygdala and prefrontal cortical regions (PFC), then specifically focusing on the innervation of the basolateral amygdala (BLA) and the medial prefrontal cortex (mPFC),

regions that are mutually interconnected. Next, we focused on the cholinergic innervation transmitting noxious information to the frontal cortex. First, we used fiber photometry to measure the population response of cholinergic cells in the HDB and VP/SI to noxious stimuli. Then to explore how cortical network elements change their activity during noxious stimuli, we performed visually guided juxtacellular recordings of various interneuron types.

1.2 Introducing the two key brain structures controlling fear states: amygdala and mPFC

The regulation of fear-related processes involves many cortical and subcortical regions, of which two areas stand out providing the top-down control of affective states: the amygdala and mPFC. These areas form a highly complex and reciprocal networks, with each region modulating distinct components of cognitive operation linked to fear. The amygdala is essential for forming stimulus-specific memory, where a particular stimulus or a set of stimuli is directly linked to threat (Tovote and Fadok, 2015). Within the mPFC, two subregions exhibit distinct functions in fear regulation. The prelimbic cortex (PL) is crucial for the learning and expression of fear (Burgos-Robles et al., 2009; Sotres-Bayon et al., 2012; Courtin et al., 2014), while the infralimbic cortex (IL) plays a key role in the extinction of learned fear (Quirk et al., 2000; Chang and Maren, 2010; Fontanez-Nuin et al., 2011; Sierra-Mercado et al., 2011; Santini et al., 2012).

The following sections will delve deeper into the structure, connections, and roles of the amygdala and mPFC in regulating cue-dependent fear learning. Additionally, the integration of the BF neuronal function into the fear-regulation networks will be explored.

1.2.1 The amygdala

The amygdala is a complex brain structure deep within the temporal lobe. It was first described by Karl Friedrich Burdach (1776–1847), who identified an almond-shaped region what is now called the basolateral amygdala (BLA; Fig. 1). The complex consists of approximately 13 nuclei, which can be further divided into various subregions. These are extensively interconnected both with each other and with different brain areas. In

humans and other vertebrates, it plays a central role in processing positive and negative emotions, forming memory traces related to these emotions, and modulating behavior patterns influenced by emotions (Phelps and LeDoux, 2005). One of its key functions is the expression of learned fear responses and the acquisition and storage of memories about the circumstances linked to these responses (Phelps and LeDoux, 2005; Duvarci and Pare, 2014; Janak and Tye, 2015; Izquierdo et al., 2016). The amygdala consists of approximately 4 major groups: the basolateral group (BLA), which includes the lateral (LA), basal (BA), and basomedial (BMA) nuclei; the cortical-like group, which contains the cortical nuclei (ACo) and the lateral olfactory tract nucleus (NLOT); the central group (CeA), which includes the lateral (CeL), medial (CeM), capsular (CeC), and intermediate (CeI) nuclei; and the medial amygdala (Fig. 1C). Additionally, there are nuclei that do not fit into the previously described groups, such as the amygdalopiriform transition area, intercalated cell masses (ITCs) and amygdalo-hippocampal area (AHA) (Sah et al., 2003). According to another interpretation, the first two groups can be merged, forming the cortico-basolateral amygdala (CBL), which includes the aforementioned nuclei. Furthermore, the centromedial group can be more accurately referred to as the extended amygdala (EA), as the central and medial amygdala extend rostromedially and form a continuous unit with the bed nucleus of the stria terminalis (BNST) (McDonald, 2003).

1.2.1.1 The basolateral amygdala complex (BLA)

As my experimental work involved delivering retrograde tracers into the basolateral group (BLA; Fig. 1A, B, C red), I will provide a more detailed anatomical description of this region.

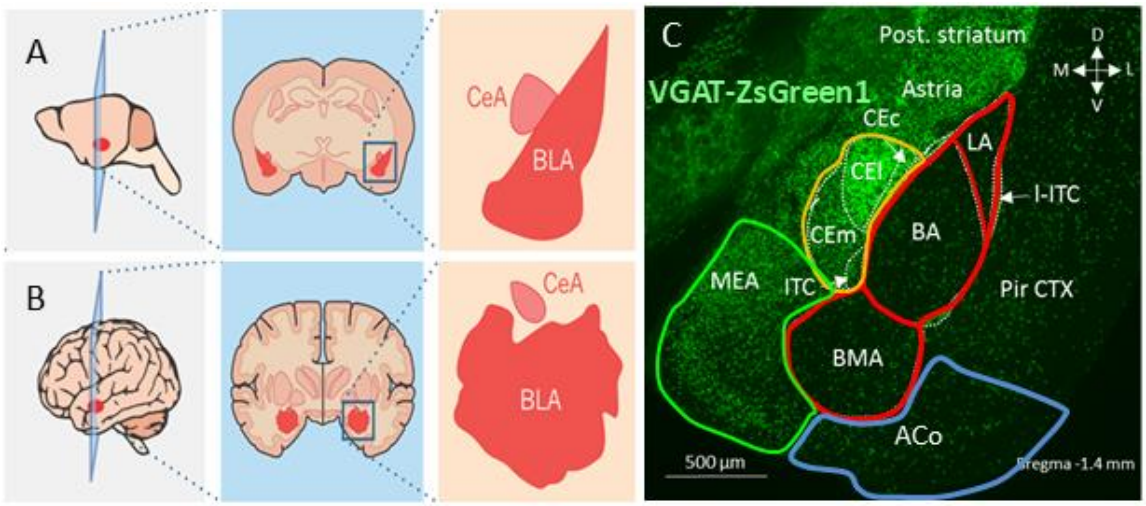

Figure 1. ***The structure and homology of the Amygdala.***
A, B*) Schematic representation of the location and homology of the amygdala in mice and humans. The fundamental pathways and functions are conserved across species (Janak and Tye, 2015).*
C*) Schematic representation of the mouse amygdala based on our results. Red: basolateral group, yellow: central group, blue: cortical-like group, green: medial amygdala. ACo, anterior cortical amygdaloid nucleus; BA, basal amygdala; BMA, basomedial amygdala; CeL, central amygdala, lateral division; CeM, central amygdala, medial division; LA, lateral amygdala; MeA, medial amygdala, anterior part; Pir, piriform cortex.*

Of the three nuclei located here, the LA is situated dorsally, while ventrally lies the BA, often referred to in the literature as the BLA. These regions are bordered laterally by the external capsule and medially by the CeA. The BLA can be further subdivided into a rostral-medial magnocellular subregion (anterior BA) and a more caudal-lateral parvocellular subregion (posterior BA). The BMA is located directly beneath the BA, adjacent to the ACo (Sah et al., 2003).

The cellular composition of the basolateral group closely resembles that of cortical structures. Our lab conducted stereological analyses to determine the ratio of gamma-aminobutyric acid-containing (GABAergic) interneurons to principal neurons in the LA and BA. A recent study found that GABAergic neurons were significantly more abundant in the BA (22%) compared to the LA (16%) in both male and female mice. This pattern was consistent across hemispheres (Vereczki et al., 2021). At least seven types of interneurons have been identified in the LA and BA of rodents, including axo-axonic cells (5.5%-6%), basket cells expressing parvalbumin (17%-20%) or cholecystokinin (7%-9%), dendrite-targeting inhibitory cells expressing somatostatin (10%-16%), neurogliaform cells containing neuropeptide Y (14%-15%), vasoactive intestinal polypeptide (VIP) and/or calretinin-expressing interneuron-selective cells (29%-38%), and GABAergic projection neurons co-expressing somatostatin and neuronal nitric oxide

synthase (5.5%-8%) (Vereczki et al., 2021). Except for the interneuron-selective interneurons (Rhomberg et al., 2018), amygdalar interneurons target functionally distinct membrane domains of principal neurons, enabling them to modulate activity in unique ways and contributing to complex network dynamics. Overall, the diversity and complexity of interneurons in the amygdala are highly similar to those in cortical networks (Freund and Buzsaki, 1996; Kepecs and Fishel, 2014). These features and their implications for network operations will be discussed in greater detail in later chapters.

1.2.1.2 The inputs and outputs of the amygdala

Inputs

The amygdala receives inputs from two primary sources: 1) cortical and thalamic pathways, which provide sensory and memory-related information, and 2) hypothalamic and brainstem pathways, which supply information related to behavior and autonomic processes (Sah et al., 2003). Among these inputs, the most significant information flow originates from cortical areas. The amygdala, particularly the BA and LA, receives direct inputs from the thalamus and indirect inputs from various cortical regions involved in processing distinct sensory modalities. These include the olfactory, somatosensory, gustatory, visceral, auditory, and visual systems. The projections from cortical areas primarily originate from glutamatergic pyramidal neurons in layer II/III and V, with their axons reaching the amygdala via the external capsule (Sah et al., 2003).

In addition to sensory inputs, the amygdala also receives direct projections from the higher-order cortical regions, including the prefrontal cortex, perirhinal cortex, and hippocampus, with the prefrontal cortex providing the most substantial input. The prefrontal cortex integrates information from multiple modalities, which converges in the BA, enabling the regulation of behaviors influenced by events of varying valence. The strong reciprocal connections of the BLA with the perirhinal cortex and hippocampus play a critical role in the formation of long-term declarative (explicit) memory. Specifically, the perirhinal cortex projects primarily to the medial part of the LA, while the ventral hippocampus (vHPC) and subiculum send axonal terminals to the BA (Sah et al., 2003).

Additionally, the amygdala receives significant projections from subcortical modulatory centers, including the locus coeruleus (giving rise to noradrenergic innervation), raphe

nuclei (sending serotonergic afferents) and ventral tegmental area (VTA, supplying dopaminergic inputs) (Sah et al., 2003). The cholinergic axons to all but one amygdala nuclei originate from the BF, the importance of which will be discussed in greater detail below (Do et al., 2016).

Outputs

Among the nuclei of the amygdaloid complex, the CeA is classically recognized as its primary output center. However, the basolateral complex also projects to numerous brain regions, including cortical, brainstem, and hypothalamic areas. Additionally, it has reciprocal connections with the sensory cortical regions mentioned earlier, projects to the vHPC involved in memory formation, the striatal regions, like the nucleus accumbens (NAc), and olfactory tuberculum, as well as the thalamus (Janak and Tye, 2015). The CeA sends efferent projections to the autonomic nervous system, enabling it to influence physiological responses, such as increased heart rate, elevated blood pressure, release of stress hormones, and the initiation of fear responses like freezing or flight. These target brain regions include the hypothalamus, the bed nucleus of the stria terminalis (BNST), and various nuclei in the midbrain, pons, and medulla, such as the periaqueductal gray (PAG), the parabrachial nucleus (PBN), and the nucleus of the solitary tract (NTS) (Sah et al., 2003). The projection from the CeA to the PAG is specifically responsible for triggering the freezing response, a behavior often studied in fear conditioning paradigms (Tovote et al., 2015).

1.2.2 The medial prefrontal cortex (mPFC)

The medial prefrontal cortex (mPFC) (based on Rose and Woolsey, 1948) is defined as the frontal lobe region receiving projections from the mediodorsal thalamus (Fig. 2C-D). This definition is consistent across mammalian species, and there is evidence of homology between the prefrontal cortex (PFC) of rodents and higher mammals (Giustino and Maren, 2015; Fig. 2A-B). The mPFC is involved in regulating fear-induced behavior, modulating emotions, decision-making, danger recognition, and contextual encoding. In rodents, the mPFC is subdivided into three regions: the anterior cingulate cortex (ACC), which regulates motor outputs related to behavior, including those linked to noxious stimulation; the prelimbic cortex (PL), which is involved in emotional and cognitive

processes like fear expression; and the infralimbic cortex (IL), which plays a role in fear extinction. The PL and IL regions are particularly relevant to the neural networks of fear regulation (Burgos-Robles et al., 2009; Herry et al., 2008; Little and Carter, 2013; Mcdonald et al., 1996; Sotres-Bayon et al., 2012).

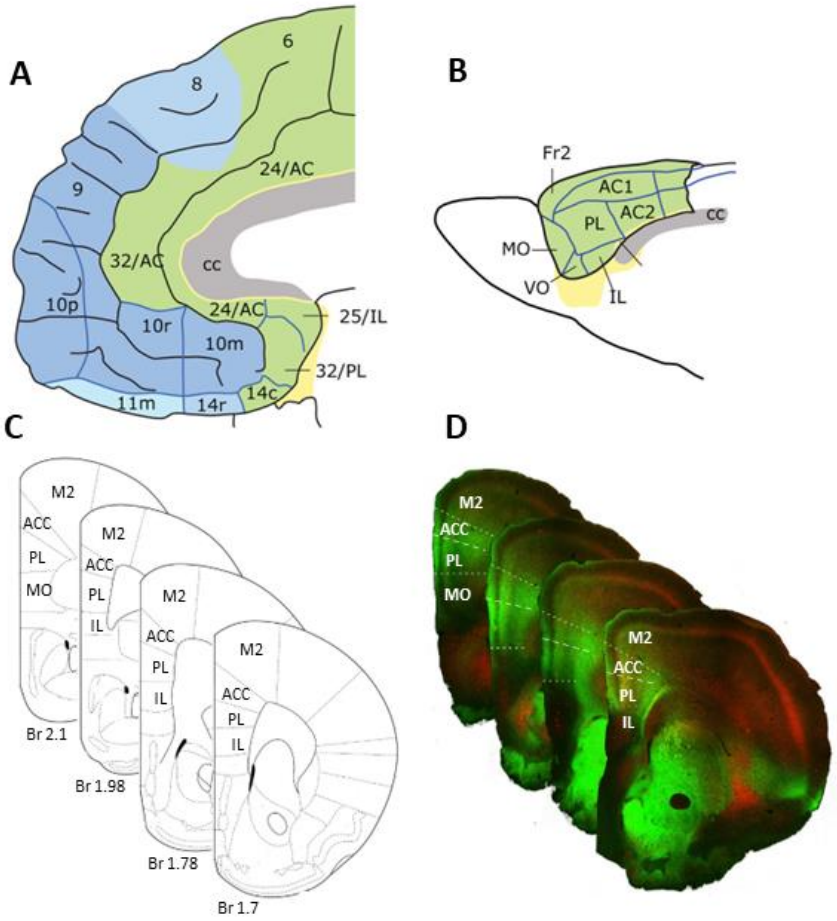

Figure 2. ***Comparison of the Human and Rodent Frontal Cortex.***
A) *Architectonic map of the medial and orbital surfaces of the human frontal lobe.* ***B)*** *Architectonic map of the medial and lateral frontal cortex of the rat. Green: agranular cortex, dark blue: granular cortex, yellow: allocortex. The color coding applies only to panels A and B. (Wallis, 2012)* ***C)*** *Schematic representation of the mouse prefrontal cortex.*
D) *Fluorescent images displaying the axonal projections from the mediodorsal thalamus to the mPFC based on our results. ACC: anterior cingulate cortex, cc: corpus callosum, FR2: second frontal area, fmi: forceps minor of the corpus callosum, IL: infralimbic cortex, M2: secondary motor cortex, MO: medial orbital cortex, PL: prelimbic cortex, VO: ventral orbital cortex. The numbers preceding the letters indicate cortical areas. Panels A and B show sagittal sections, while panel C, D presents coronal sections.*

The cell types that make up the mPFC can also be divided into two main categories: pyramidal neurons (80-90%) and interneurons (10-20%) (Gabbott et al., 2005). The pyramidal neurons are named after their characteristic morphology, as their cell bodies giving rise to dendritic branches have a pyramid-like shape. These neurons are typically located within Layers II-VI of the PL and IL regions and are capable of forming long-

range connections with distant brain areas (DeFelipe and Fariñas, 1992).

Although glutamate is the sole fast neurotransmitter of pyramidal neurons, they differ in firing properties, cell size, and morphology. Furthermore, based on molecular markers, several specialized subtypes of pyramidal neurons can be identified (Giustino and Maren, 2015).

1.2.2.1 Inputs and outputs of the mPFC

Inputs

The mPFC receives a variety of excitatory inputs, primarily from the mediodorsal thalamus, the BLA, and the hippocampus. It also receives projections from the contralateral mPFC and subcortical neuromodulatory centers, located in the brainstem. The mediodorsal thalamus provides important sensory and cognitive information related to higher-order processing, while the BLA supplies information related to emotional processing, including fear states (Burgos-Robles et al., 2009; Little and Carter, 2013; Mcdonald et al., 1996; Sotres-Bayon et al., 2012). The hippocampus is critical for contextual and declarative memory processing, with the vHPC and subiculum particularly projecting to the mPFC, which is essential for encoding context during fear-related learning (Padilla-Coreano et al., 2016; Tovote et al., 2015). Brainstem inputs include projections from regions such as the dorsal raphe nucleus, which gives rise to serotoninergic projections important for modulating waking states and cortical activation (del Cid-Pellitero and Garzón, 2011) and locus coeruleus, which supplies the mPFC with noradrenergic afferents, conveying information about novelty and stress (Arnsten, 2009; Uematsu et al., 2015). Dopaminergic inputs to the mPFC originate from the VTA (Thierry et al., 1973; Aransay et al, 2015; Abe et al., 2024). The contralateral mPFC projections contribute to bilateral processing and integration of emotional and cognitive information. Additionally, the mPFC receives significant cholinergic and GABAergic inputs from the BF, contributing to attentional and regulatory functions (Bloem et al., 2014; Do et al., 2016).

Outputs

The mPFC sends outputs to various brain regions, primarily influencing fear responses and cognitive processing. Both the IL and PL regions project to the BLA, but the PL more strongly targets the BA, while the IL projects to other areas such as the LA, BMA

(Giustino and Maren, 2015). The mPFC also sends projections to the BF. Other target areas include the insular cortex, claustrum, NAc, various thalamic nuclei, and dorsal raphe in the brainstem (Vertes, 2004). Furthermore, both the IL and PL regions of the mPFC send direct projections to the PAG, which plays a central role in the freezing response associated with fear. The rostral IL/PL regions project to the ventrolateral PAG, while the caudal parts target the dorsolateral PAG (Giustino and Maren, 2015; Rozeske et al., 2015). This direct influence on the PAG suggests that the mPFC, bypassing the amygdala, may directly modulate freezing behavior in response to fear.

1.2.3 The fear regulation networks

1.2.3.1 Fear memory formation

A critical aspect of fear memory formation is that the amygdaloid complex receives both direct and indirect sensory inputs from various sensory modalities. These pathways primarily target glutamatergic principal neurons in the BLA and are essential for the development of stimulus-associated fear learning. The information processing that begins in the BLA is relayed to CeL and CeM subdivisions of the central amygdala, which also receive direct inputs e.g. from the thalamus and PBN carrying sensory information. The activation of CeM and its impact on fear expression can occur through different mechanisms: either via direct glutamatergic excitation from the BLA or through disinhibition mediated by CeL (Janak and Tye, 2015).

Within the CeL, there are two types of neurons spiking distinctly upon fear aquisition: CeLon and CeLoff cells (Ciocchi et al., 2010; Haubensak et al., 2010). According to the current model, the CeLon neurons are activated by a conditioned stimulus (CS) and inhibit CeLoff neurons. This inhibition prevents CeLoff neurons from suppressing CeM activity, thereby allowing CeM neurons to exert their effects on fear responses (Janak and Tye, 2015). Projections from the CeM ultimately reach the PAG, a pathway believed to play a role in defensive behavior, controlling freezing or flight, as well as the lateral hypothalamus, which stimulates the sympathetic responses associated with fear-causing stress (Phelps et al., 2005).

However, neurons in the BLA do not merely relay information from upstream regions to the CeA; they actively modulate these signals over time through their cortical (mPFC, hippocampus) and subcortical (basal forebrain) connections (Duvarci and Paré, 2014).

Based on the findings of Andreas Lüthi's group (Herry at al., 2008; Senn et al., 2014), three types of fear state-related neurons can be distinguished within the BLA based on their spiking in fear responses:1) "Fear neurons", which exhibit excitatory activity in response to a CS but cease activation after extinction; 2) "Extinction neurons", which only become active during or after extinction; 3) "Extinction-resistant neurons, which maintain their CS-induced activity even after extinction.

Fear neurons primarily project to the PL cortex of the mPFC, while extinction neurons target the IL cortex. As hypothesized, the balance between these pathways determines the relative expression of fear versus extinction memory during relapse (Senn et al., 2014). Additionally, the BLA is reciprocally connected to the vHPC, with projections to the vHPC implicated in anxiety-related states (Felix-Ortiz et al., 2013). Moreover, the BF modulates fear learning via the BLA, a topic that will be discussed in detail in the next chapter.

1.2.3.2 Fear extinction

An essential aspect of fear state regulation is the ability to extinguish learned fear when the conditioned stimulus (CS) no longer poses a threat to the organism's safety. Extinction does not erase the original CS-unconditioned stimulus (US) association but instead forms a new inhibitory memory that competes with the original fear memory, with the net outcome determining behavior (Duvarci and Paré, 2014). Although, there are studies showing that memory erasing may contribute partially to memory extinction (Quirk et al., 2010; Guo et al., 2025). The activation of the IL cortex is crucial for fear extinction. Studies have shown that IL activity is suppressed during fear conditioning but increases during extinction learning (Santini et al., 2008).

Furthermore, Bukalo et al. (2015) demonstrated that *in vivo* optogenetic stimulation of the ventromedial PFC (which mainly corresponds to the IL) to BLA pathway enhances extinction memory formation without preventing relapses. Following IL principal neuron activation, extinction-related information is transmitted via the BLA to the ITCs, a specialized population of inhibitory neurons located between the CeA and the BLA. These ITC neurons primarily consist of inhibitory interneurons that project to the CeA, where they exert effects opposite to those of fear learning (Marek et al., 2013; Tovote et al., 2015).

1.3 The basal forebrain

The stimulus-associated fear learning can be split to two main components: (1) acquisition/consolidation and (2) extinction, which are opposing, competing processes. However, their precise regulation remains poorly understood. It is still unclear what the exact functions of other brain regions involved in regulation are and how the transition between acquisition/consolidation and extinction is modulated. One highly promising candidate for this role is the BF. This brain region is known to play a role in learning and memory processes and has both afferent and efferent connections with the mPFC and amygdala. Additionally, its physical location between these two structures makes it well-positioned for regulatory functions (Hasselmo and Sarter, 2011; Mesulam et al., 1983; Solari and Hangya, 2018; Zaborszky, 2002; Knox, 2016).

The BF is a heterogeneous structure found in the medial and ventral regions of the cerebral hemispheres, and includes the medial septum/ventral limb of the diagonal band (MS/VDB), the horizontal limb of the diagonal band (HDB), the substantia innominata (SI), the nucleus basalis magnocellularis (NBM), and a portion of pallidal areas (ventral pallidum (VP), globus pallidus GP)), where cholinergic projecting neurons can be observed (Zaborszky et al., 1999). Neurons in this region are diverse in terms of neurotransmitter content, morphology, and connectivity patterns, making it a significant challenge for neurobiologists to fully understand its function. Based on findings, three major neuron types can be distinguished in the BF based on their neurotransmitter content: cholinergic, glutamatergic, and GABAergic neurons (Semba, 2000).

1.3.1 Cholinergic neurons of the basal forebrain

Among the aforementioned cell types, the most studied population is the acetylcholine-containing (ACh) neurons, which play a crucial role in modulating cortical states, attention, plasticity, fear learning, and extinction learning (Wilson and Fadel, 2016). Furthermore, dysfunction or widespread loss of these neurons is strongly associated with the severe cognitive decline observed in Alzheimer's disease (Schliebs and Arendt, 2011). In the mammalian BF, cholinergic neurons are classified into four main groups based on the work of Mesulam and colleagues (Mesulam et al., 1983; Wilson and Fadel, 2016). The first three groups (Ch1–3) consist of neurons located within the MS, VDB and HDB

regions, projecting to the hippocampus, olfactory bulb, and prefrontal cortex. The fourth group of BF cholinergic neurons is scattered across the NBM, VP, and SI regions, innervating all layers of the neocortical regions, including projections to the mPFC and BLA (Do et al., 2016; Wilson et al., 2016).

The BF cholinergic cells receive widespread innervation from various brain regions. The densest projections originate from the striatum—specifically, the caudate-putamen and NAc regions—the lateral hypothalamus, and CeA (Do et al., 2016). A smaller proportion of inputs comes from different cortical areas, including the mPFC (1.5%), as well as from brainstem structures such as the PAG, VTA, and PBN (Hu et al., 2016). Notably, projections from the CeA synapse specifically onto those BF cholinergic neurons that send axonal terminals to the BLA (Gielow and Zaborszky, 2017). This suggests that the amygdala may influence cholinergic innervation from the BF, a pathway (BF cholinergic neurons → BLA) that has been shown to play a role in promoting fear learning and inhibiting extinction learning (Gielow et al., 2017; Jiang et al., 2016).

In contrast, during fear expression, the CeM becomes activated, inhibiting the BF cholinergic projections to the BLA, thereby reducing ACh release in the BLA (Gielow et al., 2017). Based on these findings, it is conceivable that BF cholinergic neurons exhibit differential activity patterns during fear learning and fear expression—being activated during fear learning and inhibited during fear expression.

1.3.2 Non-cholinergic neurons of the basal forebrain

In addition to cholinergic neurons, the BF contains two other neuron types. These cells are found throughout the entire BF, do not form clearly distinct populations, and their projections, similar to those of cholinergic neurons, innervate various cortical areas. GABA-containing cells are present in a significantly higher number, with approximately seven times more of them compared to their cholinergic counterparts (Sarter and Bruno, 2002). Some of these GABAergic neurons are long-range projecting neurons, targeting not only the neocortex and the BLA but also the pallidum, striatum, midbrain, and habenula (McDonald et al., 2011; Do et al., 2016).

A subgroup of BF GABAergic neurons, distinguished by the presence of a calcium-binding protein parvalbumin (PV), synapse onto inhibitory interneurons in the hippocampus and cortex (Freund and Antal, 1988; Freund and Meskenaite, 1992;

Borhegyi et al., 2004; Hangya et al., 2009). Since cortical GABAergic inhibitory interneurons innervate pyramidal cells, the activation of BF GABAergic PV cells lead to dis-inhibition of pyramidal cells via suppressing the spiking in local cortical interneurons (Toth et al., 1997). If this cortical disinhibition occurs rhythmically, then it may contribute to the generation of 40 Hz gamma oscillations in the cortex (Kim et al., 2015). Borhegyi et al. identified two distinct populations of these neurons in the MS that exhibit bursting activity synchronized to different phases of the theta rhythm: one group fires at the trough, and the other near the peak. Anatomical analysis revealed extensive local connections between these neurons, suggesting a mechanism for their synchronized activity and influence on the hippocampus through rhythmic disinhibition at specific phases of the theta cycle (Borhegyi et al., 2004). Other study found that BF GABAergic PV cells exhibit phasic activation in response to punishment and optogenetic inhibition of these cells during punishment impaired cue-outcome association formation, indicating their role in associative learning (Hegedüs et al., 2024).

Very little information is available in the literature regarding the BF glutamatergic neurons. However, one subset of these cells, identified by the expression of vesicular glutamate transporter 2 (VGLUT2) and projecting from the septum to the hippocampus, has been found to play a role in movement organization. Their activation precedes the initiation of movement and regulates movement speed. As the firing rate of septal VGLUT2 neurons increases, the firing rate of hippocampal CA1 pyramidal neurons also increases, leading to an overall acceleration of movement speed (Fuhrmann et al., 2015). Another recent study demonstrates that BF VGLUT2 neurons send projections to key brain regions involved in arousal and reward/aversion processing, including the lateral habenula and VTA, as well as neighboring BF cholinergic and PV neurons. Additionally, optogenetic activation of BF VGLUT2 neurons triggered avoidance behavior, a response not observed with the stimulation of BF cholinergic or PV neurons. (McKenna et al., 2021).

1.4 Cortical networks and interneurons

1.4.1 Cortical networks

After exploring the connections and functions of the amygdala and mPFC in fear

regulation, as well as their innervation by BF cholinergic neurons, I shift to the second part of my thesis. Here, I introduce the structure of cortical networks, the role of ACh as a key neurotransmitter in learning, and its specific effects on different types of inhibitory interneurons.

The cerebral cortex in mice, like in other mammals, is organized into six distinct layers, each playing a crucial role in processing sensory information, motor control, and higher cognitive functions. Despite being thinner and less convoluted than the human cortex, the mouse neocortex follows the same laminar structure, with variations in cell composition, connectivity, and function across different regions (Wallis, 2012).

Layer I: The outermost layer largely consists of cell bodies of different interneurons but rich in axons, dendrites, and synapses as well. It serves as an integration hub, where top-down projections from other cortical and subcortical areas modulate cortical activity. Neuromodulators such as ACh and serotonin (5-HT) exert significant influence in this layer, shaping network dynamics (Manes et al., 2022).

Layer II: This layer contains small pyramidal neurons, and inhibitory interneurons that contribute to local processing. It primarily engages in intracortical communication, receiving inputs from other cortical areas and playing a role in associative processing.

Layer III: Slightly deeper than Layer II, this layer contains medium-sized pyramidal neurons that project to other cortical areas, both within the same hemisphere (association fibers) and to the opposite hemisphere via the corpus callosum (commissural fibers). In mice, this layer is particularly important for interhemispheric communication and sensory integration.

Layer IV (present in sensory cortices): As the primary recipient of sensory inputs from the thalamus, Layer IV is densely packed with small stellate neurons and pyramidal cells that process and relay sensory information to other layers. In primary sensory areas such as the somatosensory cortex, this layer is especially prominent, forming the well-studied barrel cortex in mice, which processes tactile information from the whiskers (Simons and Woolsey, 1979).

Layer V: This layer contains large pyramidal neurons, including corticospinal and corticobulbar projection neurons that send outputs to subcortical structures such as the brainstem and spinal cord. In the motor cortex, Layer V is particularly thick and includes Betz cells, which are among the largest neurons in the brain and are critical for motor

control (Naka and Adesnik, 2016).

Layer VI: The deepest layer, Layer VI, consists of a diverse population of pyramidal and fusiform neurons. It plays a key role in feedback regulation by sending projections back to the thalamus, modulating thalamic inputs based on ongoing cortical activity. This cortico-thalamic loop is essential for attention, sensory gating, and state-dependent cortical processing (description of layers are based on the work of Ramón y Cajal, S).

This structural organization of layers varies significantly between different functional regions, reflecting their specialized roles in sensory processing, association, and motor control. One of the key distinctions lies in the presence or absence of Layer IV, which serves as the primary recipient of thalamo-cortical inputs (Lewis, 1878; Kemper and Galaburda, 1984; Donoghue and Wise, 1982).

In primary sensory cortices, such as the primary somatosensory cortex (S1) and primary visual cortex (V1), Layer IV is highly developed and densely packed with small stellate neurons and pyramidal cells, which receive and process incoming sensory information.

In contrast, agranular regions such as the mPFC and the secondary motor cortex (M2) lack a well-defined Layer IV. Instead of a dense population of stellate neurons, these areas have a more continuous flow of information between Layers II/III and V/VI, facilitating integrative processing and executive control rather than direct sensory inputs. The absence of a clear granular layer in association cortices aligns with their role in higher-order cognitive functions and motor planning, rather than direct sensory representation (Shipp 2005, 2013).

As mentioned, cortical circuits primarily consist of excitatory (pyramidal, stellate) neurons, characterized by strong recurrent connections, and a smaller population of inhibitory interneurons that regulate local activity. The fundamental role of inhibition is to maintain balance within the network by temporarily suppressing excitation with a precise manner, thereby enabling complex and rapid dynamics. To maintain this balance and enhance computational capabilities, an incredibly diverse interneuronal populations have evolved, allowing for precise regulation of different membrane domains of glutamatergic pyramidal neurons. Some interneurons inhibit only the dendritic shafts-, while others target the somatic region of pyramidal neurons or even other interneurons. In the following section, I will introduce the main categories of inhibitory interneurons in cortical regions, as well as describe those interneurons that are the focus of my research.

1.4.2 Cortical interneurons

In the cortex, GABAergic inhibitory neurons are classified into four main functional groups based on their axonal targets: perisomatic region-targeting interneurons (PTIs), dendrite-targeting interneurons, interneuron-selective interneurons (ISIs), and GABAergic projection neurons (Fig. 3).

1.4.2.1 Perisomatic region-targeting interneurons (PTIs)

These interneurons exert strong control over the firing of principal neurons by innervating the soma, proximal dendrites, or axon initial segment (AIS). This category includes axo-axonic cells (AACs) or chandelier cells (ChCs) and basket cells (BCs). AACs exclusively target the AIS of pyramidal neurons (Szentágothai, 1975; Somogyi, 1977), whereas BCs' axons form pericellular baskets around the cell bodies and proximal dendrites of target neurons. Both interneuron types effectively control spiking in their postsynaptic targets (Miles et al., 1996; Veres et al., 2014; Veres et al., 2017). BCs can be further divided into parvalbumin-positive (PVBCs) and cholecystokinin and cannabinoid receptor type 1-expressing subtypes (CCKCB1BCs) (Freund 2003; Freund and Katona, 2007).

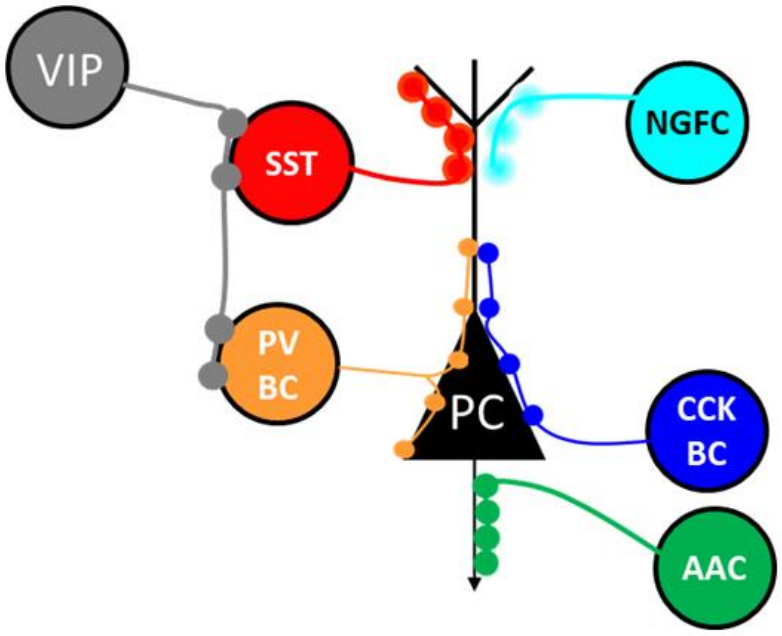

Figure 3. ***Schematic representation of inhibitory interneuron connectivity onto a pyramidal cell (PC).*** *Different interneuron subtypes target distinct compartments of the pyramidal cell:*
VIP (vasoactive intestinal polypeptide) interneurons *(gray) inhibit SST and PV interneurons.*

SST (somatostatin) interneurons *(red) primarily target the distal dendrites of the pyramidal cell.*
NGFC (neurogliaform cells) *(cyan) provide widespread inhibition at the dendritic level.*
PVBC (parvalbumin-positive basket cells *(orange) target the perisomatic region of the pyramidal cell.*
CCKBC (cholecystokinin-positive basket cells *(blue) also innervate the perisomatic region.*
AAC (axo-axonic cells) *(green) synapse on the axon initial segment.*

1.4.2.1.1 Parvalbumin basket cells (PVBCs)

PVBCs (Fig. 3 orange) are fast-spiking interneurons characterized by their ability to sustain high-frequency trains of action potentials (40–200 Hz) with minimal spike frequency adaptation, promoted by fast afterhyperpolarization. They have the lowest input resistance and the fastest membrane time constant among interneurons, allowing for rapid synaptic responses (Connors and Gutnick, 1990; Cauli et al., 1997; Markram et al., 2004). They contain PV, which has been correlated with their fast-spiking capability since the 1980s (Kawaguchi et al., 1987). As typical for each neocortical region, PV cells receive major input from local pyramidal cells, the thalamus and other cortical areas, including the BLA in the mPFC and mediate fast, precise inhibition of target neurons (Nagy-Pál et al., 2023; Gabernet et al., 2005; Cruikshank et al., 2007; Fekete et al., 2024). They contribute to both feedforward and feedback inhibition, precisely regulating the timing of excitatory input integration and action potential generation in principal cells, while also playing a key role in the initiation and maintenance of fast gamma-frequency cortical rhythms (Miles et al., 1996; Traub et al., 2004; Bartos et al., 2007; Cardin et al., 2009; Gulyas et al., 2010; Veres et al., 2017). Additionally, PVBCs and CCKBCs may innervate each other in the hippocampus and mPFC, but not in the BLA, (Dudok et al., 2021; Andrasi et al., 2017; Fekete et al., 2024).

1.4.2.1.2 Cholecystokinin and cannabinoid receptor type 1 - expressing basket cells (CCKCB1BCs)

CCKCB1BCs, (Fig. 3 dark blue) in contrast, exhibit a regular-spiking, adapting firing pattern with slower membrane time constants and receive diverse modulatory inputs from subcortical regions (Armstrong and Soltesz, 2012; Freund and Katona, 2007). They express cannabinoid receptor type 1 (CB1) and, in some cases, vesicular glutamate transporter 3 (VGLUT3) or calbindin (Calb) (Somogyi et al., 2004, Rovira-Esteban et al., 2017). One of the most important differences between CCKCB1BCs and PVBCs is that the GABA release from the axon terminals of CCKCB1BCs is controlled by

endocannabinoid-mediated retrograde signaling. When their postsynaptic targets depolarize, endocannabinoids are released, activating CB1 receptors on presynaptic terminals, which in turn reduces neurotransmitter release — a phenomenon known as depolarization-induced suppression of inhibition (DSI) at short-term (Freund, 2003; Wilson and Nicoll, 2001, Dudok et al., 2024). If CB1 receptor activation takes longer time, then long-term depression can be induced at these axon terminals (iLTD) (Chevalyere and Castillo, 2004). These mechanisms make CCKCB1BCs a highly plastic, fine-tuning system that is more susceptible to both short- and long-term modulatory influences (Freund, 2003; Freund and Katona, 2007).

1.4.2.1.3 Chandelier (ChCs) or axo-axonic cells (AACs)

ChCs, also known as AACs (Fig. 3 green), were first described in the 1970s by János Szenthágotai (Szentágothai, 1975) and are distinguished by their vertically oriented axonal terminals, or "cartridges," which selectively innervate the AISs of pyramidal neurons (Somogyi, 1977). These GABAergic interneurons typically express PV and, in some cases, Calb, calretinin (CR), as well as vasoactive intestinal polypeptide receptor 2 (VIPR2), which has recently been identified as an additional marker (Schneider-Mizell et al., 2021; Tasic et al., 2018). Like PVBCs, AACs are fast-spiking cells and are considered to provide effective synaptic inhibition on their targets (Veres et al., 2014). However, their impact on pyramidal neurons may be complex, as GABAergic inputs to the AISs can be depolarizing rather than inhibitory due to chloride ion concentration shifts (Szabadics et al., 2006; Woodruff et al., 2009). In the S1, AACs initially depolarize the AISs during early development but shift to hyperpolarizing or shunting effects in adulthood (Pan-Vázquez et al., 2020). Notably, while thalamo-cortical inputs to BCs produces strong but rapidly depressing synaptic responses, AACs exhibit weak initial responses that facilitate over time, enabling sustained spiking (Zhang et al., 2022), highlighting their separate role from BCs.

Overall PVBCs, CCKCB1BCs, and AACs represent functionally specialized inhibitory interneuron subtypes. PVBCs provide both feedforward and feedback inhibition and generate rhythmic activities, while CCKCB1BCs enable the “fine tuning” of inhibition. AACs uniquely gate pyramidal neuron firing through AIS-targeted synapses, making them an important regulator of pyramidal cell output. Together, these interneurons orchestrate cortical dynamics through complementary mechanisms, balancing excitation

and inhibition across temporal and spatial scales.

1.4.2.2 Dendrite-targeting interneurons

1.4.2.2.1 Somatostatin-expressing interneurons (SST INs)

Somatostatin-expressing interneurons (SST INs; Fig. 3 red), also known as SOM INs, are a diverse group of inhibitory interneurons that play a crucial role in modulating cortical activity. Defined by their expression of the neuropeptide somatostatin (SST), one group of these interneurons primarily target the apical dendrites and spines of pyramidal neurons and constitute approximately 30% of all inhibitory cells in the cortex (Xu and Callaway, 2009; Yavorska and Wehr, 2016). While receiving input from both cortical and subcortical regions, SST INs are able to regulate dendritic computations through both feedforward and feedback inhibition (Miles et al., 1996; Murayama et al., 2009; Karnani et al., 2016a).

Among SST INs, Martinotti cells (MCs) represent a well-characterized subgroup. These are the most abundant SST IN type, distributed across all cortical layers but particularly concentrated in superficial layers. They possess ascending axons that arborize in Layer I, where they form synapses on the dendritic tufts and spines of pyramidal neurons (Martinotti, 1889; Karube et al., 2004; Wang et al., 2004). MCs typically exhibit a regular adapting firing pattern but can also display bursting activity. They can be further classified into those expressing CR and those that do not (CR−), with distinct functional and physiological properties (Bernado et al., 2011).

In contrast, non-Martinotti SST INs encompass a range of anatomical subtypes, including subsets of basket, bitufted, horizontal, and multipolar cells. Additionally, some SST inhibitory neurons function as long-projecting GABAergic neurons, extending their influence beyond local circuits (Reyes et al., 1998; Ma et al., 2006; McGarry et al., 2010; Suzuki and Bekkers, 2010).

Functionally, SST INs play an essential role in regulating cortical information flow by primarily inhibiting dendrites of principal neurons. Through their involvement in disynaptic inhibitory circuits between principal neurons, they contribute to surround activity suppression, a phenomenon where a pyramidal cell’s spiking is reduced in response to a stimulus outside its classical receptive field (Silberberg and Markram, 2007; Fino and Yuste, 2011; Adesnik et al., 2012). In the mouse visual cortex, unlike principal

neurons, SST INs in the superficial layers exhibit increased activity when the receptive field surround is stimulated. This difference arises from the preferential excitation of SST INs by horizontal cortical axons (Adesnik et al., 2012). Through these mechanisms, SST INs serve as critical modulators of cortical dynamics, shaping sensory processing and cognitive functions.

1.4.2.2.2 Neurogliaform cells (NGFCs)

Neurogliaform cells (NGFCs; Fig. 3 light blue), first described by Ramón Cajal as "spiderweb" or "arachniform" cells due to their morphology, are characterized by a small, round soma and thin, varicose dendrites radiating in all directions to form a dense stellate plexus around the cell body. These GABAergic interneurons exhibit a dense axonal arborization that typically remains close to their somato-dendritic profile. While predominantly abundant in cortical Layer I —where they constitute over 90% of neurons — NGFCs are distributed across all cortical layers (Kawaguchi and Kubota, 1997; Krimer et al., 2005; Overstreet-Wadiche and McBain, 2015). Immunocytochemically, most neocortical NGFCs express neuropeptide Y (NPY), reelin, and COUPTFII, with a minority positive for nNOS (Miyoshi et al., 2010).

Functionally, NGFCs mediate feedforward inhibition onto pyramidal cell's dendrites, but unlike typical interneurons, their synaptic boutons are positioned farther from dendritic spines and shafts, highlighting a role in volume transmission rather than precise synaptic signaling (Olah et al., 2009). This "cloud-like" GABA release engages both GABA(A) and GABA(B) receptors, enabling slow, prolonged inhibition that broadly suppresses local microcircuits (Tamas et al., 2003). Additionally, NGFCs form electrical synapses not only among themselves but also with other interneurons, including BCs and AACs, facilitating synchronized network activity (Simon et al., 2005).

These cells are also important in the integration of feedback inhibition. For instance, in the medial entorhinal cortex, Layer I NGFCs receive excitatory input from Layer II pyramidal neurons and inhibit apical dendrites of principal cells (Szocs et al., 2022). Furthermore, their cholinergic input specificity allows fine-tuning of circuit functions, highlighting their adaptability across brain regions (Brombas et al., 2014; Abs et al., 2018).

In summary, NGFCs represent a morphologically and functionally distinct interneuron class, utilizing volume transmission to exert broad inhibitory control. Their diverse

connectivity, the usage of GABA(A) and GABA(B), and regional specialization enable them to shape neural dynamics, while remaining responsive to subcortical neuromodulation.

1.4.2.3 Interneuron-selective interneurons (ISIs)

VIP ISIs (Fig 3. grey) are a distinct subpopulation of GABAergic inhibitory neurons found in various brain regions, including the neocortex, amygdala, and hippocampus (Acsady et al., 1996; Pi et al., 2013; Krabbe et al., 2019; Francavilla et al., 2018; Tyan et al., 2014; Rhomberg et al., 2018). As their name 'interneuron-selective' implies, they specifically innervate other interneurons and are distinguished by their expression of the neuropeptide VIP (Acsady et al., 1996; Hajos et al., 1996). They also display remarkable diversity in morphology, molecular markers, and electrophysiological properties.

Regarding their morphology, VIP ISIs encompass several types, including bipolar and bitufted morphologies (Acsady et al., 1996; Cauli et al., 1997; Porter et al., 1998). At the molecular level, these interneurons frequently co-express markers such as CR and ChAT (Porter et al., 1998; Amir, 2020). It has to be mentioned that a subpopulation of VIP interneurons also express CCK and CB1 (Acsady et al., 1996; Hajos et al., 1996; Galarreta et al., 2004; Sugino et al., 2006; Rhomberg et al., 2018), but these interneurons have multipolar morphology and are BCs (Hajos et al., 1996; Katona et al., 1999; Rhomberg et al., 2018), distinct from ISIs.

A key role of VIP ISIs is disinhibition, as they suppress the activity of other inhibitory interneurons, particularly those expressing SST and PV. This disinhibitory mechanism enhances the excitability of principal neurons and facilitates selective amplification of local circuit processing (Letzkus et al., 2011; Pfeffer et al., 2013; Pi et al., 2013). These interneurons are also involved in processing sensory information across multiple modalities, including tactile, auditory, and visual inputs (Mesik et al., 2015; Ibrahim et al., 2016; Kuchibhotla et al., 2017). Furthermore, VIP ISIs are activated by reinforcement signals such as reward and punishment, with widespread cortical activation potentially serving as a global learning signal that strengthens functional connectivity across cortical representations (Pi et al., 2013; Szadai et al., 2022).

In summary, VIP ISIs represent a diverse and functionally significant class of inhibitory neurons that modulate cortical circuits through disinhibition. They contribute to sensory

processing, arousal regulation, learning, and plasticity, primarily by controlling the activity of other interneurons and fine-tuning principal neuron excitability.

1.5 Cholinergic modulation and salient/noxious information processing

Cholinergic signaling in the cortex is highly complex, involving various receptor types, cell populations, and mechanisms that together shape cortical processing. ACh functions as a neuromodulator through volume transmission, influencing cell excitability and network activity over extended periods. This process can enhance the responsiveness of cortical and hippocampal pyramidal neurons (Picciotto et al., 2012; Sarter et al., 2014).
In addition to its modulatory role, ACh also participates in synaptic transmission (Takacs et al., 2018). Both the modulatory function and synaptic transmission are achieved via nicotinic (nAChRs) and muscarinic (mAChRs) receptors, each with distinct localization and signaling mechanisms. nAChRs located on dendrites and cell bodies can mediate direct postsynaptic effects, while on axon terminals, they contribute to glutamate release and the depolarization of cortical interneurons (Hogg et al., 2003). Additionally, mAChRs boost pyramidal neuron activity and reduce the transmitter release, promoting oscillatory patterns (Brown, 2012). Together, these cellular and circuit mechanisms underscore the intricate role of cholinergic signaling in regulating cortical dynamics.

1.5.1 The role of ACh linked to noxious stimuli.

Cholinergic signaling plays a crucial role in the brain's ability to respond to salient and noxious stimuli, significantly influencing sensory processing, attention, and emotional learning. BF cholinergic neurons are particularly attuned to novel sensory inputs, acting as key players in encoding the salience of such stimuli. These neurons activate rapidly, with response times comparable to conventional synaptic transmission, enabling precise, time-locked communication of salient information to the neocortex (Richardson and DeLong, 1990; Wilson and Rolls, 1990a; Zhang et al., 2019, Hangya 2015).
Phasic ACh release plays a pivotal role in enhancing associative learning by modulating cortical circuits in a layer- and cell type-specific manner. In Layer I, ACh depolarizes most interneurons via nAChRs, including VIP ISIs and other Layer I interneurons, which

inhibit PVBCs. This disinhibition (i.e., inhibiting PVBCs) reduces synaptic inhibition of pyramidal neurons, thereby enhancing pyramidal neuron activity and facilitating sensory and learning processes (Letzkus et al., 2011; Christophe et al., 2002; Arroyo et al., 2012). ACh also exhibits activity-dependent effects on NGFCs in Layer I, activating them through nAChRs during low firing rates and inhibiting them via mAChRs during high firing rates (Brombas et al., 2014). In Layers II/III, pyramidal neurons themselves do not express nAChRs, but interneurons in these layers do, leading to cholinergic modulation that typically reduces pyramidal cell firing rates by enhancing GABAergic inhibition (Poorthuis et al., 2013). In Layer IV of the visual cortex, ACh improves neuronal gain and response reliability, facilitating sensory processing (Goard and Dan, 2009; Soma et al., 2012). Meanwhile, in Layers V and VI, both nAChRs and mAChRs modulate pyramidal neurons and interneurons, producing diverse effects such as suppression or facilitation, depending on the context (Poorthuis et al., 2013; Luchicchi et al, 2014).

This intricate, layer-specific cholinergic modulation underscores the complexity of ACh's role in regulating cortical activity, enabling precise adjustments to sensory input, attention, and learning across cortical networks.

2.Objectives

Based on the findings discussed in the previous chapter, it is evident that the BF plays a crucial role in the regulation of fear learning and behavior. However, further research is needed to better understand the precise localization, neurochemical properties, and behavioral functions of BF cells projecting to different brain regions. Anatomical studies are particularly important because, in recent years, numerous functional studies have been conducted on the activity of BF cholinergic and non-cholinergic cells, yet the detailed neuroanatomical investigations supporting these findings have been lacking (Sarter, 2008).

In the first part of my thesis, we focused on the cholinergic innervation of the amygdala and mPFC networks by the BF, carrying salient/noxious information to the cortical areas. We aimed to understand whether specific subregions receive distinct projections from the BF and whether individual cholinergic neurons can simultaneously innervate these subregions. To address this, we asked the following questions:

1) What are the projection patterns of cholinergic neurons originating from the HDB and VP/SI?

2) Do specific subregions of the amygdala and mPFC receive distinct cholinergic projections from different BF nuclei?

3) Can individual cholinergic neurons simultaneously innervate both the amygdala and mPFC?

4) Do cholinergic neurons in the VP/SI and HDB co-express transporters for other neurotransmitter molecules, such as VGLUT3 and VGAT?

The second part of my introduction outlines the structure of cortical networks, emphasizing the diversity and functional roles of inhibitory interneurons. It also highlights their dynamic behavior during noxious stimulation, particularly when ACh is released from BF terminals in the cortex. My research aimed to further explore how noxious stimuli alter cortical network activity in a cell-type-specific manner. To explore this issue, the following questions were posed:

1) Are cholinergic neurons in the HDB and VP/SI activated during noxious stimulation?

2) How do specific types of cortical inhibitory interneurons respond to noxious stimulation, and is BF cholinergic input necessary for shaping their activity? Our results

advance our understanding of how painful or noxious stimuli alters cortical network dynamics by linking cholinergic signaling to cell-type-specific interneuron activity, bridging a critical gap in salient information processing.

3.Materials and Methods

3.1 Animals.

Table 1 collects all the mice used for these experiments (Table 1). All experiments were performed in male and female mice 5-16 weeks of age. All experiments were approved by the Committee of the Scientific Ethics of Animal Research (22.1/360/3/2011) and all procedures involving animals were performed according to methods approved by Hungarian legislation (1998 XXVIII. section 243/1998, renewed in 40/2013.) and institutional guidelines of ethical code. All procedures complied with the European Convention for the Protection of Vertebrate Animals used for Experimental and Other Scientific Purposes (Directive 86/609/CEE and modified according to the Directives 2010/63/EU). All effort was taken to minimize animal suffering and the number of animals used.

Table 1. ***Animals used in the experiments.***

Animals	cataloge #	Company
ChAT-IRES-Cre	#006410	JAX
CAG-LSL-ZsGreen1	#007906	JAX
CAG-LSL-tdTomato	#007914	JAX
BAC-VGLUT3-iCre	#018147	JAX
BAC-CCK-dsRed		HUN-REN IEM Medical Gene Technology Unit
VIP-IRES-Cre	#010908	JAX
NPY-IRES-Cre	#027851	JAX
Pvalb-IRES-Cre	#017320	JAX
BAC-CCK/gfpcoIN_sb		HUN-REN IEM Medical Gene Technology Unit
Nkx2.1-CreER	#14552	JAX
LSL-Flpo	#28584	JAX
VGAT-IRES-Cre	#016962	JAX
SST-IRES-Cre	#013044	JAX
NPY-IRES-Cre x BAC-CCK/gfpcoIN_sb		Generate in the HUN-REN IEM Medical Gene Technology Unit
BAC-VGLUT3-iCre x BAC-CCK/gfpcoIN_sb		Generate in the HUN-REN IEM Medical Gene Technology Unit
Nkx2.1-CreER x LSL-Flpo		Generate in the HUN-REN IEM Medical Gene Technology Unit
Pvalb-IRES-Cre x CAG-LSL-ZsGreen1		Generate in the HUN-REN IEM Medical Gene Technology

		Unit
VIP-IRES-Cre x BAC-CCK/gfpcoIN_sb		Generate in the HUN-REN IEM Medical Gene Technology Unit
VIP-IRES-Cre x CAG-LSL-ZsGreen1		Generate in the HUN-REN IEM Medical Gene Technology Unit
NPY-IRES-Cre x CAG-LSL-ZsGreen1		Generate in the HUN-REN IEM Medical Gene Technology Unit
VGAT-IRES-Cre x CAG-LSL-ZsGreen1		Generate in the HUN-REN IEM Medical Gene Technology Unit

3.2 Tracing experiments.

Mice were anaesthetized with 125 mg/kg ketamine and 5 mg/kg xylazine and mounted to a stereotaxic frame. Eyes were coated with corneal gel (Recugel Ophthalmic Gel), and body temperature was maintained with small animal heating pads (Supertech Instruments, Pecs, Hungary). The skin was removed from the skull, so the cranial sutures were clearly visible. The mouse head was set horizontally based on the level of the bregma and lambda. Anterior-posterior and medio-lateral coordinates were measured from the bregma. The skull was carefully drilled with a dental bur (Foredom), then dorso-ventral coordinates were measured from the level of the dura mater. The performed surgeries are detailed in Table 2 grouped and numbered by the experiments. **1)** To label BF neurons projecting to the amygdala region, we used Cholera Toxin B (CTB, 0.5 mg/99.5 µl distilled water, List Biological Laboratories) or Fast Blue (FB, 5% in in 0.9% saline, Polysciences), which were iontophoretically injected (2/2 s on/off duty cycle, 2 µA pulses, for 5 min for CTB, 2/2 s on/off duty cycle, 5 µA pulses, for 7-10 min for FB) into the LA, BA or BMA unilaterally (Table 2; exp. 1) using a Drummond Recording Nanoject II (Drummond Scientific). **2)** To label BF neurons projecting to the mPFC, FluoroGold (FG, 2% in 0.9% saline, Fluorochrome) was injected iontophoretically (2/2 s on/off duty cycle, 2 µA pulses, for 5 min; AP/ML/DV; Table 2; exp. 2). These retrograde tracers were applied to the brain via a glass pipette (ID = 0.530 mm ± 25 µm, OD 1.14 mm, World Precision Instruments) which was filled first with 50% glycerol (tap water: glycerol, 1:1) and then by the tracer. After 3-5 days following the injections, animals were anesthetized again with ketamine/xylazine mixture as above and perfused under deep anesthesia first with saline (0.9%) and then with 4% paraformaldehyde dissolved in 0.1 M phosphate buffer (PB, pH: 7.4, 100 mL/animal, Sigma-Aldrich). Brains were then removed and cut into

50-80 µm-thick coronal sections with a Vibratome (VT1000S, Leica). **3)** To analyze the axonal arborization of BF cholinergic neurons projecting to the amygdala and the PFC, we injected 100-100 nl of AAV5.Ef1a.DIO.eYFP (gift from Karl Deisseroth; Addgene viral prep # 27056-AAV5, RRID: Addgene_27056) to the HDB and VP/SI within the same ChAT-Cre animals (Table 2; exp. 3). **4)** To individually investigate the cholinergic projections of these BF nuclei, we injected 30 nl of AAV8.CAG.Flex.GFP virus (gift from Dr. Ed Boyden, UNC Vector Core) to the HDB or VP/SI into different ChAT-Cre mice (Table 2; exp. 4). **5)** To investigate the glutamatergic projections of the VP/SI, we injected 30 nl of AAV8.CAG.Flex.GFP virus to the VP/SI of VGLUT3-Cre mice (Table 2; exp. 5). Virus was injected with a Nanoject III Programmable Nanoliter Injector (Drummond Scientific). **6)** To investigate the dual projection of BF cholinergic cells to the BLA and mPFC, we injected 3x100 nl AAV5.Ef1a.DIO.eYFP to the mPFC unilaterally into ChAT-Cre mice. This approach allowed retrograde labeling of BF cholinergic neurons, expressing eYFP in their cell bodies as well as in their remote axons after 6-8 weeks. In these surgeries, the glass pipettes were used as in retrograde tracing, but instead of glycerol, mineral oil (Sigma-Aldrich) was filled to the pipettes first, followed by introducing the virus. Injection speed was set to 3 nl/s until a clear change in the meniscus (mineral oil–virus border) was observed, then speed was set to 1 nl/s. Once the injection was completed sutures were used for wound closure. In order to assure complete closure of the incision, minimal amounts of Vetbond were dropped in between sutures through a sterile syringe/needle. After 4-5 weeks following the surgery, animals were anaesthetized and perfused the same way as described for retrograde tracing. Following tissue processing, we compared the normalized axonal fluorescent intensity (utilizing NIS elements AR 5.3) - obtained by anterograde virus tracing (HDB, VP/SI) - within the BLA and mPFC.

Table 2. ***Tracing experiments***

Experiment	Animal	tracer/virus	volume	brain region	type	coordinates (AP/ML/DV mm)
1)	C57Bl6 wild type mice	CTB or FB	ionthophoretic	BA	retrograde	-1.5/3.2/-4.2
	C57Bl6 wild type mice	CTB or FG	ionthophoretic	LA	retrograde	-1.7/3.4/-3.6
	C57Bl6 wild type mice	CTB or FG	ionthophoretic	BMA	retrograde	-1.7/2.8/-4.6
2)	C57Bl6 wild type mice	CTB or FG	ionthophoretic	mPFC	retrograde	2.2, 1.9, 1.5/0.3/-1
3)	ChAT-Cre	AAV5.Ef1a.DIO.eYFP	100-100 nl	HDB + VP/SI	anterograde	**HDB** 0.5/0.7/-5.0 + **VP/SI** 0.5/1.5/-4.4
4)	ChAT-Cre	AAV8.CAG.Flex.GFP	30 nl	HDB	anterograde	0.5/0.7/-5.0
	ChAT-Cre	AAV8.CAG.Flex.GFP	30 nl	VP/SI	anterograde	0.5/1.5/-4.4
5)	VGLUT3-cre	AAV8.CAG.Flex.GFP	30 nl	VP/SI	anterograde	0.5/1.5/-4.4
6)	ChAT-Cre	AAV5.Ef1a.DIO.eYFP	3x100nl	mPFC	retrograde-anterograde	2.2, 1.9, 1.5/0.3/-1
7)	ChAT-Cre	3/3 AAV2/5.CAG.Flex.GcaMP6f	100 nl	HDB	fiber photometry	0.5/0.7/-5.0
	ChAT-Cre	3/3 AAV2/5.CAG.Flex.GcaMP6f	100 nl	VP/SI	fiber photometry	0.5/1.5/-4.4
8)	Nkx2.1-Cre x Rosa26-LSL-Flp	3/15 AAV5.EF1a.eYFP.fDIO	3*100 nl	M2	juxtacellular recording	2.0/2.5/-0.5

3.3 Preparation of optic fiber implants for fiber photometry.

For our fiber photometry measurements, we used optical fibers with a 400 µm diameter (Thorlabs), which were affixed to ceramic ferrules (Thorlabs) using adhesive (Loctite 405). The preparation of these optical fiber cannulas followed a detailed process: 1) a fiber stripping tool was employed to carefully remove the protective coating from the fiber, and 2) the fiber was then scratched at the desired length with a fiber optic scribe and subsequently broken. It was critical to ensure that the fiber break resulted in a flat, smooth glass surface. Once a sufficient number of fibers of the appropriate length were prepared, they were secured into the ceramic ferrules using Loctite 405 adhesive. In cases where the 400 µm tick fibers were cleanly broken, additional polishing was unnecessary. After the glue had fully dried, the fibers were ready for implantation.

3.4 Fiber photometry surgery.

The mouse was removed from its home cage and anesthetized using isoflurane. Once immobility was achieved and the breathing rate slowed, it was taken out of the chamber and secured in a stereotaxic apparatus using ear bars. Isoflurane delivery was maintained through a nose cone. The skin was cleaned with alternating applications of Betadine (or chlorhexidine) and alcohol (or saline). A circular area of skin, with a radius of 5-20 mm, was excised from the top of the skull using surgical forceps and scissors. The edges of the remaining skin were glued to the skull with veterinary tissue glue (3M Vetbond). The exposed skull was mechanically cleaned with a scalpel and disinfected with Betadine (Povidone-iodine). A dental bur was used to drill a small hole in the occipital region, where a 1 mm screw was inserted to stabilize the later cemented optic fiber. Another hole, with a diameter of 0.6-1 mm, was drilled above the target area for the insertion of a glass capillary containing viral vectors (AAV2/5.CAG.Flex.GcaMP6f; Table 2; exp. 7), followed by a mono fiber-optic cannula. The viral solution (200 nl total volume) was injected under pressure using a pneumatic microinjector (WPI, Nanoliter injector) over 5-10 minutes. After the injection, the needle/capillary was retracted, and the microinjector was replaced with a stereotaxic cannula holder (Doric Lenses Inc.) to position the fiber-optic cannula 200-300 µm above the injection site. Cement was applied while the cannula holder remained in place to ensure the cannula stayed positioned correctly. Once the cement hardened, the animal was removed from the stereotaxic frame and placed in a clean cage on a heating source for recovery.

3.5 Fiber photometry measurement.

In these experiments, we used ChAT-Cre mice, which were injected with AAV2/5.CAG.Flex.GcaMP6f (Table 2; exp. 7) into either the HDB or VP and implanted with an optical fiber positioned above these brain regions. The objective was to assess whether these BF nuclei activate in response to noxious stimuli. Following the recovery period, the mice were handled for three days to ensure they could be connected to the fiber photometry cable without the need for isoflurane anesthesia. On the experimental days, the mice were connected to the fiber photometry system (Doric Lenses Inc.) and placed into a shocking chamber. Each mice received seven 1-second long, 0.7 mA scrambled shocks, while neuronal activity was recorded using the Doric Neuroscience Studio software. This procedure was repeated over three consecutive days for each mouse. The resulting CSV files were then analyzed using custom scripts developed by Bálint Király. Mice were then perfused and fixed brain tissue were sectioned for anatomical inspection.

3.6 Tamoxifen treatment.

To investigate the *in vivo* activity of AACs in the cortex in response to noxious stimulation, it was first necessary to label these cells. However, a suitable reporter mouse line for selectively labeling AACs was not available at the time of experiments. Therefore, we utilized a tamoxifen-dependent induction of Cre expression followed by viral labeling. To achieve this, Nkx2.1-CreER mice were crossed with Rosa26-LSL-Flp mice, and neonatal mice (P0) received an intraperitoneal tamoxifen injection. Following administration, tamoxifen induces Cre recombinase expression specifically in Nkx2.1-positive cells, which excises the stop codon upstream of the FLP promoter. Consequently, only these cells are able to express the FLP-dependent AAV5.EF1a.eYFP.fDIO virus (Table 2; exp. 8) (Taniguchi et al., 2013).

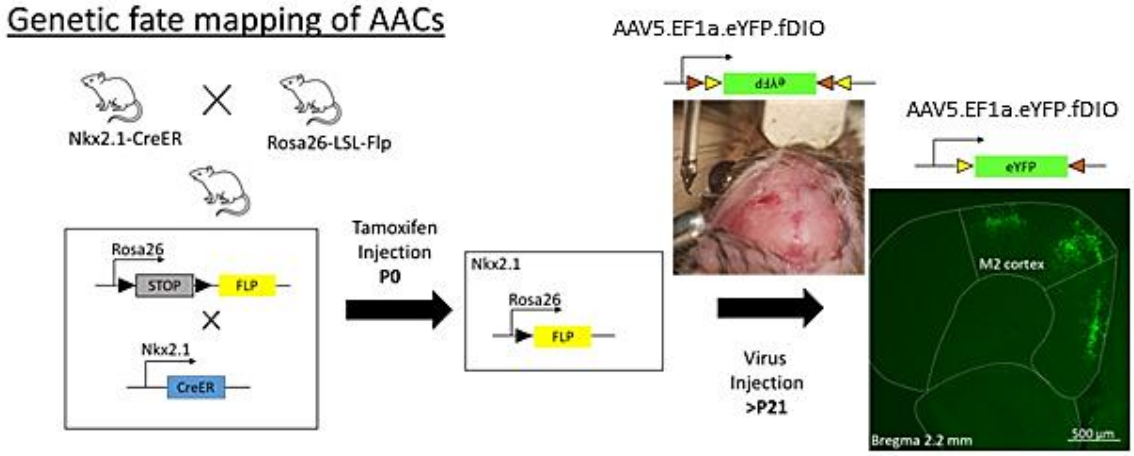

Figure 4. ***Visualizing AACs in frontal cortices.***
Schematic representation of the genetic strategy used to target axo-axonic cells (AACs). ***Left:*** *Breeding strategy utilizing* ***Nkx2.1-CreER*** *and* ***Rosa26-LSL-Flp*** *mice. Tamoxifen injection at postnatal day 0 (P0) activates Cre recombinase expression in Nkx2.1-expressing cells, the precursors of AACs. This leads to the removal of the stop codon upstream of the FLP gene, enabling the labeling of AACs using FLP-dependent viral vectors at a later time point (****Taniguchi et al., 2013****).* ***Middle:*** *The experimental workflow illustrates a surgical procedure using an "L" pipette for side-angle injection of the AAV5.EF1a.eYFP.fDIO virus into the M2 cortex at postnatal day 21 (P21) or later. This approach enables the selective labeling of AACs within the targeted cortical region.* ***Right:*** *A confocal image illustrates eYFP expression in AACs in the M2 cortex.*

3.7 Virus tracing for *in vivo* measurements.

Injecting a virus into a specific area (M2), where *in vivo* visually guided juxtacellular recordings were planned to be performed, presents several challenges. Drilling the skull above the target area during virus injection is not feasible, as it would damage the dura and surface veins, making later two-photon targeted electrophysiological recordings impossible. To overcome this potential constrain, we needed a method that allowed us to inject the virus into the M2 cortex without the vertical approach. We achieved this by using glass pipettes bent into an "L" shape. First, we pulled the glass pipettes, then with a heat source, we heated the base of the taper of the capillary to its melting point and carefully bent it at a 90-degree angle. The resulting L-shaped pipette maintains the same flow capacity as a standard pipette while enabling access to the M2 cortex from the side of the skull, preserving the integrity of the skull above the M2 cortex. Using a dental bur a hole was drilled at the most lateral part of the skull 2 mm anterior from bregma, where the “L” shaped glass capillary containing the viral vector was inserted (Table 2; exp. 8, Figure 4). The vectors or buffer containing the tracer molecules (300-400 nl/total volume) were injected under pressure using a pneumatic microinjector (WPI, Nanoliter injector), injection time 5-10 minutes. After 4-5 weeks following the viral injection, animals are

ready for *in vivo* surgery.

3.8 Aseptic surgery.

The mouse was removed from its home cage and anesthetized using isoflurane. Once immobility was achieved and respiration frequency began to decrease, it was taken out of the chamber and secured in a stereotaxic apparatus using ear bars, while isoflurane delivery was maintained through a nose cone. The skin was prepared by alternating applications of Betadine or chlorhexidine with alcohol or saline. A circular section of skin, with a radius of 5-20 mm, was excised from the top of the skull using surgical forceps and scissors. The edges of the remaining skin were glued to the skull bones with veterinary tissue glue (3M Vetbond). The exposed skull was then mechanically cleaned with a scalpel and disinfected with Betadine (Povidone-iodine). Two, or at most three, holes (~0.7 mm) were drilled into the skull bones—one in the frontal part and one (or two) in the occipital part. Small screws (1 mm) were inserted into these holes to support headplate stability. Following screw placement, the skull was coated with a thin layer of cyanoacrylate glue (e.g., Loctite 401). This step served two purposes: (a) to stabilize the skull bones relative to each other, preventing movement when the mouse initiated motion, and (b) to preserve a clear, transparent skull, allowing for the avoidance of thick veins beneath it.

Before visually guided juxtacellular recording, a small (~1-2 mm^2) cranial window was created on the skull above the M2 cortex using a precision drill (Foredom), and the bone within the window was removed. A small drop of liquid agar solution (Agarose High EEO, 45°C) was applied to the window and partially covered with a small piece of glass coverslip, ensuring that two-thirds of the cranial window was covered, while the uncovered portion allowed access to the brain tissue with a recording pipette. The glass coverslip was then glued to the skull. To prevent desiccation of the window, the chamber on the animal's head was filled with Ringer's solution or saline.

Before silicone probe recordings, the cranial window was drilled on the lateral side of the skull, and the silicone probe was inserted horizontally (Fig. 23A) in the M2 cortex to minimize cortical extrusion around the probe.

The surgical procedure lasted 30-60 minutes. After surgery, isoflurane anesthesia was replaced by an intraperitoneal urethane injection (dose: 650 mg/kg). The mouse was then positioned under the objective of a two-photon microscope, and *in vivo* neuronal and

population activity was recorded (Spike2 software) in the anesthetized mice. After a recording session lasting for 60-180 minutes, the mouse was over-anesthetized using isoflurane, decapitated, and the extracted brain was post-fixed with 4% paraformaldehyde.

3.9 Preparation of pipette for *in vivo* juxtacellular recording.

Pulling a pipette for *in vivo* visually guided juxtacellular recordings presents several challenges. First, the pipette must be robust enough to navigate in three dimensions through agarose gel and live brain tissue to target fluorescent cells. Second, it must have the appropriate physical properties for extracellular spike detection, requiring a resistance of 10-15 MΩ. Achieving these specifications required an iterative, experimental approach. Using a pipette puller (Sutter Instruments, Model P-1000), we systematically adjusted the pulling steps and parameters until the desired pipette was produced. The final protocol consisted of three steps: the first two were crucial for setting the taper's length and strength, while the third step defined the tip diameter (aprox. 1 µm).

3.10 *In vivo* measurement.

After the animal has gone through the preparation for *in vivo* juxtacellular recordings ("Aseptic surgery"), then the mouse was placed under the two-photon microscope in a stereotaxic frame (Thorlabs; Fig. 5A-B). Electrical stimuli for noxious stimulation (1 mA, 2 ms) were administered through two wires positioned 1 cm apart, attached to the left hind paw. Stimulus timing was managed using Spike2 software, delivering a single pulse every 30 seconds for a total of 20 repetitions. Pipettes were filled with a 3–4% Neurobiotin solution in 0.5 M NaCl, combined with either Alexa-594 or Alexa-488 for visualization under the microscope (Fig. 5C1-2), and were maneuvered using Luigs-Neumann micromanipulators. A grounding electrode was placed in the saline solution surrounding the craniotomy chamber to minimize recording noise. A 4x magnification objective guided the glass pipette into the brain, after which it was swapped for a 20x objective to achieve higher resolution. Spike detection was accomplished by targeting fluorescent cells with the pipette. To avoid tissue damage during lateral and dorso-ventral pipette movements, the pipette was retracted from the brain into the agar. Only minor adjustments—on the scale of a few micrometers—were made within the brain tissue to precisely target the cells. Once spikes were detected, cell recording began using Spike2

software. After a 3-minute baseline recording, electrical stimulation was applied, consisting of 20 shocks over 10 minutes (0.7–1 mA; Fig. 5D). Following the recordings, cells were loaded with 3–4% Neurobiotin by applying incremental current pulses until membrane rupture allowed diffusion of Neurobiotin (Fig 5E). This process was repeated for 3–4 cells per animal. After measurement and filling, the positions of recorded cells were noted for future anatomical identification (Fig 5F).

After the animal underwent preparation for silicone probe recordings, its head was secured with a headplate in a stereotaxic frame (Luigs and Neumann), enabling electrical stimulation of the tail, using the same protocol as in juxtacellular recording. A wire inserted into the temporal bone served as a reference electrode. Extracellular activity in the M2 cortex (N=5 animals) was recorded using 64-channel silicon probes (ASSY-77 H10, Cambridge Neurotech) stained with fluorescent DiI. Wideband neural signals (0.1–7.500 Hz) were amplified (gain: 192×) and digitized at 30 kHz (Intan Technologies). Spike detection and automatic clustering were performed using Kilosort 2.5 (https://github.com/MouseLand/Kilosort/releases/tag/v2.5.2), with manual refinement of cell grouping conducted in Phy2 (https://github.com/cortex-lab/phy).

3.11 Immunostaining.

Fixed brain sections were washed 3 times for 10 minutes in 0.1M PB, then a blocking solution (10% NDS, Normal Donkey Serum, 0.5% Triton-x 100 (10%), 0.1M PB) was applied for 30 minutes. The sections were incubated in a solution containing primary antibodies (Table 3) in addition to 2% NDS, 0.5% Triton-x 100 and 0.1M sodium azide dissolved in 0.1M PB for 1 day at room temperature, followed by 2 hours of incubation in the secondary antibody containing solution (1% NDS, 0.1M PB). The applied primary antibodies are detailed in Table 3 grouped and numbered by the experiments: for the retrograde tracing combined with ChAT immunostaining (1); for the visualization of GFP containing axons (3); for the quantification of different neurochemicals markers (ChAT/VAChT, VGLUT3, VGAT) in the amygdala (2,4); and for the identification of specific *in vivo* measured interneurons: NGFCs (5); PVBCs (6); AACs (7); CCKCB1BCs (8); VIP ISIs (9). After the incubations, the sections were rinsed in 0.1M PB, and mounted on slides in Vectashield (Vector Laboratories).

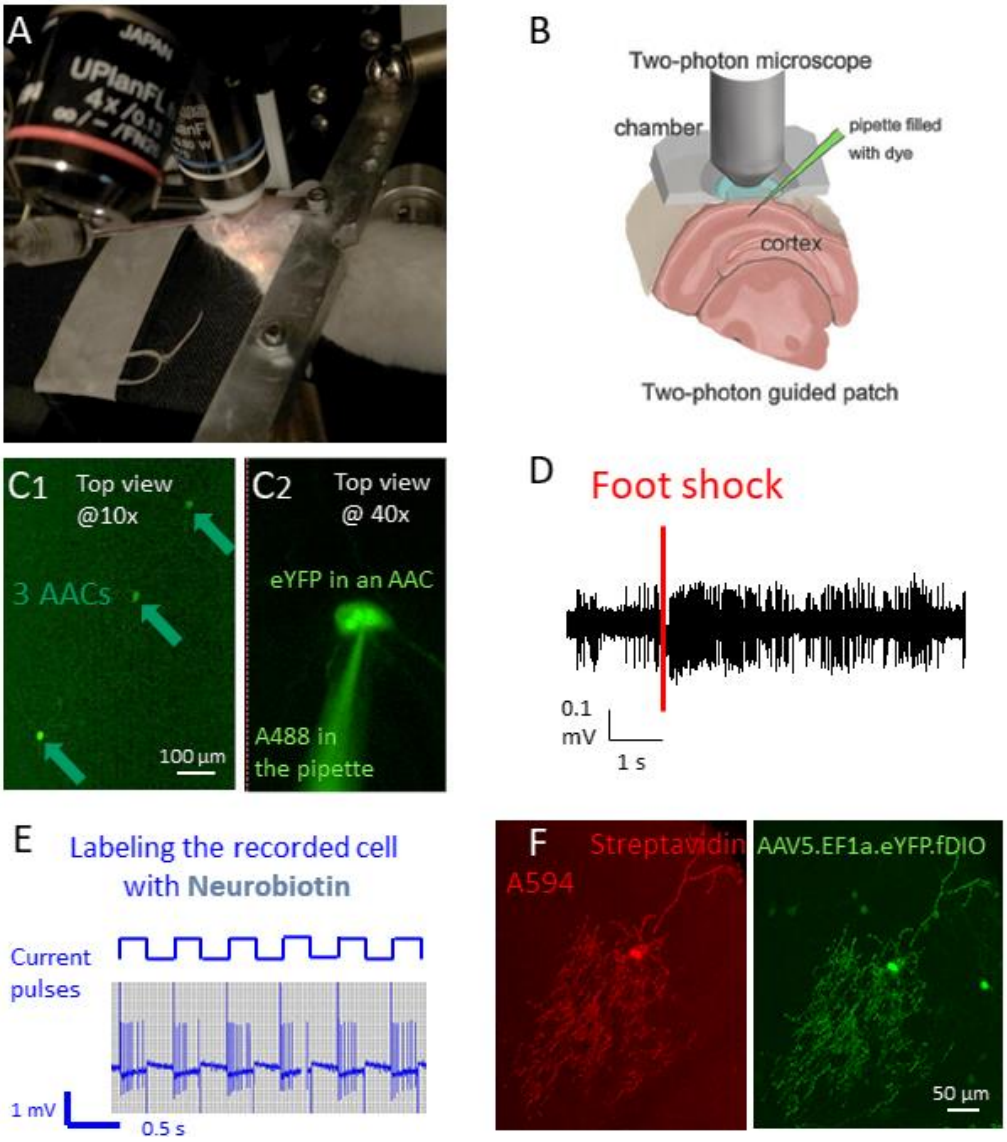

Figure 5. ***In Vivo Visually Guided Juxtacellular Recordings.***
(A-B) Real and schematic representation of the experimental workflow. Mice were anesthetized with urethane and fixed under a two-photon microscope using an implanted metal bar. A glass pipette was carefully inserted into the brain through a pre-prepared craniotomy.
(C1) Target cells were visually identified, and (C2) the pipette was precisely navigated to juxtacellular position. Magnification was achieved using a 16x optical zoom, with additional enhancement provided by digital zoom.
(D) Example trace showing the response of an AAC to noxious stimuli, with the red line indicating the onset of foot shock.
(E) Process of labeling recorded neurons with Neurobiotin. Positive current pulses were applied in increasing magnitude, ranging from 1 nA to 9 nA, until rhythmic firing was observed, confirming successful diffusion of Neurobiotin through the membrane into the cell.
(F) Left: Streptavidin staining of the recorded and labeled neurons. Right: Fluorescent viral labeling of the recorded AAC.

Table 3. ***Immunostaining used in the experiments.***

immuno #	primary ab	provider	catalog #	concentration	Secondary Ab	provider	concentration
1/Retrograde tracing	Guinea pig anti-FG	Protos Biotech	NM-101 FluGgp	1:5000	A488 DAGp or Cy3 DAGp	Jackson ImmunoResearch	1:500
	Goat anti-CTB	List Biological Laboratory	703	1:20 000	Cy3 DAG	Jackson ImmunoResearch	1:500
2/ ChAT immuno	Rabbit anti-ChAT	SYSY	297013	1:5000	A647 or Cy3 DAR	Jackson ImmunoResearch	1:500
3/ GFP staining	Goat anti-GFP	Frontier Institute Co. Ltd	GFP-Go-Af1480	1:1000	A488 DAG	Jackson ImmunoResearch	1:500
4/ Amygdala neurochemical	Rabbit anti-ChAT	SYSY	297013	1:5000	A488 DAR	Jackson ImmunoResearch	1:500
content	Rabbit anti-VAChT	Frontier Institute Co. Ltd	VAChT-Rb-Af1000	1:1000	A488 DAR	Jackson ImmunoResearch	1:500
	Goat anti-VGLUT3	Frontier Institute Co. Ltd	VGLuT3-Go-Af870	1:1000	Cy3 DAG	Jackson ImmunoResearch	1:500
	Guinea pig anti-VGAT	Frontier Institute Co. Ltd	VGAT-GP-Af1000	1:1000	Cy5 DAGp	Jackson ImmunoResearch	1:500
5/ NGFCs	Streptavidin	Invitrogen (ThermoFisher)	434315	1:5000	Cy3		
6/ PVBCs	Streptavidin	Invitrogen (ThermoFisher)	434315	1:5000	Cy3		
	Mouse anti-Kv2.1	neuromab	75-014	1:1000	A647 DAM	Jackson ImmunoResearch	1:500
7/ AACs	Streptavidin	Invitrogen (ThermoFisher)	434315	1:5000	Cy3		
8/ CCKCB1BCs	Streptavidin	Invitrogen (ThermoFisher)	434315	1:5000	Cy3		
	Goat anti-CB1	Frontier Institute Co. Ltd	CB1-Go-Af450	1:5000	A647 DAM	Jackson ImmunoResearch	1:500
9/ VIP ISIs	Rabbit anti-VIP	ImmunoStar	20077	1:2000	A647 DAR	Jackson ImmunoResearch	1:500
	Streptavidin	Invitrogen (ThermoFisher)	434315	1:5000	Cy3		

3.12 Confocal microscopy.

Multicolor large images from different brain regions and filled neurons were taken with a C2 confocal laser scanning microscope (Nikon Europe, Amsterdam, The Netherlands) using 10x (Plan Fluor 10x, N.A. 0.3, xy: 1.25 µm/pixel) and 20x objectives (CFI Super Plan Fluor 20X, N.A. 0.45, xy: 0.58 µm/pixel). Multichannel images at a high resolution were acquired in channel series mode. This way quantitative analysis and localization maps of retrogradely labeled BF cells could be performed on the same images. To quantify the neurochemical content of retrogradely labeled BF neurons, the NIS-Elements software was used. Then, large images were exported to Neurolucida software (10.53 software, MBF Bioscience), where the position of retrogradely labeled neurons as well as the brain structures and landmarks (ventral border of the slice, anterior commissure, midline) were indicated. This process was repeated at multiple coronal planes of the BF (0.62, 0.14, and -0.34 mm from bregma) in all injected animals. The drawings from the corresponding coronal planes were aligned and mapped onto the appropriate coronal section taken from the mouse brain atlas (Paxinos et al., 2004) using Adobe Photoshop (version 3.0, Adobe Inc.).

To reveal the neurochemical content of axon terminals in the amygdala region, confocal images were taken from each nuclei/subnuclei using a C2 microscope with a 60x objective (CFI Plan Apo VC60X Oil objective, N.A. 1.40; z (n=50) step size: 0.13 µm, xy: 0.08 µm/pixel). High resolution fluorescent images (2048x2048 pixel) from the injection sites in the HDB and VP/SI as well as amygdala region were taken using a 4x objective (C2 confocal laser scanning microscope, Plan Fluor 4x, N.A 0.13, xy: 1.54 µm/pixel). To quantify the VGAT content of BF cholinergic neurons, images were

acquired in the HDB and VP/SI with a C2 confocal laser scanning microscope using a 10x objective (Plan Fluor 10x, N.A. 0.3, z (n=10) step size: 25.88 μm, xy: 1.25 μm/pixel).

3.13 Axon arborization and injection parameter maps.

To determine the proportion of the labeled axons in each amygdala nucleus and prefrontal cortical area, we used two methods: 1) for Figures 9, 11, 12, 18 we imported the confocal images into the Adobe Photoshop, quantified the pixels representing axons in the region of interest and compared it to the total number of pixels from the axonal arborization within the amygdala or prefrontal cortical regions. 2) For Figures 6 and 10, we quantified the normalized fluorescence intensity using NIS-Elements software by dividing the mean fluorescence intensity (MFI) of each region of interest (ROI) by the MFI of the darkest ROI within the same sample. To determine the borders of the amygdala nuclei based on soma distributions, we mapped the amygdala region at the coronal plains using NeuN staining (1:1000, Millipore) or we used reconstructed maps from the mouse brain atlas. In the case of the PFC, we only used edited pictures from the mouse brain atlas. All maps containing injection location and spread were made based on the mouse brain atlas (Paxinos et al., 2004). Data are presented as mean ± SD.

3.14 Pavlovian fear conditioning and analysis.

Cue-dependent fear conditioning consisted of a chamber with black dotted white background, slightly curved walls, metal rod floor, white illumination and was cleaned with 70% ethanol (context A). First, mice were allowed to habituate to this context for 5 min at Zeitgeber time (ZT) 2–3 h, then returned to their home cage. After 1 h, mice were transferred back to context A, where, after a 120 s-long acclimation period, three different protocols were used. (1) only CS group (n = 14): CS (7.5 kHz sound for 20 s) was presented 7 times without US (with 110 ± 23 s intervals; mean ± SD); (2) unsigned US group (n = 12): 7 CS and 7 US (mild electrical shocks, 2 mA for 1 s) were presented randomly [with 111 ± 21 s intervals for CS and 110 ± 33 s intervals for US (mean ± SD)]; (3) signed US group (n = 13): 20 s-long CS presentations were co-terminated with the 1 s-long US, pairs repeated 7 times at random intervals (110 ± 23 s; mean ± SD). On the next day at ZT 1–2 h, for testing cued fear expression, after a 120 s-long acclimation, mice were subjected to a 20 s-long CS in a novel context (context B: square chamber with white background, paper floor, red illumination, cleaned with 1% acetic acid). Freezing

(as an index of fear) was post hoc measured manually on video recordings with an in-house software (H 77, courtesy of Prof. József Haller, Institute of Experimental Medicine, Budapest, Hungary) by trained observers blind to the animal treatment. Freezing was defined as no visible movement of the body except that required for respiration. Freezing levels are expressed as a percentage (duration of freezing within the CS/total time of the CS or duration of freezing during baseline/total time of the baseline, respectively). The methods applied here are identical to those described in Veres et al. (2023).

3.15 Statistical analysis

To assess the difference in freezing levels during the fear condition (Fig. 21B), we employed Kruskal–Wallis ANOVA (K-W ANOVA) with a post hoc Dunn's test, as the data did not follow a normal distribution according to the Shapiro–Wilk test.

For comparing first spike latencies among Type 1 VIP/CCK ISIs, NPY/NGFCs, Type 2 PVBCs, and AACs (Fig. 26B), we randomly selected 100 first spike latencies from each group (due to high variance in the total number of first spikes) and applied Kruskal–Wallis ANOVA (K-W ANOVA) with a post hoc Dunn's test, given the non-normal distribution detected by the Shapiro–Wilk test.

To examine the effects of hexamethonium and NBQX on Type 1 VIP/CCK ISIs (Fig. 27D), we used the Mann–Whitney test, as the data did not meet normality assumptions. All statistical analyses were conducted using OriginPro 2021.

3.16 Personal contribution to the results

The *in vivo* silicone probe recordings and analyses in anesthetized mice (Fig. 23) were conducted by Daniel Magyar, while I prepared the corresponding figure.

Antero-retrograde viral labeling (Fig. 12) was performed by Zsofia Reeb, with the associated analysis and figure completed by me.

I was responsible for analyzing all fear conditioning behavioral experiments presented in Figure 21 (Veres et al., 2023).

Figure 20 was created by Orsolya Papp, while I conducted the corresponding cell counting.

Immunostaining on juxtacellularly recorded and filled interneurons (Figs 24-25) were done by Petra Nagy-Pal.

All remaining experiments, immunostaining, analyses, and figures were done by me.

4.Results

4.1 Cholinergic innervation of the amygdala region by two basal forebrain areas, the HDB and VP/SI.

First, we aimed to investigate the overall cholinergic innervation of the amygdala region given rise by the HDB and VP/SI. To this end, we injected a high volume of AAV5.Ef1a.DIO.eYFP, a Cre-dependent adeno-associated virus vector (AAV) into the HDB and VP/SI of ChAT-Cre mice (100-100 nl to each area, Fig. 6A, n=3, Fig. 7A). After analyzing the cholinergic projection patterns in multiple coronal planes within the amygdala region, we found that the BA received the strongest cholinergic innervation – based on normalized fluorescence intensity – from these two BF areas (Fig. 6B-C). Cholinergic innervation extended also to the BMA, the medial division of the CeM, the anterior- and posteromedial cortical amygdaloid nucleus (ACo, PMCo), the anterolateral portion of the amygdalohippocampal area (AHiAL), and the piriform cortex (Pir) with comparable innervation levels among them (Fig. 6B-C). Conversely, the anterior and posterior sections of the medial amygdala (MeA, MeP), the lateral nucleus of the LA, the lateral division of the central amygdala (CeL), and the posteromedial part of the amygdalohippocampal area (AHiPM) received only sparse cholinergic innervation (Fig. 6B-C). Taken together, these findings demonstrate that the amygdala region, particularly the BA and BMA, receives robust cholinergic innervation from the HDB and VP/SI.

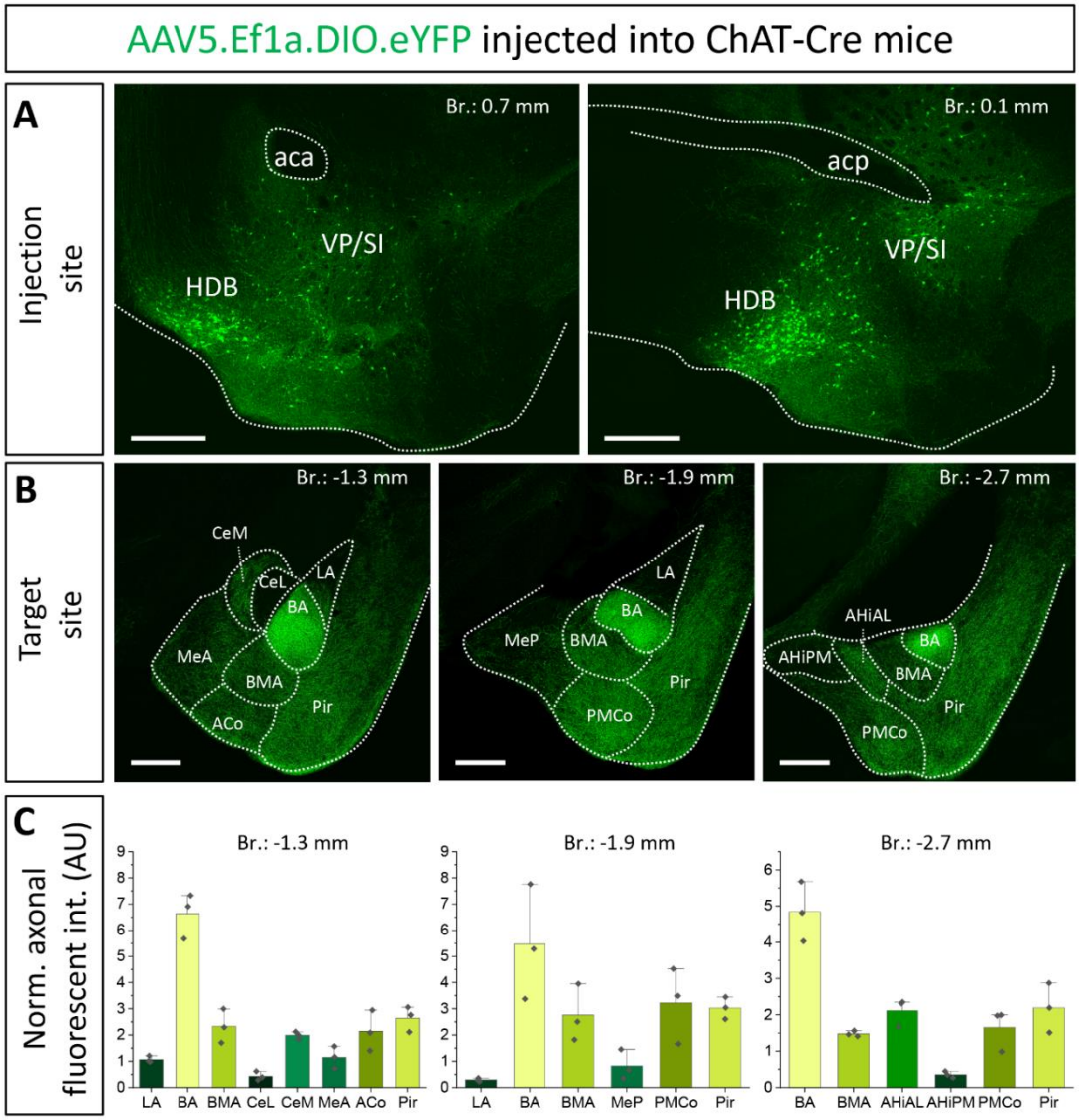

Figure 6. ***Cholinergic innervation of the amygdala region by two basal forebrain nuclei, the HDB and VP/SI.***
***(A**1, 2**)** Example injection sites in the HDB and VP/SI in ChAT-Cre mice, 100 nL of AAV5.Ef1a.DIO.eYFP was injected to each area. Scale bar: 500 μm. **(B**1–3**)** Coronal images taken at different amygdala planes showing distribution of cholinergic projections from the HDB and VP/SI. Scale bar: 500 μm. **(C)** Normalized axonal fluorescent intensity (AU) graph comparing the abundance of cholinergic innervation within the amygdala region originating from the HDB and VP/SI. Aca, anterior commissure, anterior part; ACo, anterior cortical amygdaloid nucleus; acp, anterior commissure, posterior part; AHiAL, amygdalohippocampal area, anterolateral part; AHiPM, amygdalohippocampal area, posteromedial part; BA, basal amygdala; BMA, basomedial amygdala; CeL, central amygdala, lateral division; CeM, central amygdala, medial division; HDB, nucleus of the horizontal limb of the diagonal band; LA, lateral amygdala; MeA, medial amygdala, anterior part; MeP, medial amygdala, posterior part; Pir, piriform cortex; PMCo, posteromedial cortical amygdaloid nucleus; SI, substantia innominata; VP, ventral pallidum.*

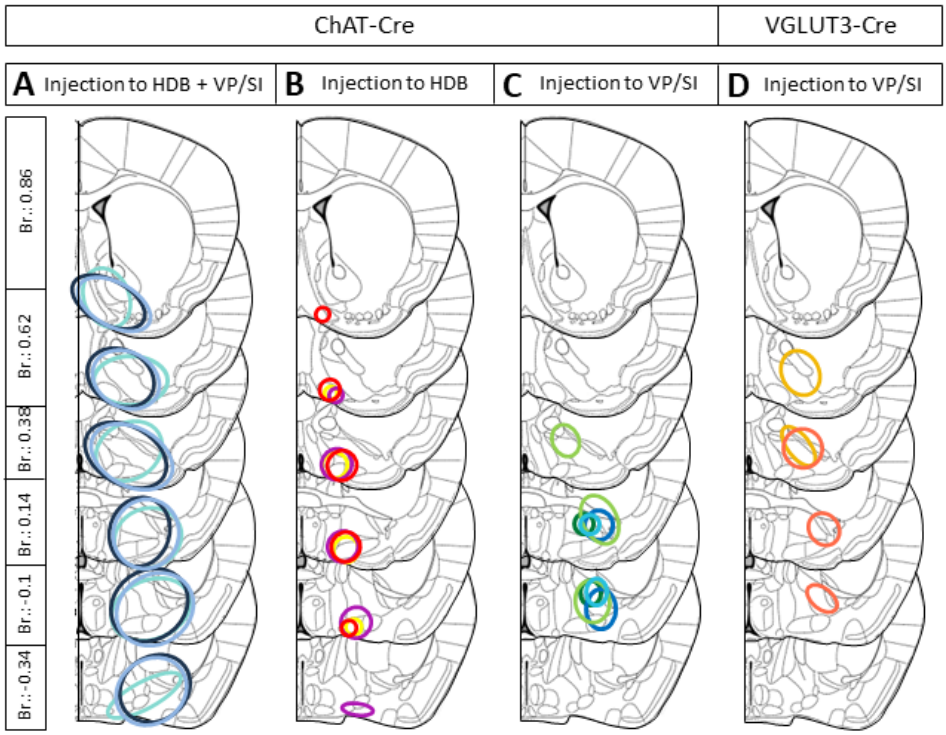

Figure 7. ***Reconstructed maps showing the localization and spread of virus injections used for BF anterograde labeling.***
(A) *Localization and spread of 100+100nl AAV5.Ef1a.DIO.eYFP virus injection to the HDB and VP/SI in ChAT-Cre mice (n = 3). Different colors represent different animals. These injections appertain to Figures 1, 4.* ***(B, C)*** *Localization and spread of 30nl AAV8.CAG.flex.GFP virus injected to the HDB (**B**, n = 3) or VP/SI (**C**, n = 4) in ChAT-Cre mice. Different colors represent different animals. These injections appertain to Figures 3, 5, and color codes are the same as in the corresponding figures.* ***(D)*** *Localization and spread of 30nl AAV8.CAG.flex.GFP virus in the VP/SI (n = 2) in VGLUT3-Cre mice. Different colors represent different animals.*

4.2 Localization of BLA-projecting cholinergic neurons shows separation within the BF.

To distinguish the sources of cholinergic innervation invading the BLA between the VP/SI and HDB, retrograde tracer Fast Blue (FB) or Cholera Toxin B subunit (CTB) was injected into the three distinct nuclei of the BLA: LA (Fig. 8A1, n=2), BA (Fig. 8A2, n=4) and BMA (Fig. 8A3, n=2). In coronal sections obtained from these injected mice, we determined the location of the somata of BLA-projecting neurons in the BF (Fig. 8B1). We found that BA-projecting BF neurons were located primarily in the VP/SI region (based on the mouse brain atlas (Paxinos et al., 2004)). In contrast, BMA-projecting BF neurons were found dominantly in the HDB (but also partially in the lateral preoptic area (LPO), median preoptic nucleus (MnPO), medial preoptic area (MPA)), forming a

separate neuronal population, the location of which overlapped minimally with BA-projecting BF neurons (Fig. 8C1-C3). Injecting a retrograde tracer into the LA resulted in only a small number of labeled neurons located in the HDB (Fig. 8C1), a finding consistent with the low number cholinergic fibers observed in anterograde tracing (Fig. 6B-C). After performing immunostaining against choline acetyltransferase (ChAT), the enzyme, responsible for the acetylcholine synthesis (Jope, 1979), we evaluated the cholinergic content of the amygdala-projecting BF neurons. We found that more than 60% of BA-projecting BF neurons were cholinergic (Fig. 8B1-3 130/212; n= 4 mice), while this ratio was around 25% (24/91; n= 2 mice) among BMA-projecting BF neurons. Altogether, these results show that neurons in the VP/SI preferentially innervate the BA, while those neurons located in the HDB project predominantly to the BMA and to a lesser extent to the LA. The difference in the ratio of BF cholinergic neurons innervating the distinct amygdala nuclei is in accord with our anterograde labeling, showing a more profound presence of cholinergic fibers in the BA in comparison with the surrounding areas (Fig. 6B-C).

4.3 Cholinergic cells from the HDB and VP/SI project to the amygdala region in a mutually exclusive manner.

To confirm that cholinergic neurons in separate BF regions innervate different amygdala nuclei, we injected a small amount (30 nl) of AAV8.CAG.Flex.GFP either into the HDB (Fig. 9A, n=3, Fig. 7B) or into the VP/SI (Fig. 9D, n=4, Fig. 7C) of ChAT-Cre mice. This approach enabled us to specifically investigate the cholinergic axonal projections originated from the HDB and VP/SI within the amygdala region. In line with our retrograde tracing data, we observed that ChAT+ neurons in the HDB projected mostly to the BMA and other surrounding areas, such as the MeA, ACo, dorsal endopiriform nucleus (DEn), Pir, but largely avoiding the BA (Fig. 9B, C, G). Although, there were some labeled axons in the LA, this connection appeared to be weak compared to other neighboring fields, an observation, which is in accord with the results shown in Fig. 6B-C, and Fig. 8C1. On the other hand, ChAT+ neurons in the VP/SI almost exclusively innervated the BA, with marginal projections into the CeM, BMA and Pir (Fig. 9E-G).

These results show that cholinergic fibers from the HDB and VP/SI parcel the amygdala region in a mutually exclusive manner.

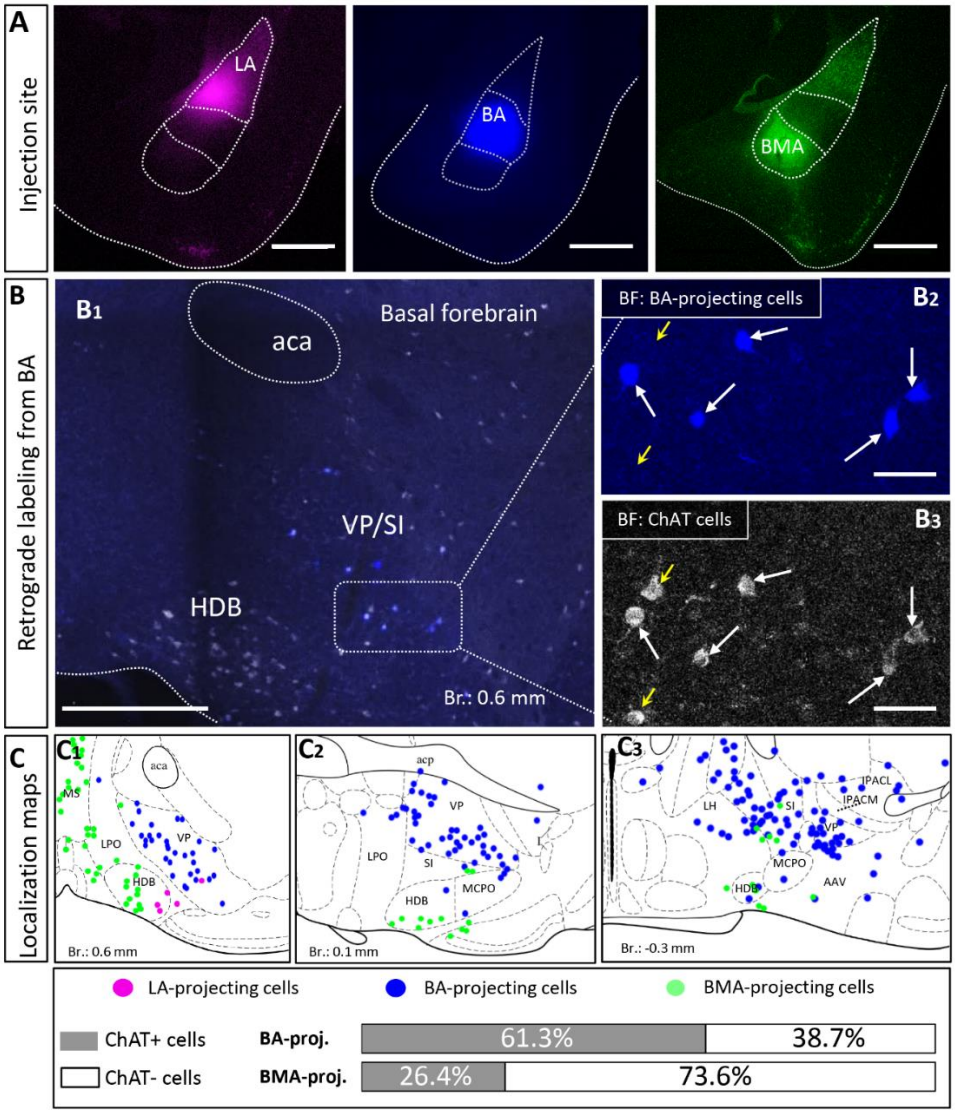

Figure 8. ***Distribution and cholinergic content of retrogradely labeled BLA-projecting BF neurons.*** ***(A)*** *Pseudo-colored images showing the injection sites in different BLA regions.* ***(A1)*** *lateral amygdala, (LA);* ***(A2)*** *basal amygdala, (BA);* ***(A3)*** *basomedial amygdala, (BMA). Scale bar: 500 μm.* ***(B1)*** *An example large image taken from the basal forebrain (Br.: 0.62 mm, BF) showing BA-projecting BF cells in blue, and ChAT-immunoreactive cells in white. Scale bar: 500 μm.* ***(B2, 3)*** *20x magnification images taken from the BF showing expression of ChAT (choline acetyltransferase,* ***B3****) in BA-projecting BF cells* ***(B2)****. Small yellow arrows indicate non-retrogradely labeled ChAT-expressing cells. Big white arrows indicate ChAT-positive BA-projecting cells. Scale bar: 50 μm.* ***(C1–3)*** *Positions of retrogradely labeled BLA-projecting BF neurons in different coronal planes of the BF. 61.3 ± 7.08% of BA-projecting BF cells expressed ChAT (130/212; n = 4 mice), while the presence of ChAT was observed in 26.37 ± 7.71% of BMA-projecting BF cells (24/91; n = 2 mice). Purple: LA-projecting cells, Blue: BA-projecting cells, Green: BMA-projecting cells. Aca, anterior commissure, anterior part; HDB, nucleus of the horizontal limb of the diagonal band; IPACL, interstitial nucleus of the posterior limb of the anterior commissure, lateral part; IPACM, interstitial nucleus of the posterior limb of the anterior commissure, medial part; LH, lateral hypothalamic area; LPO, lateral preoptic area; MCPO, magnocellular preoptic nucleus; MS, medial septal nucleus; SI, substantia innominata; VP, ventral pallidum.*

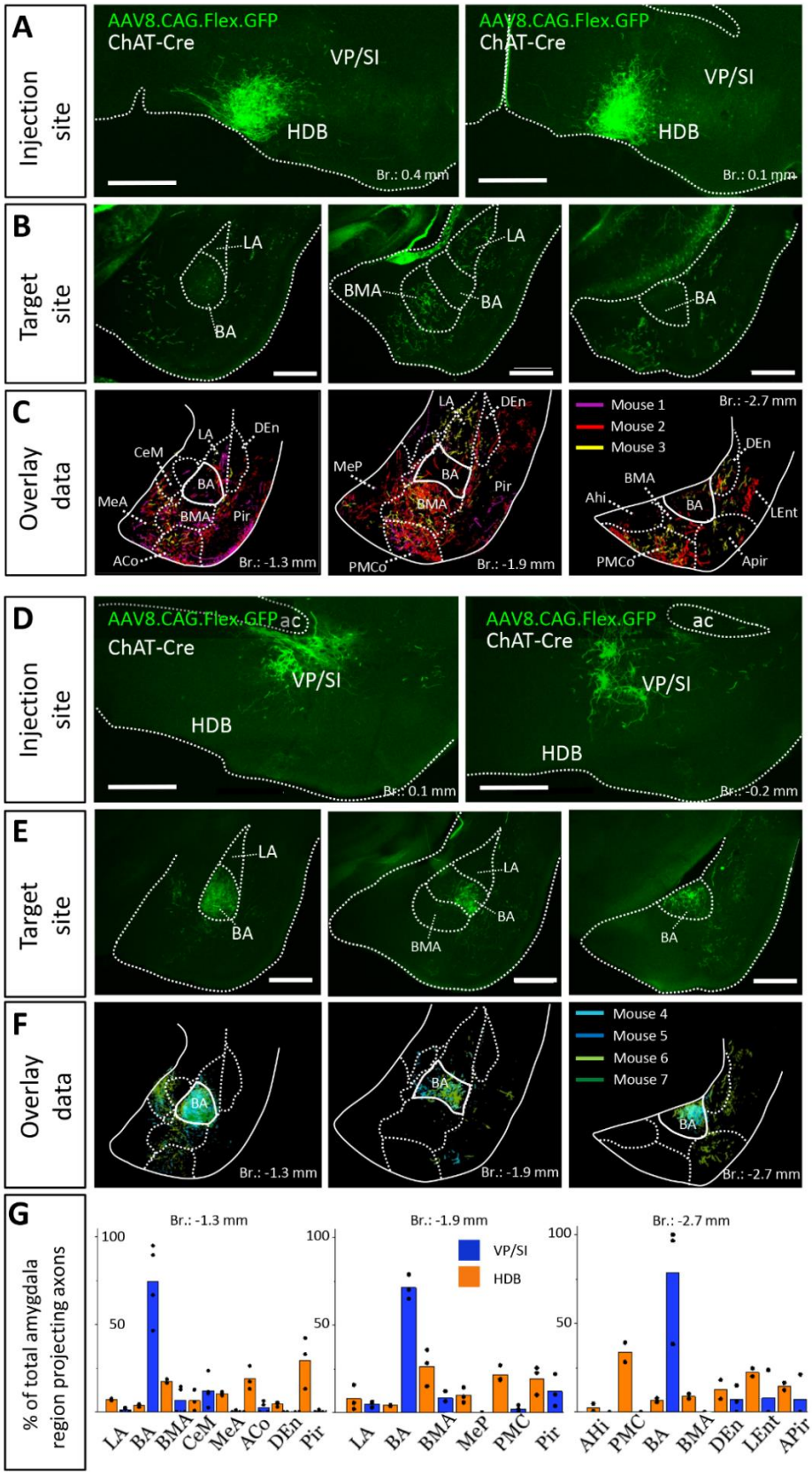

Figure 9. ***Distribution of anterogradely labeled cholinergic projections in the amygdala region from the HDB or VP/SI.***
(A) *Example injection sites in the HDB in ChAT-Cre mice. Small volume (30 nL) of AAV8.CAG.flex.GFP*

was injected to the target area. Scale bar: 500 μm. ***(B)*** *Coronal images taken at different amygdala planes showing cholinergic projections from the HDB. Scale bar: 500 μm.* ***(C)*** *Overlaid representative cholinergic projections from the HDB. Axons visualized in different animals (n = 3) are shown in different colors. Borders of distinct amygdala regions were drawn based on NeuN staining.* ***(D)*** *Example injection sites in the VP/SI in ChAT-Cre mice. 30 nL AAV8.CAG.flex. GFP was injected to the target area. Scale bar: 500 μm.* ***(E)*** *Coronal images taken at different amygdala planes showing cholinergic projections from the VP/SI. Scale bar: 500 μm.* ***(F)*** *Overlaid representative cholinergic projections from the VP/SI. Axons revealed in different animals (n = 4) are shown in distinct colors. The borders of distinct amygdala regions are drawn based on NeuN staining.* ***(G)*** *Percentage of amygdala region-projecting HDB or VP/SI cholinergic axons in each nucleus/region. ACo, anterior cortical amygdaloid nucleus; AHi, amygdalohippocampal area; APir, amygdalopiriform transition area; BA, basal amygdala; BMA, basomedial amygdala; CeM, central amygdala, medial division; DEn, dorsal endopiriform nucleus; LA, lateral amygdala; LEnt, lateral entorhinal cortex; MeA, medial amygdala, anterior part; Mep, medial amygdala, posterior part; Pir, piriform cortex; PMCo, posteromedial cortical amygdaloid nucleus.*

4.4 Cholinergic inputs from the HDB and VP/SI overlap in the mPFC, with VP/SI showing a preference for dorsal and HDB for ventral innervation of the PFC.

Previous studies uncovered that the mPFC and BLA are reciprocally interconnected cortical regions playing a role in similar cognitive processes (Arruda-Carvalho and Clem, 2015; Burgos-Robles et al., 2009; Herry et al., 2008; Little and Carter, 2013; Sotres-Bayon et al., 2012; Weiskrantz, 1956). Therefore, we analyzed the cholinergic projections from the HDB and VP/SI towards the PFC in the same mice as we did for the innervation of the amygdala region (Figs 6 and 9). Upon analyzing the cholinergic projection patterns towards the PFC (Fig. 10A, same injections as shown in Fig. 6), we observed that cholinergic fibers covered the cingulate cortex area 1 and 2 (Cg1, Cg2), as well as the PL and IL cortices and the medial orbital cortex (MO) in a similar manner (Fig. 10B-C). Additionally, these fibers exhibited a slightly weaker innervation to the secondary motor cortex (M2) (Fig. 10B-C).

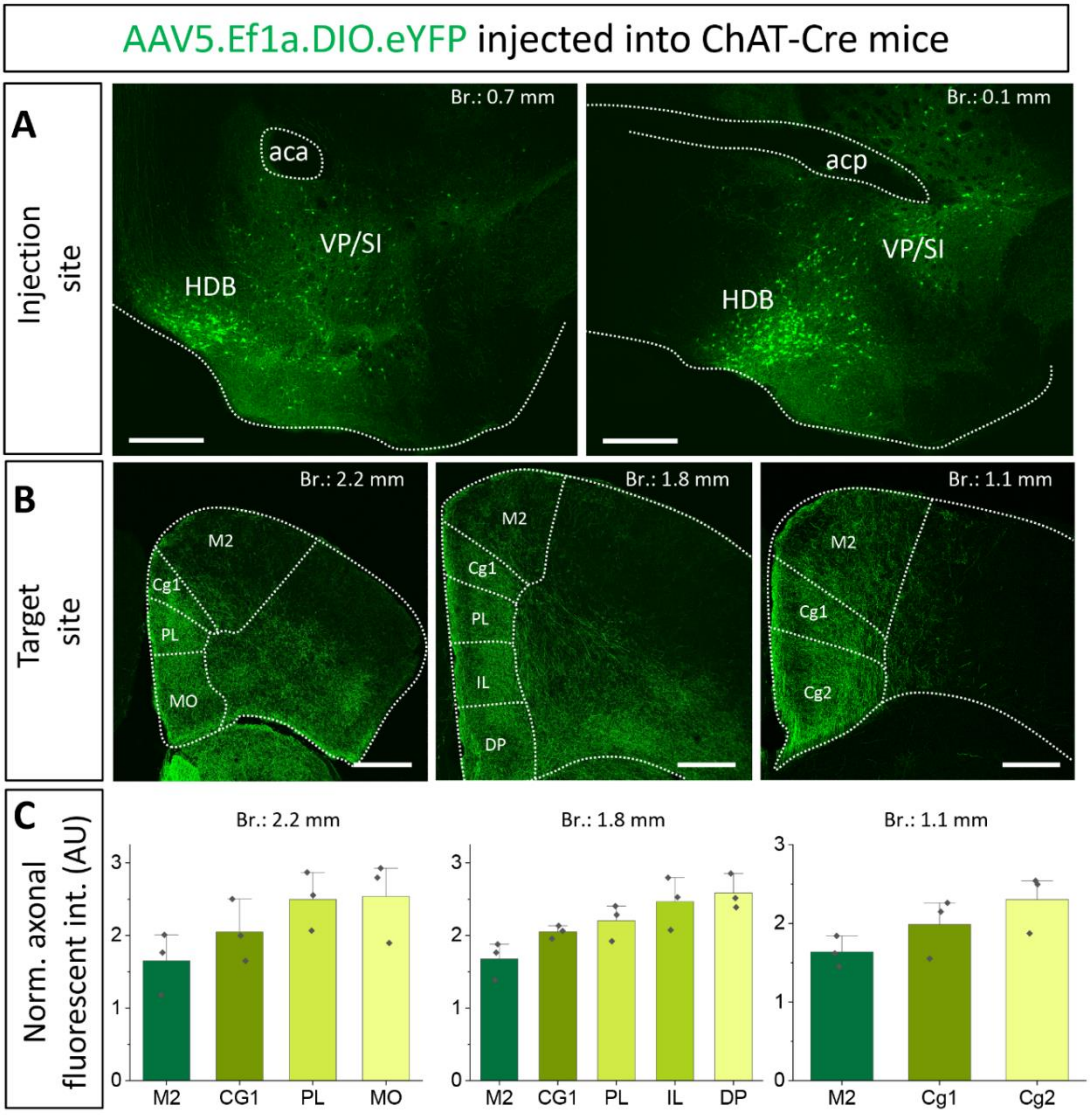

Figure 10. ***Cholinergic innervation of the prefrontal cortex by the HDB and VP/SI.***
***(A**1, 2) Example injection sites in the HDB and VP/SI in ChAT-Cre mice. Large volume (100 nL) of AAV5.Ef1a.DIO.eYFP was injected to each area. Scale bar: 500 μm. Same images as shown in Figure 1A.* ***(B**1–3) Coronal images taken at different prefrontal cortical planes showing cholinergic projections from the HDB and VP/SI. Scale bar: 500 μm.* ***(C)** Normalized axonal fluorescent intensity (AU) graph comparing the abundance of cholinergic innervation within the PFC region originating from the HDB an VP/SI. Aca, anterior commissure, anterior part; acp, anterior commissure, posterior part; Cg1, cingulate cortex, area 1; Cg2, cingulate cortex, area 2; DP, dorsal peduncular cortex; IL, infralimbic cortex; LO, lateral orbital cortex; M1, primary motor cortex; M2, secondary motor cortex; MO, medial orbital cortex; PL, prelimbic cortex; VO, ventral orbital cortex.*

Based on small injections targeted separately into the HDB or VP/SI (injections shown in Fig. 9), we found that both BF areas projected to the mPFC, namely the ACC/Cg1, PL and IL cortices. However, the HDB tended to project to the vPFC, including the MO, lateral orbital cortex (LO), ventral orbital cortex (VO), dorsal peduncular cortex (DP), Cg2 (Fig. 11A, B, E), while the VP/SI innervated the dPFC (including the M2, Cg1 and PL; Fig. 11C-E). The most conspicuous differences were found at the level of 2.4 mm

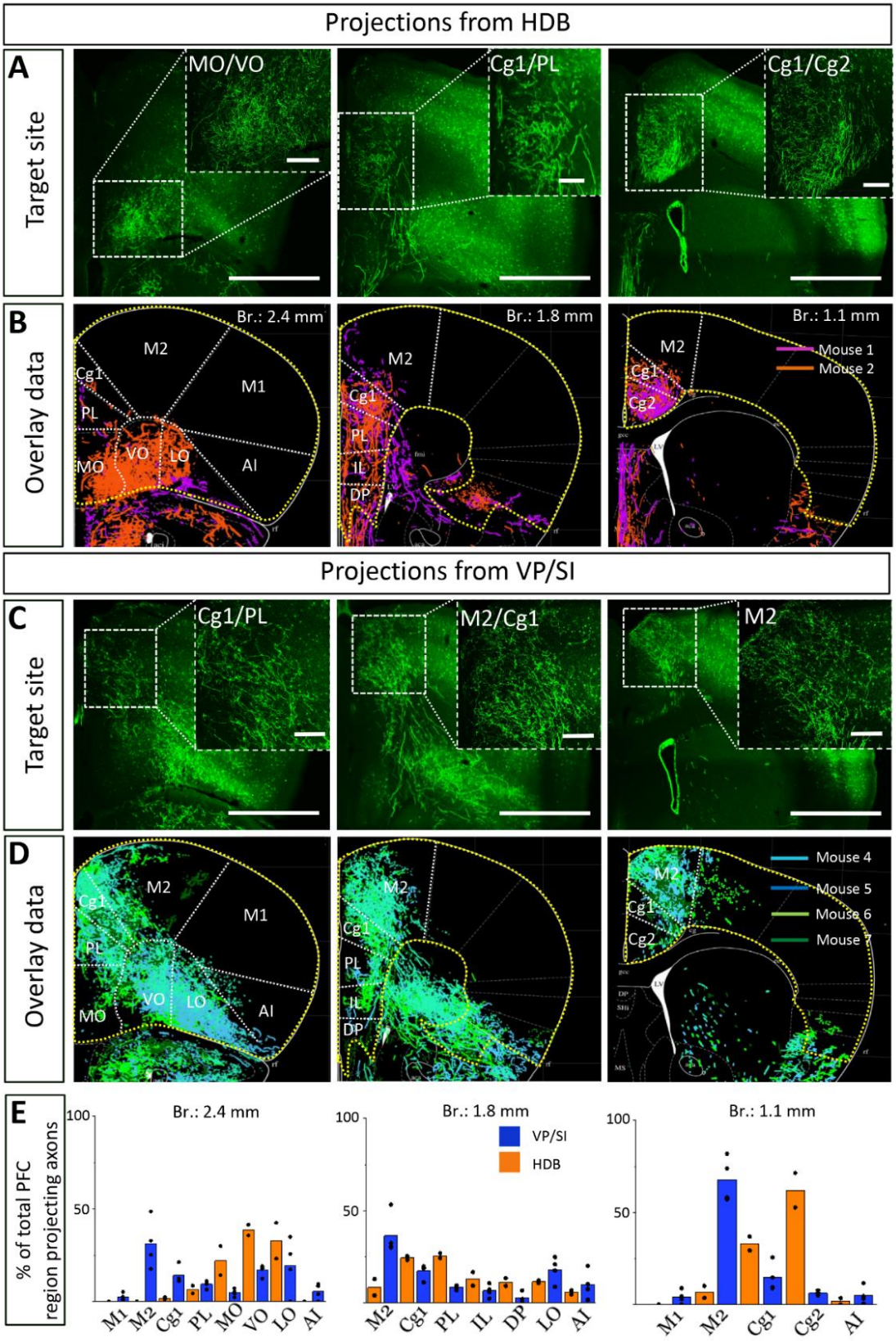

Figure 11. ***Cholinergic afferents from the HDB and VP/SI highly overlap in the mPFC but show separation in the dorsal and ventral parts of the PFC.***
(A, C) *Images taken at different prefrontal cortical planes showing cholinergic projections from the HDB*

*(**A**) and VP/SI (**C**) (injection sites presented in Figure 3). Scale bar: 1000 μm. (**B, D**) Overlaid representative cholinergic projections from the HDB (**B**) or VP/SI (**D**). Axons represented in different colors were obtained from different animals (n = 2–4). Maps of the PFC were modified from the mouse brain atlas (Paxinos and Franklin, 2004). (**E**) Percentage of PFC-projecting cholinergic axons in each cortical region from the HDB or VP/SI. AI, agranular insular cortex; Cg1, cingulate cortex, area 1; Cg2, cingulate cortex, area 2; DP, dorsal peduncular cortex; IL, infralimbic cortex; LO, lateral orbital cortex; M1, primary motor cortex; M2, secondary motor cortex; MO, medial orbital cortex; PFC, prefrontal cortex; PL, prelimbic cortex; VO, ventral orbital cortex.*

from the bregma, where the HDB predominantly innervated the MO, while the VP/SI had prominent projections to the PL, Cg1 and M2 (Fig. 11B, D). At the bregma level of 1.1 mm, there was a similar exclusive projection pattern: cholinergic cells in the HDB innervated the Cg2, but not the M2, while cholinergic cells in the VP/SI gave rise to projections to the M2, but not to the Cg2 (Fig. 11B, D). Altogether, these results show that cholinergic innervation originated from the HDB and VP/SI terminates in the differential parts of the PFC and amygdala regions. Namely, ChAT+ neurons in the HDB send axons to the vPFC and mPFC as well as to the most amygdala areas, apart from the BA, while ChAT+ neurons in the VP/SI prefer to terminate in the dPFC, mPFC and BA.

4.5 Significant portion of BF cholinergic neurons exhibit dual projections to both the mPFC and BLA.

The next question we asked was whether the same BF neurons send axonal collaterals into the mPFC and BLA, or separate populations of neurons innervate these two brain structures. To reveal the logic underlying the cholinergic control of these regions, first we performed retrograde-anterograde virus tracing in ChAT-Cre mice by injecting AAV5.Ef1a.DIO.eYFP into the mPFC (Fig. 12B, n=5). This approach reveals whether neurons projecting to a given area have axonal collaterals in other brain regions, too. Thus, AAV injection into the mPFC may visualize axons in the BLA if a portion of BF cholinergic neurons simultaneously project to these regions. Our retrograde-anterograde virus tracing demonstrated the presence of ChAT+ neurons in the BF (Fig. 12C, Fig. 13) that innervate both the mPFC (Fig. 12B) and BLA (Fig. 12D-E). The somata of retrogradely labeled ChAT+ cells were found in both the HDB and VP/SI along the BF (Fig. 13), revealing the area where the dual projecting cholinergic neurons were located. Based on overlaid images (Fig 12E), extracted from 5 animals, we found that BA received

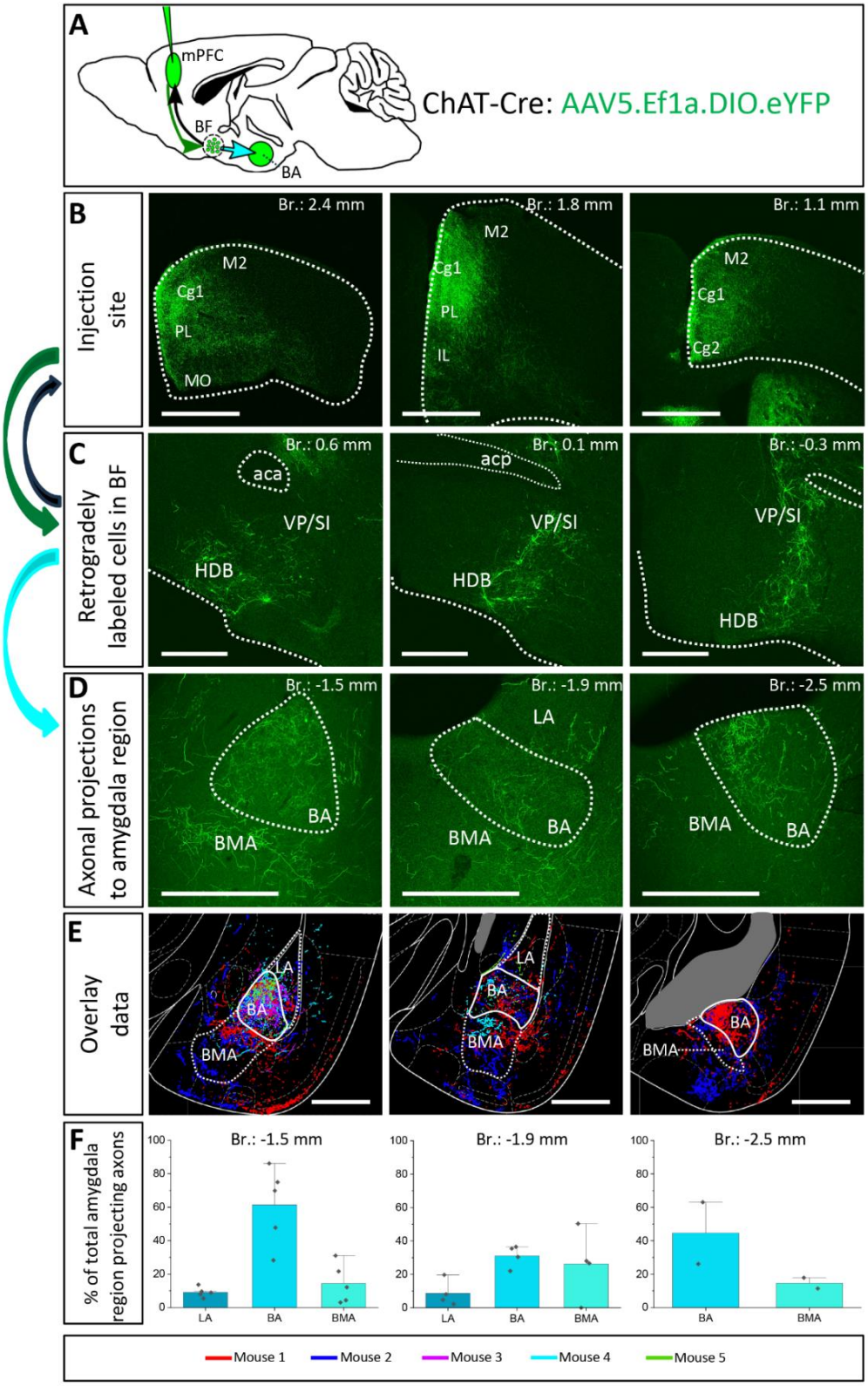

Figure 12. ***Retrograde-anterograde virus tracing demonstrates the presence of a cholinergic neuronal population with dual projection toward the mPFC and BLA.***
(A) *Schematic representation of retrograde-anterograde Cre-dependent axonal labeling. AAV5.Ef1a.DIO.eYFP was injected into the mPFC (3 × 100 nL) in ChAT-Cre mice (n = 5). Green arrow shows retrograde spread of the Cre-dependent virus retrogradely to BF cholinergic cells. Black arrow*

indicates anterograde labeling of axons toward the injection site. Cyan arrow shows anterograde labeling of axons toward the amygdala. ***(B)*** *Coronal images taken from the injection sites in the mPFC showing cholinergic fibers from retrogradely labeled cholinergic BF cells. Scale bar: 1000 μm.* ***(C)*** *Coronal images of retrogradely labeled cell bodies of processes of cholinergic neurons in the BF. Scale bar: 500 μm.* ***(D)*** *Fluorescent images of BLA-projecting axon collaterals in the BA of those BF cholinergic neurons, which also innervated the mPFC. Scale bar: 500 μm.* ***(E)*** *Overlaid representative axonal projections in the BLA originating from dual projecting cholinergic BF cells. Axons revealed in different animals (n = 5) are shown in distinct colors. Scale bar: 500 μm.* ***(F)*** *Percentage of BLA-projecting cholinergic axons in the BA, BMA and LA. BA, basal amygdala; BMA, basomedial amygdala; Cg1, cingulate cortex, area 1; Cg2, cingulate cortex, area 2; IL, infralimbic cortex; LA, lateral amygdala, M1, primary motor cortex; M2, secondary motor cortex; MO, medial orbital cortex; PL, prelimbic cortex; HDB, nucleus of the horizontal limb of the diagonal band; SI, substantia innominata; VP, ventral pallidum.*

a substantial cholinergic innervation from dual projecting neurons, with the strongest innervation found at the level of -1.5 mm from the bregma (Fig. 12E-F). BMA also received axon collaterals from the dual projection, while there were barely any fibers in the LA (Fig. 12E-F). Our results provide evidence that the mPFC-BLA circuit receives dual cholinergic innervation from both the HDB and VP/SI.

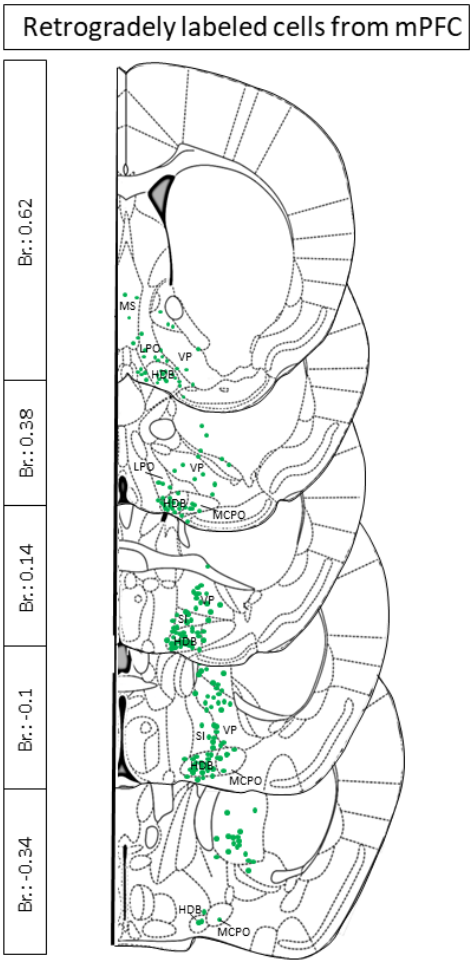

Figure 13. ***Localization of retrogradely labeled cholinergic BF neurons from retrograde- anterograde virus tracing.***

Green dots represent retrogradely labeled BF cholinergic neurons projecting to the mPFC. The area covered by greens dots defines the source of single and double- projecting cholinergic neurons in the BF. Aca, anterior commissure, anterior part; HDB, nucleus of the horizontal limb of the diagonal band; LPO, lateral preoptic area; MCPO, magnocellular preoptic nucleus; MS, medial septal nucleus; SI, substantia innominata; VP, ventral pallidum.

To further validate the observation that cholinergic neurons simultaneously innervate the mPFC and BLA, we injected different retrograde tracers (FG and FB) into the mPFC and BA (Fig. 14A-C, Fig. 15, n=3), areas receiving the strongest innervation from cholinergic cells with dual projections (Fig. 12). In line with our previous tracing results, retrogradely labeled neurons from the mPFC were located both in HDB and VP/SI (Fig. 14D-E1, E3), while BA-projecting cholinergic cells were mostly found in the VP/SI (Fig. 14D-E1, E3). Importantly, we identified a population of dual-projecting cells in the VP/SI (Fig. 14F), accounting for 30.07±12.5% (Fig. 14G, 109/355, n=3) of the retrogradely labeled cells, the vast majority of which (92.7%) was immunopositive for ChAT (Fig. 14E4, G, 101/355, n=3), leaving a small portion (2.2±1.2%, Fig. 14G, 8/355, n=3) of dual-projecting cells immunonegative for ChAT. These results confirm that BF cholinergic cells can regulate the interaction between the mPFC and BLA simultaneously and/or independently.

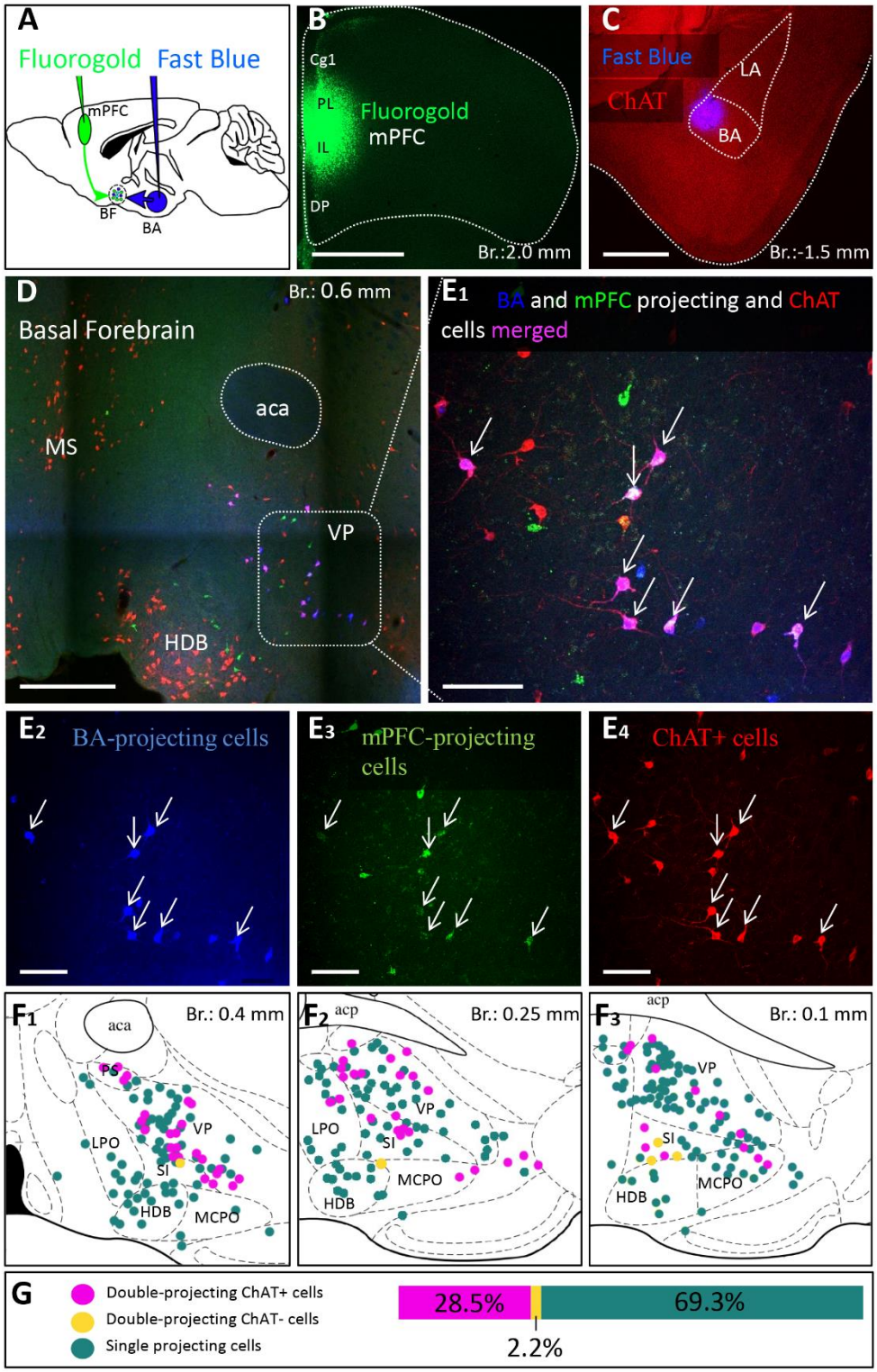

Figure 14. ***Double-retrograde labeling of BF neurons that project to the mPFC and BA.***
(A) *Experimental design: iontophoretic injection of Fluorogold into the mPFC and Fast Blue to the BA.* ***(B)*** *Example coronal image taken at the injection site in the mPFC showing Fluorogold labeling in the PL and IL regions. Scale bar: 1000 µm.* ***(C)*** *Example coronal image taken from the same animal showing the injection site of Fast Blue labeling in the BA. Scale bar: 500 µm.* ***(D,E1-4)*** *10x and 20x magnification coronal images at a BF plane showing BA-projecting* ***(E2)****, mPFC-projecting* ***(E3)*** *and ChAT-immunopositive* ***(E4)*** *cells in the VP/SI. White arrows indicate double-labeled cholinergic neurons. Scale bar:* ***(D)*** *500 µm, (E1-4) 100 µm.* ***(F1–3)*** *Localization of double-projecting cholinergic neurons shown in*

purple in different planes of the BF. ***(G)*** *Bar graph showing that 28.5 ± 12.48% (n = 3, 101/355) of retrogradely labeled neuros were double-projecting and ChAT-positive, while only 2.2 ± 1.22% (n = 3, 8/355) were double-projecting and ChAT-negative. 69.3 ± 11.5% of retrogradely labeled neurons were single-projecting (n = 3, 246/355). Purple: double-projecting ChAT-positive neurons; Yellow: double-projecting ChAT-negative neurons; Green: single-projecting neurons. Aca, anterior commissure, anterior part; BA, basal amygdala; Cg1, cingulate cortex, area 1; DP, dorsal peduncular cortex; HDB, nucleus of the horizontal limb of the diagonal band; IL, infralimbic cortex; LA, lateral amygdala; LPO, lateral preoptic area; MCPO, magnocellular preoptic nucleus; MS, medial septal nucleus; PL, prelimbic cortex; PS, parastrial nucleus; SI, substantia innominata; VP, ventral pallidum.*

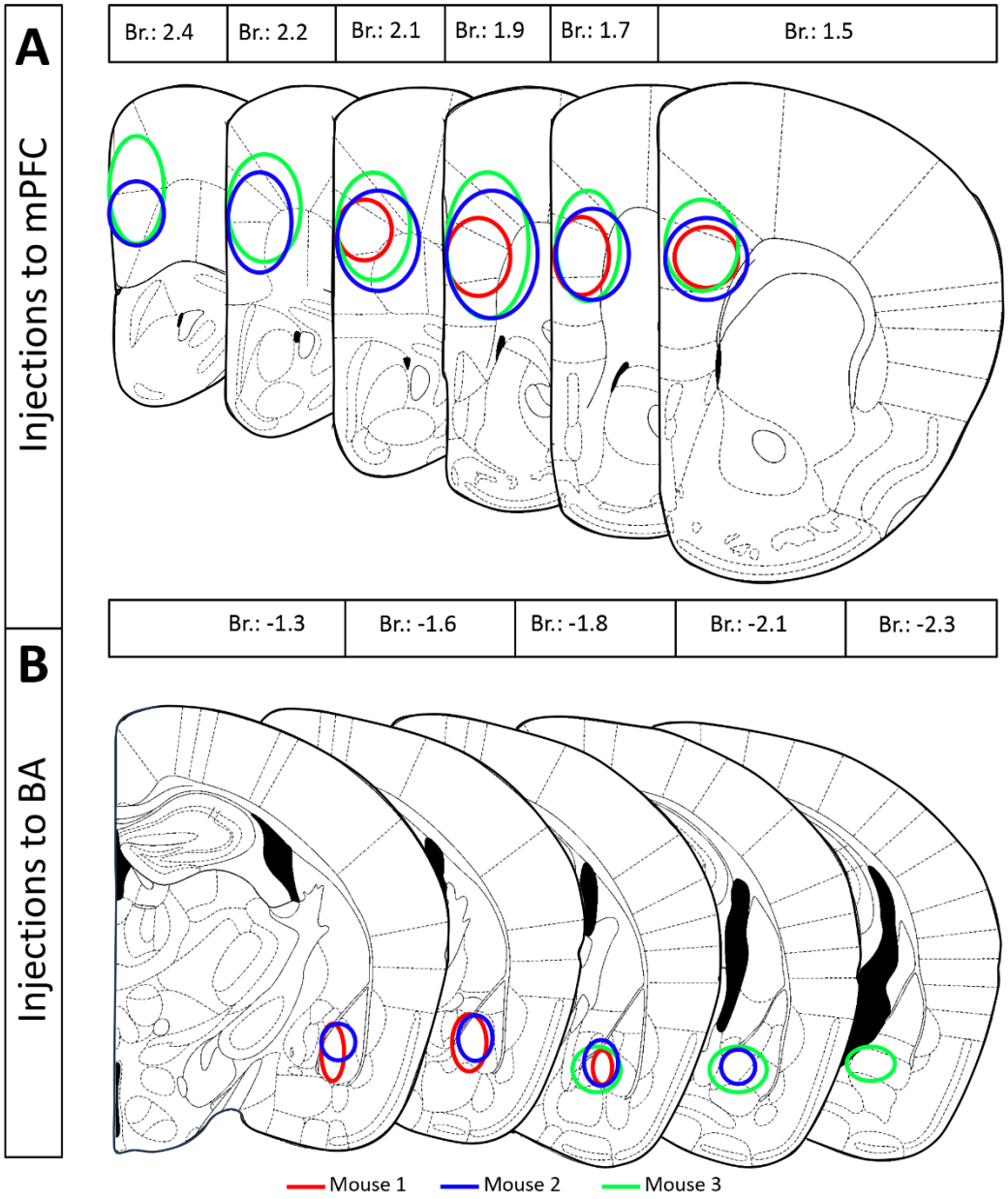

Figure 15. ***Reconstructed maps showing the localization and spread of retrograde tracers used for double-retrograde tracing.***
(A) *Localization and spread of Fluorogold in the mPFC (n = 3).* ***(B)*** *Localization and spread of Fast Blue in the BA (n = 3). Different colors represent different animals.*

4.6 ChAT and VGLUT3 cells form highly overlapping populations within the VP/SI

A previous study obtained in rats has uncovered (Poulin et al., 2006) that BF cholinergic neurons projecting to the BLA express VGLUT3. To clarify whether amygdala-projecting cholinergic neurons also contain VGLUT3 in mice, we revealed the neurons expressing VGLUT3 by crossing VGLUT3-Cre and Ai14 reporter mice. In offspring, we performed immunostaining against ChAT that allowed us to quantify the number of cholinergic neurons in the HDB and VP/SI that expressed VGLUT3, too. We observed that 71.19% (168/236, n=2; Fig. 16) of cholinergic neurons in the VP/SI expressed VLGUT3, whereas this ratio was 33.69% (94/279, n=2; Fig. 16) in the HDB.

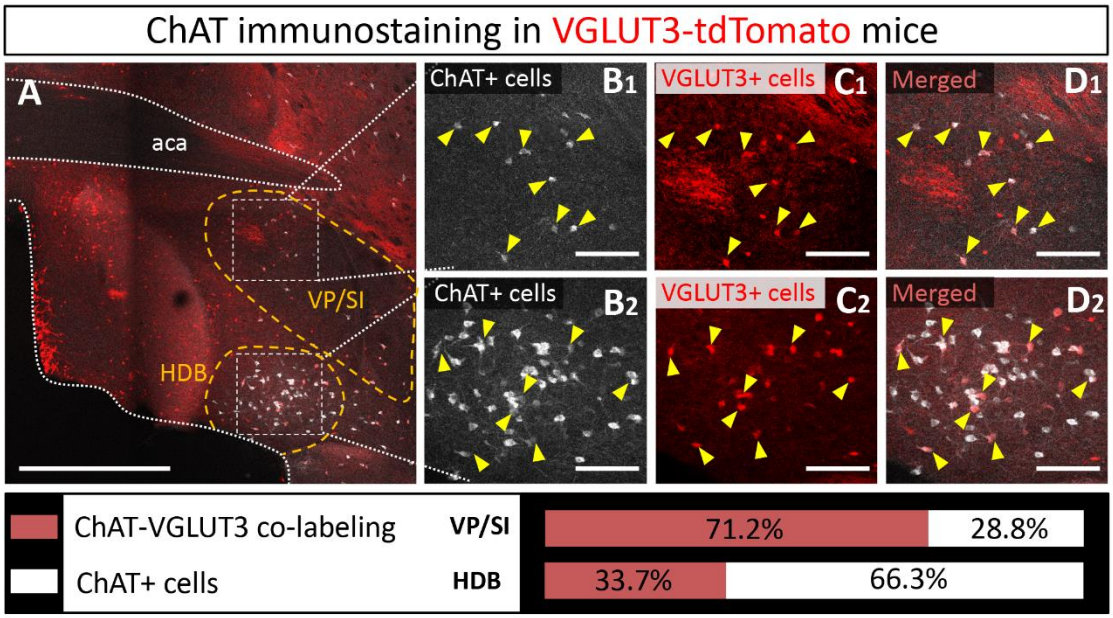

Figure 16. ***Ratio of ChAT and VGLUT3 co-labeling in the HDB and VP/SI.***
(A) *Example coronal slice taken at the BF, showing ChAT content of VGLUT3-expressing neurons. The yellow dashed lines represent the borders of the HDB and VP/SI, where the co-labeling was counted. Scale bar: 500 µm.* ***(B)*** *ChAT+ cells in the VP/SI* ***(B1)*** *and HDB* ***(B2)****. Scale bar: 100 µm.* ***(C)*** *VGLUT3+ cells in the VP/SI* ***(C1)*** *and HDB* ***(C2)****. Scale bar: 100 µm.* ***(D)*** *Merged images taken at the VP/SI* ***(D1)*** *and HDB* ***(D2)****. Scale bar: 100 µm. Yellow arrows indicate co-labeled neurons. Bottom graph showing the ratio of co-labeling in the VP/SI and HDB, respectively.*

Knowing that most cholinergic cells also contain VGLUT3 in the VP/SI, we administered 30 nl AAV8.CAG.Flex.GFP into the VP/SI of VGLUT3-Cre mice to explore the projection patterns and cholinergic phenotype of VGLUT3+ neurons and their axons in the PFC and amygdala region (Fig. 17, Fig. 7D). We found that 64% (Fig. 17A, 89/139, n=2) of VGLUT3+ neurons were also positive for ChAT at the injection site, and these

cells exhibited similar projection patterns towards the amygdala (Fig. 17B) and PFC (Fig. 17D), mirroring our observations obtained in ChAT-Cre mice. The most prominent difference was that VGLUT3+ axons in the BA could not be observe in posterior amygdala planes (from Br.: -1.8mm to -2.9 mm), while fewer axons were found in the M2 cortex (Fig. 18). However, more prominent projections were seen in the anterior insular cortex (AI, Fig. 17D, Fig. 18). Additionally, ChAT immunostaining revealed that VGLUT3+ axons contained ChAT enzyme in both the BA (Fig. 17C) and mPFC (mainly Cg1, PL) (Fig. 17E), further supporting the observation that VGLUT3+ and ChAT+ neurons form overlapping populations in the VP/SI.

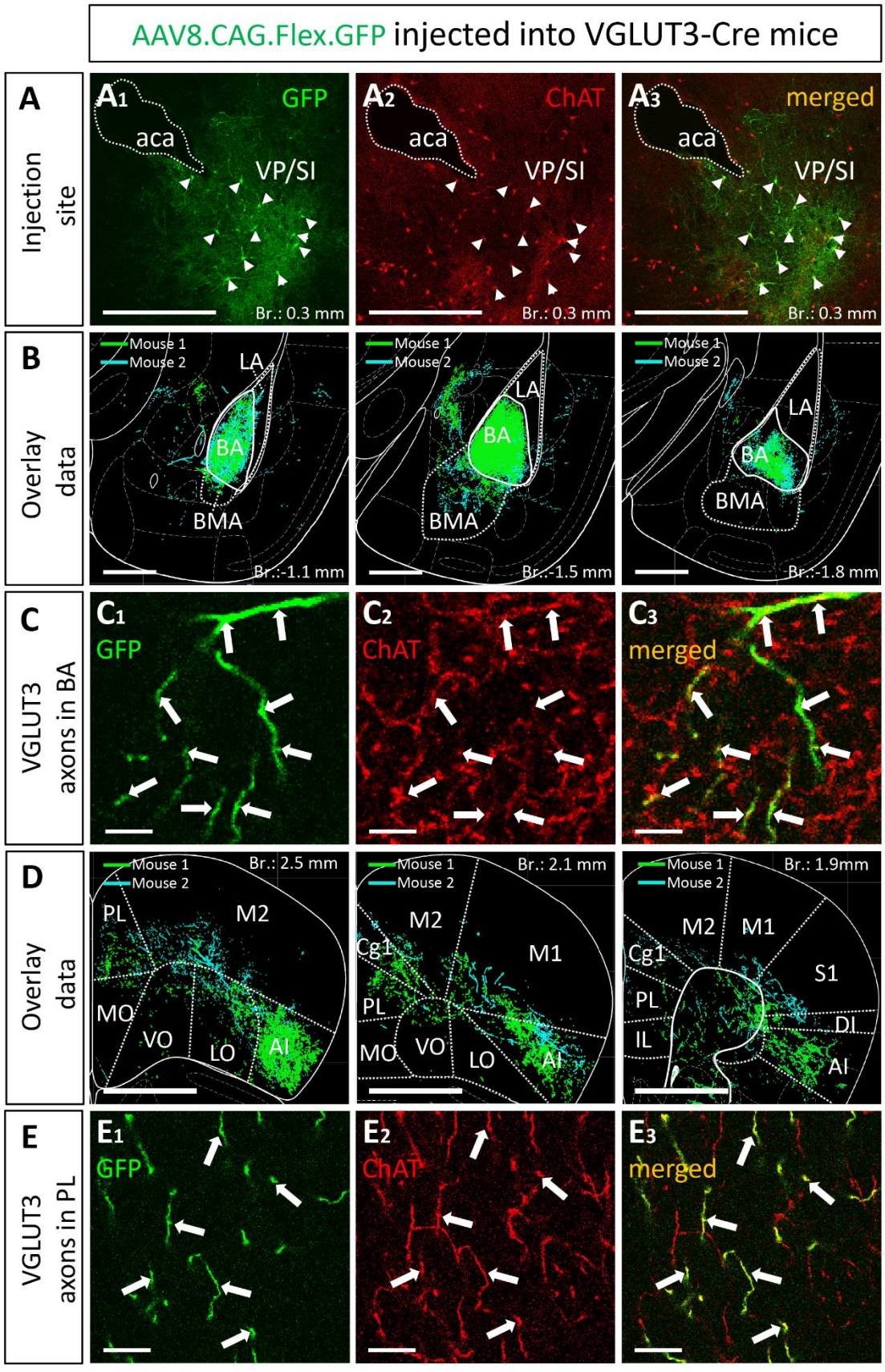
AAV8.CAG.Flex.GFP injected into VGLUT3-Cre mice
A
Injection site
A1
GFP
aca
VP/SI
Br.: 0.3 mm
A2
ChAT
aca
VP/SI
Br.: 0.3 mm
A3
merged
aca
VP/SI
Br.: 0.3 mm
B
Overlay data
Mouse 1
Mouse 2
LA
BA
BMA
Br.:-1.1 mm
Mouse 1
Mouse 2
LA
BA
BMA
Br.:-1.5 mm
Mouse 1
Mouse 2
LA
BA
BMA
Br.:-1.8 mm
C
VGLUT3 axons in BA
C1
GFP
C2
ChAT
C3
merged
D
Overlay data
Mouse 1
Mouse 2
Br.: 2.5 mm
PL
M2
MO
VO
LO
AI
Mouse 1
Mouse 2
Br.: 2.1 mm
M2
Cg1
M1
PL
MO
VO
LO
AI
Mouse 1
Mouse 2
Br.: 1.9mm
M2
M1
Cg1
S1
PL
DI
IL
AI
E
VGLUT3 axons in PL
E1
GFP
E2
ChAT
E3
merged

Figure 17. ***VGLUT3-expressing neurons within the VP/SI show ChAT immunoreactivity and project to the mPFC and BA.***
(A) *Coronal image taken from the BF showing the injection site* ***(A1)*** *in the VP/SI in VGLUT3-Cre mice. Small amount (30 nL) of AAV8.CAG.flex.GFP was injected to the target area. Cholinergic cells were visualized with ChAT immunostaining* ***(A2)*** *to reveal the cholinergic content of VGLUT3-expressing BF cells* ***(A3)*** *in the VP/SI. Scale bar: 500 µm. White arrowheads: double labeled neurons.* ***(B)*** *Overlaid representative glutamatergic projections in the BLA originating from VP/SI cells. Axons revealed in different animals (n = 2) are shown in distinct colors. Scale bar: 500 µm.* ***(C)*** *60x magnification fluorescent images showing VGLUT3-GFP* ***(C1)*** *and ChAT* ***(C2)*** *co-labeling* ***(C3)*** *within the BA. Scale bar: 5 µm. White arrows: double labeled axons.* ***(D)*** *Overlaid representative glutamatergic projections in the mPFC originating from VP/SI cells. Axons revealed in different animals (n = 2) are shown in distinct colors. Scale bar: 1000 µm.* ***(E)*** *60x magnification fluorescent images showing VGLUT3-GFP* ***(E1)*** *and ChAT* ***(E2)*** *co-labeling* ***(E3)*** *within the PL. Scale bar: 10 µm. White arrows: double labeled axons. Aca, anterior commissure, anterior part; AI, agranular insular cortex; BA, basal amygdala; BMA, basomedial amygdala; Cg1, cingulate cortex, area 1; IL, infralimbic cortex; LA, lateral amygdala, LO, lateral orbital cortex; M1, primary motor cortex; M2, secondary motor cortex; MO, medial orbital cortex; PL, prelimbic cortex; VO, ventral orbital cortex; S1, primary somatosensory cortex; DI, dysgranular insular cortex; SI, substantia innominata; VP, ventral pallidum.*

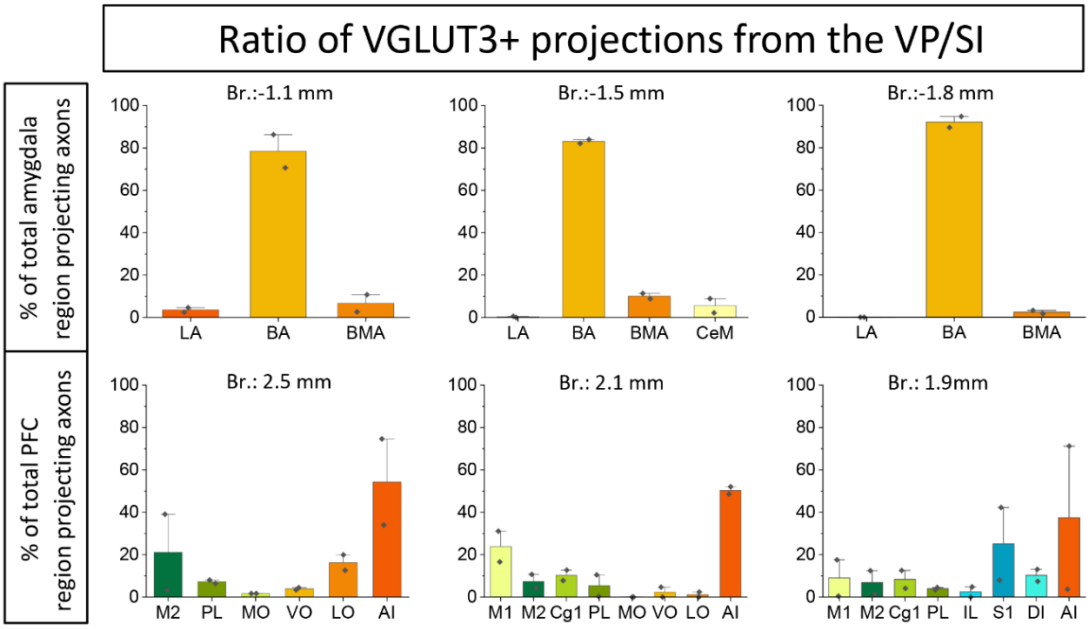

Figure 18. ***Ratio of glutamatergic (VGLUT3) projections in the amygdala and PFC subregions originating from the VP/SI.***
(A) *Percentage of amygdala region-projecting VP/SI glutamatergic axons in each nucleus/region at different bregma levels.* ***(B)*** *Percentage of PFC region-projecting VP/SI glutamatergic axons in each nucleus/region at different bregma levels. These graphs appertain to Figure 17.*

Collectively, these data predict that most cholinergic axon terminals within the BA should also contain VGLUT3 immunolabeling, whereas the ratio of the double labeled axonal boutons for ChAT and VGLUT3 should be substantially less in other amygdala areas. In agreement with this hypothesis, we found that, among all amygdala areas, the BA had the highest ratio of axon terminals immunoreactive for both ChAT and VGLUT3 (Fig. 19A). Interestingly, this ratio was not homogeneous within this nucleus: its anterior part (Fig. 19A, C, 63.28%± 8.58, 324/512, n=3) contained twice as many double immunopositive

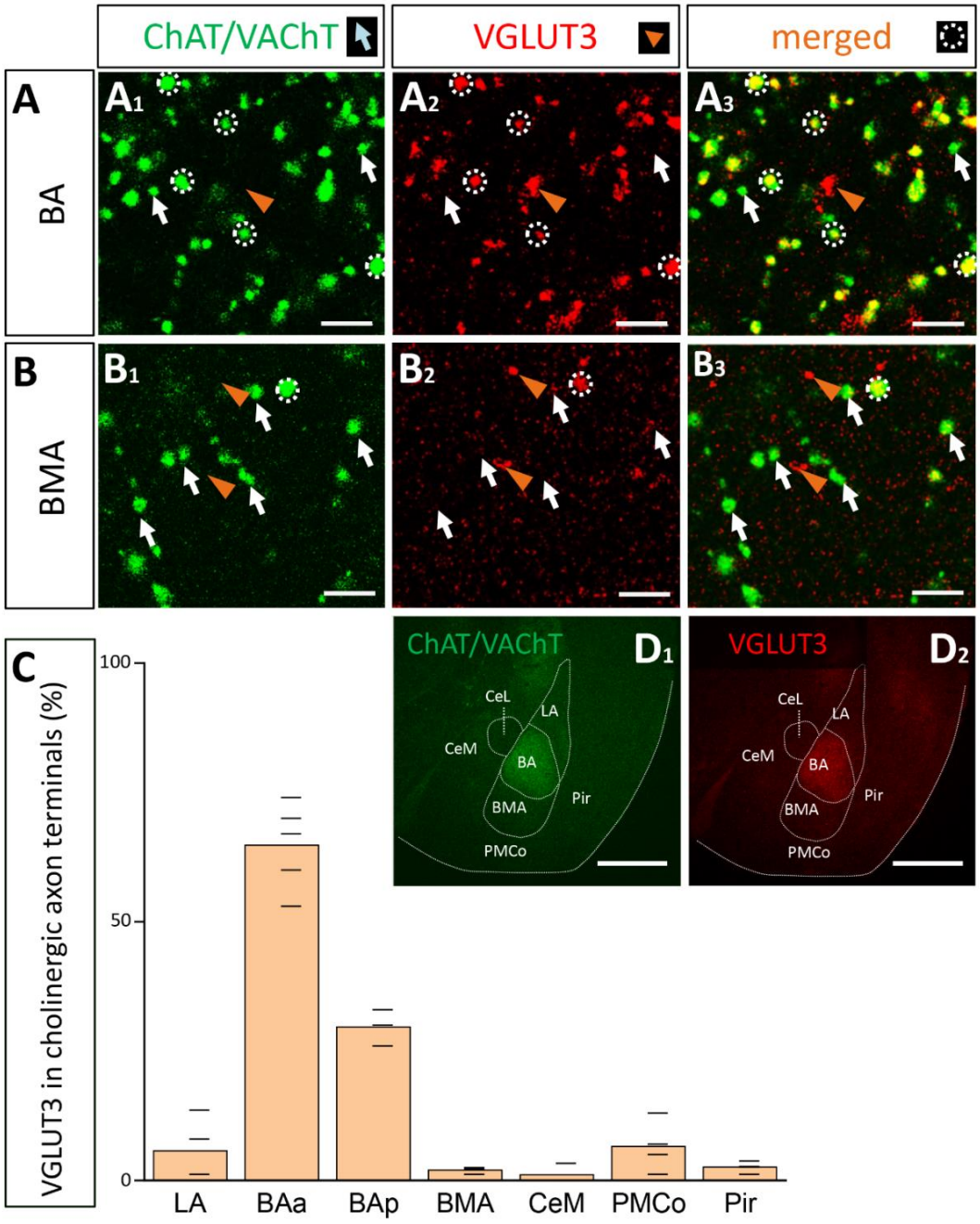

Figure 19. ***Cholinergic axon terminals in the BA co-express VGLUT3.***
(A) *Cholinergic (**A**1; green. ChAT/VAChT) and glutamatergic axon terminals (**A**2; red. VGLUT3) revealed by immunostaining showing high co-occurrence in cholinergic boutons in the BA **(A**3**)**. Scale bar: 3 μm. White arrows point to ChAT/VAChT-containing boutons. Orange arrowheads indicate VGLUT3-containing boutons. White dotted circles indicate double labeled, i.e., cholinergic and VGLUT3-immunostained boutons. Scale bar: 3 μm.* ***(B)*** *Cholinergic (**B**1; green) and VGLUT3-containing axonal boutons (**B**2; red) form largely non-overlapping populations in the BMA. Scale bar: 3 μm.* ***(C)*** *Graph showing that the VGLUT3 content in cholinergic axon terminals is the highest in the anterior BA (BAa; 64.8 ± 8.35%; n = 3, 332/512) and posterior BA (BAp; 29.67 ± 3.51%, n = 3, 89/300), while the co-expression is lower in surrounding amygdala nuclei: LA (5.82 ± 6.33%, n = 2, 17/292), BMA (2.38 ± 0.68%, n = 2, 6/252), PMCo (6.85 ± 4.93%, n = 2, 24/350), Pir (2.57 ± 1.05%, n = 2, 8/311), CeM (1.69 ± 1.92%, n = 2, 3/177).* ***(D)*** *Images taken at low magnification from ChAT/VAChT (**D**1; green) and VGLUT3 (**D**1; red) immunostained sections showing high expression levels for these proteins in the BA, but not in surrounding amygdala regions. Scale bar: 500 μm. BAa, basal amygdala, anterior part; BAp, basal*

amygdala, posterior part; BMA, basomedial amygdala; CeM, central amygdala, medial division; LA, lateral amygdala; Pir, piriform cortex; PMCo, posteromedial cortical amygdaloid nucleus.

axonal boutons than its posterior part (Fig. 19C, 29.67%± 3.51, 89/300, n=3). This observation might explain why fewer VGLUT3+ fibers were observed in caudal amygdala planes (Fig. 17B). As expected, in neighboring regions, the co-expression of ChAT and VGLUT3 was minimal (Fig. 19B, C). These results together suggest that cholinergic pathways from the VP/SI typically contain VGLUT3, while ChAT+ fibers located in other amygdala regions - originating primarily from the HDB - express this glutamate transporter at a much lower level. In addition, these observations further strengthen the conclusion that the BA and its surrounding regions receive cholinergic control from two distinct BF sources that differ in their VGLUT3 content.

4.7 GABAergic phenotype is not characteristic for cholinergic neurons in the HDB and VP/SI in adult mice.

Previous studies convincingly demonstrated that GABA can be released from cholinergic axon terminals in the neocortex (Saunders et al., 2015), hippocampus (Takács et al., 2018) and striatum (Lozovaya et al., 2018). To assess whether cholinergic neurons in the HDB and VP/SI are also GABAergic, we visualized inhibitory cells in the BF by crossing VGAT-Cre with Ai9 reporter mice (CAG-LSL- ZsGreen1, Fig. 20A1, B1), whereas ChAT content of neurons was revealed by immunostaining (Fig. 20A2, B2). We found that 96.98% (546/563, n=3) of cholinergic neurons expressed the reporter protein under the control of VGAT promoter in the HDB, whereas this ratio was 58.8% (137/233, n=3) in the VP/SI (Fig. 20E, dark green). To confirm the GABAergic nature of cholinergic afferents in the BLA, we examined the VGAT immunoreactivity in cholinergic axon terminals. To our surprise, we observed no co-expression of VGAT and cholinergic markers (ChAT; VAChT) (Fig. 20F, 0.75%, 3/400, n=2) in axonal boutons at the amygdala level. To resolve this contradiction, we labeled BF GABAergic cells in adult VGAT-Cre mice by injecting AAV8.CAG.Flex.GFP vector simultaneously into the HDB and VP/SI (Fig. 20C1, D1). After 4 weeks following the injections, we performed immunostaining against ChAT (Fig. 20C2, D2) and counted the GFP content of cholinergic cells in the BF (Fig. 20C3, D3). Under these circumstances, we found that

there were only a few neurons co-expressing ChAT and GFP both in the HDB (3.06%, 19/620, n=3) and VP/SI (1.19%, 3/253, n=3) (Fig. 20E, light green). These data are in line with the findings that cholinergic axon terminals do not contain VGAT immunolabeling in the amygdala (Fig. 19F). Thus, our results collectively show that in adult mice, GABA is not typically present in cholinergic neurons in the HDB and VP/SI.

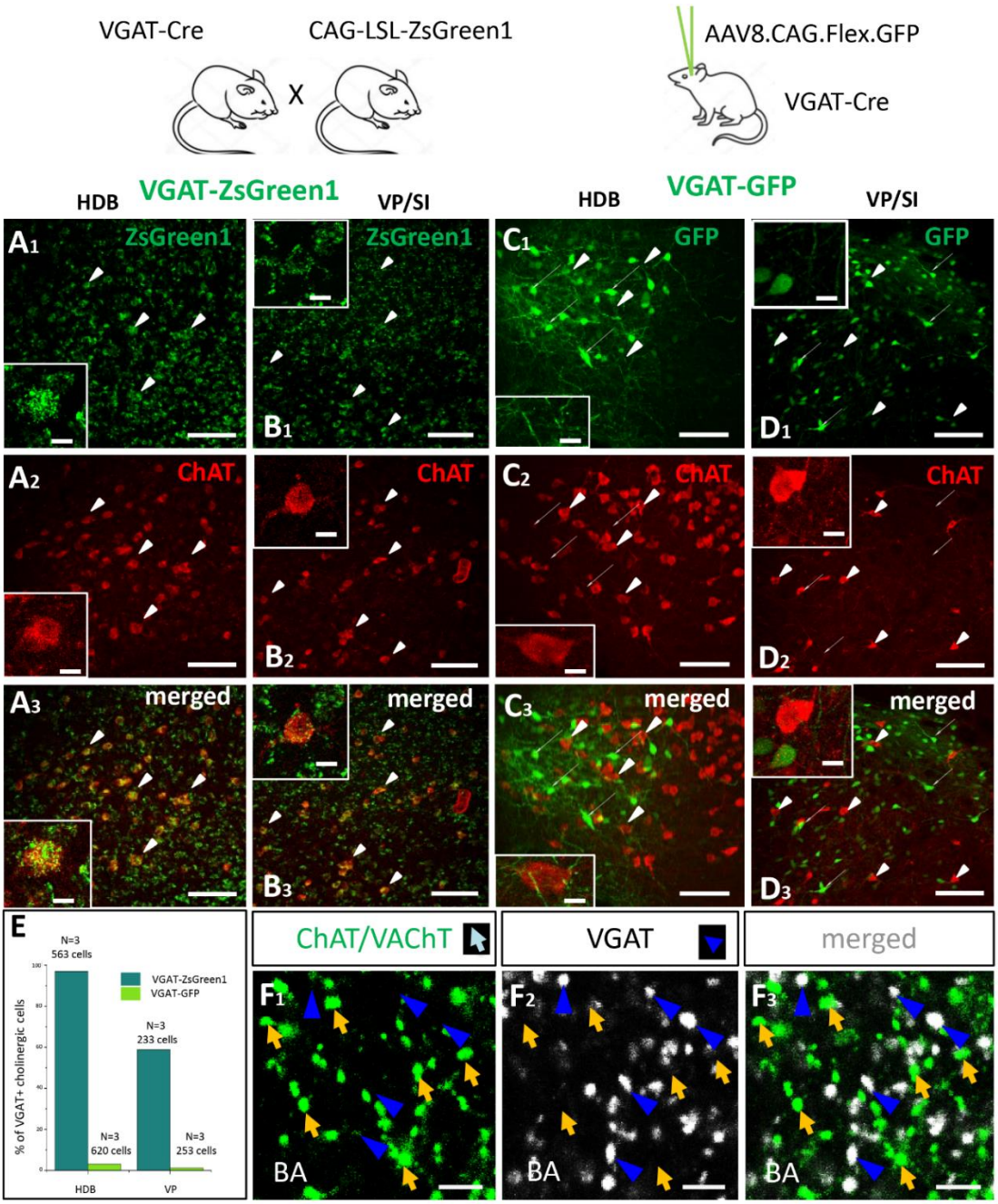

Figure 20. ***Cholinergic cells in the HDB and VP/SI do not express VGAT in adult mice.***
(A,B) *Visualizing GABAergic cells in the HDB* ***(A1)*** *and VP/SI* ***(B1)*** *within the BF, in VGAT-ZsGreen1 offspring generated by breeding VGAT-IRES-Cre and CAG-LSL-ZsGreen1 mice. Scale bar: 50 μm. Insets: images taken at higher magnification of a GABAergic BF neuron containing ChAT immunolabeling. Scale bar: White arrowheads point to co-labeled ChAT/VGAT-ZsGreen1 cells. 5 μm.* ***(C,D)*** *Virus labeling of*

*GABAergic cells in the HDB **(C1)** and VP/SI **(D1)** by injecting AAV8.CAG.Flex.GFP into VGAT-Cre mice. Scale bar: 50 μm. Insets: images taken at higher magnification showing GABAergic and cholinergic cells intermingled in the BF. Scale bar: White elongated arrowheads point to ChAT positive cells, while narrow white arrows indicate VGAT-GFP neurons. 5 μm. **(A2–D2)** ChAT immunostaining revealing cholinergic cells in the BF. Scale bar: 50 μm. **(A3,B3)** Merged images showing co-expression of VGAT and ChAT both in the HDB and VP/SI in VGAT-ZsGreen1 mice. Scale bar: 50 μm. **(C3,D3)** Merged images showing that cholinergic cells in the HDB and VP/SI do not contain VGAT in AAV-injected VGAT-Cre mice. Scale bar: 50 μm. **(E)** Percentage of VGAT-expressing cholinergic cells in the HDB (Dark green, 96.7%, 546/563, n = 3) and VP/SI (Dark green, 58.8%, 137/233, n = 3) in VGAT-ZsGreen1 and AAV-injected VGAT-Cre (Light green, HDB: 3.06%, 19/620; VP/SI: 1.19%, 3/253, n = 3) mice. **(F1–3)** Cholinergic (**F1; green. ChAT/VAChT) and GABAergic (F2; white. VGAT) axon terminals showing non-overlapping populations in the BA (F3)**. Scale bar: 3 μm. Orange arrows show ChAT/VAChT-containing boutons. Dark blue arrowheads point to VGAT-immunoreactive boutons.*

4.8 Electrical stimulation as noxious signal.

In animals, three primary fear responses can be distinguished based on the proximity of the danger source: fight, flight, and freezing (LeDoux, 2000; Tovote et al., 2015). In experiments investigating whether fear-regulating neural pathways in the brain have been activated, the presence and duration of the freezing response are analyzed (Janak and Tye, 2015; Tovote et al., 2015). One of the most commonly used methods in neuroscience to study the structural and functional organization of these pathways is Pavlovian fear conditioning (Fig. 21A1). Here, I describe an experiment, as an exemplar, we performed to examine the neuronal circuits involved in associative learning. In this procedure, experimental mice were placed in an unfamiliar environment (context A) to explore their surroundings, a behavior referred to as "exploration", when mice form spatial map of the novel environment (Tovote et al., 2015). During the fear conditioning phase, the presentation of a neutral conditioned stimulus (CS) is co-terminated with an unconditioned stimulus (US), such as an aversive stimulus (e.g., an electric shock) (signed US; Fig. 21A2). The pairing of CS with US several times forms an association memory. To test the memory formation on a subsequent day, the animal is placed into a different environment (context B) and the CS is presented several times. If the association between CS and US has been formed, then mice will show freezing behavior during CS presentation in the context B (Fig. 21B). If we present the same number of CS and US to mice, but independent of each other, i.e., un-paired during conditioning (unsigned US; Fig. 21A2), the association between the CS and US will not be formed, indicated by CS-induced low freezing observed in the context B (Fig. 21B). These results show that CS and US presentations need to be delivered close in time and in a structured manner, so the

animal will form a fear memory trace, when CS will predict the US, proxied by freezing. Irrespective whether the US is delivered linked to CS or independently from it, mice typically show aversive behavior, like jumping, vocalization and fight response triggered by electric foot shock. These behavior signs indicate that US clearly induces an aversive emotional state.

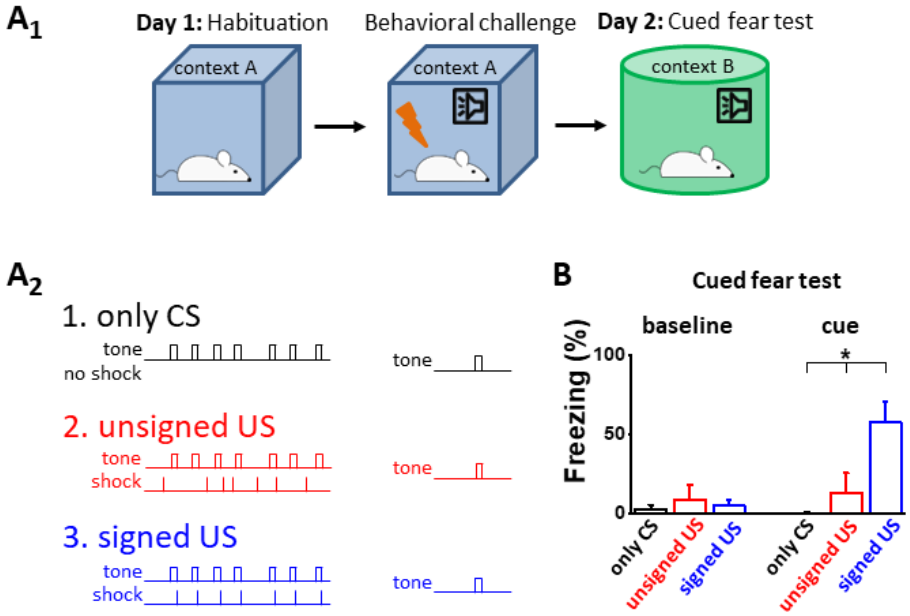

Figure 21. ***Electrical stimulation is a highly potent learning signal.***
(A1) *Experimental design.* ***(A2)*** *The three mouse groups with different combinations of CS (tone) and US (shock) presentation.* ***(B)*** *Freezing tested on the consecutive day was elevated only in the signed US group, therefore, the other two conditioning paradigms can serve as assessments of the effects of the sensory inputs on the network. Asterisk indicates significant difference (K-W ANOVA $p = 3\times10-6$, only CS vs. unsigned US $p = 0.39$, only CS vs. signed US $p = 2\times10-6$, unsigned US vs. signed US $p = 0.003$). Box represents mean, whiskers SEM. Only CS group n = 14, unsigned US group n = 12, signed US group n = 13 (Veres et al., 2023).*

4.9 Cholinergic cells in the HDB and VP/SI show increased activation upon noxious stimulation

After investigating the projection characteristics and neurochemical properties of BF cholinergic cells, next we wanted to see if these cell groups have a role in the transmission of noxious signals towards the amygdala and cortical areas. To this end, we used fiber photometry, a technique which involves using optical fibers to deliver light into brain regions where neurons express fluorescent indicators suitable to monitor changes in intracellular Ca^{2+} concentrations. These indicators emit fluorescence signals when

neurons are active, proxied by Ca^{2+} elevation, allowing researchers to measure and analyze neural activity by detecting changes in light collected through the optic fiber. In our experiments ChAT-cre mice were injected with AAV2/5.CAG.Flex.GcaMP6f virus, then an optical fiber was implanted 100 μm above the HDB or VP/SI (Fig. 22A). After the recovery period, mice received mild electrical shocks (7 times/day for 3 days, 0.7mA), while fluorescent signals in cholinergic cells were measured. After analyzing the results, we observed that cholinergic cells were activated upon noxious stimulation (Fig. 22C-D). These data, in line with previous observations (Hangya et al., 2015), suggest that BF cholinergic neurons are profoundly excited by foot shocks, findings that imply their significant role in salient information processing.

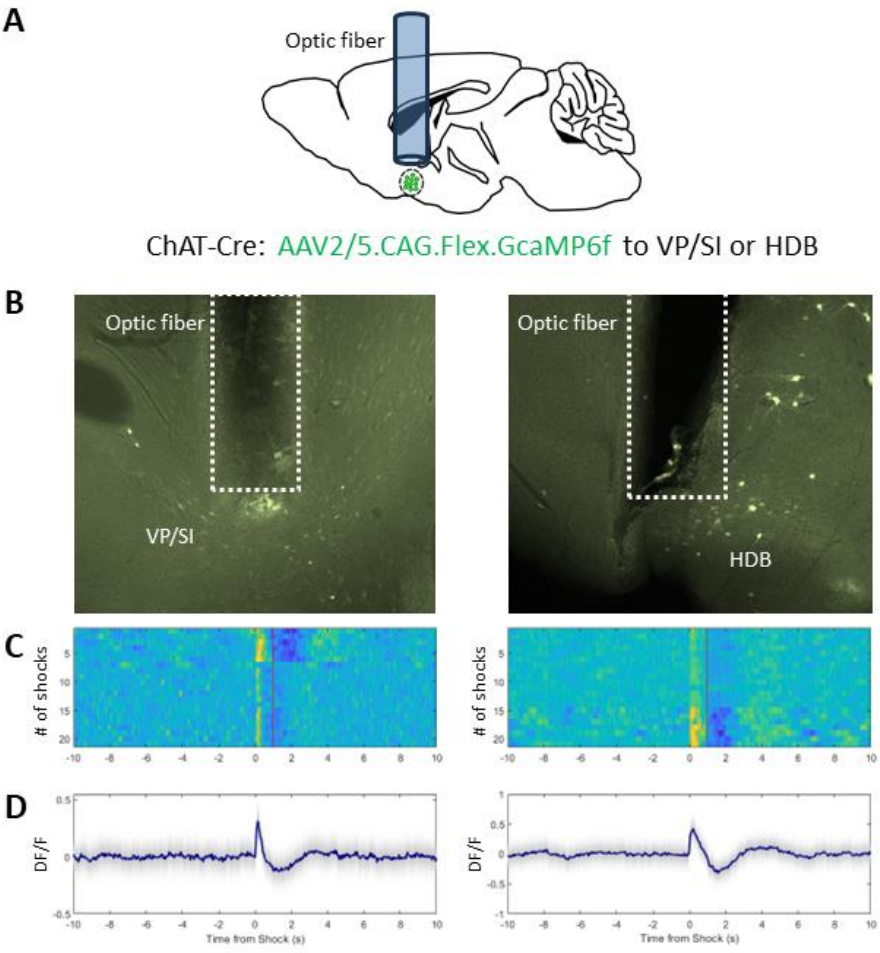

Figure 22. ***VP/SI and HDB cholinergic neurons are activated in response to noxious stimulation.*** *(**A**) Schematic representation of the experimental setup. (**B**) Pseudocolored fluorescent images illustrating the injection site and optic fiber placement in the VP/SI or HDB. (**C**) Heatmaps depicting cholinergic cell activation in the VP/SI and HDB, with warmer colors indicating higher activation and cooler colors indicating inactivation. Time 0 marks the foot shock onset, and the red line denotes the end of the foot shock at 1 second. (**D**) Peristimulus graphs showing ΔF/F changes in the VP/SI (n=2) and HDB (n=1) following noxious stimulation.*

4.10 Cortical processing of noxious stimulation

After determining the projection patterns of BF cholinergic neurons towards the frontal cortices and showing that these neurons are activated by noxious stimulation, we moved forward with our experiments in understanding how cortical network operation is changed upon delivery of electrical shocks. We have chosen two different approaches: 1) *in vivo* silicone probe recordings and 2) *in vivo* juxtacellular recordings visually guided by two-photon imaging in urethane-anesthetized mice in the M2 cortex. The first method has a great advantage in recording multiple neurons at the same time, and gathering information about putative principal cells and interneurons, while lacking cell type specificity. Meanwhile the second method can record the action potentials of individual neurons specifically followed by labelling the measured cells with Neurobiotin for subsequent anatomical identification. With silicone probe recordings we collected data from many neurons, the majority of which were likely principal neurons, while with juxtacellular recordings different types of genetically defined inhibitory cells were sampled in distinct transgenic mouse lines.

We selected the M2 cortex for four main reasons: 1) its location on the dorsal brain surface allows easy access for two-photon-guided juxtacellular recording, 2) it receives dense cholinergic innervation from the basal forebrain, primarily the VP/SI (Fig. 10B, Fig. 11C, D), 3) like the mPFC, it has reciprocal connections with the BLA (based on our unpublished observations) and 4) M2 cortical neurons respond similarly to foot shocks as those neurons located in the PFC and BLA (our unpublished observation), indicating that basic principles of circuit mechanisms driven by aversive stimulation may be shared by these neuronal networks.

4.10.1 Noxious stimulus-driven spiking in cortical neurons

With silicone probe recordings, we found three main response types among cortical neurons: 1) excitation (N= 29, 32.93%; Fig. 23C1-2), 2) inhibition (N= 46, 52.27%; Fig. 23D1-2) and 3) no response (N= 13, 14.77%; Fig. 23E) to noxious stimuli. Excitatory responses could further be dissected based on their response length, with 26.13% of the cells (N=23; Fig. 23C1) exhibiting a short and rapid increase in activity immediately after

(173.68±119 ms, N= 419) the foot shock delivery, and a smaller subset (N=6, 6.8%; Fig. 23C2) with an also immediate, but sustained (2s) excitation. Inhibitory responses in spiking could also be divided into similar groups, where 17.05% of cells (N=15; Fig. 23D1) showed a short decrease in activity following the foot shock, and another subset (N=31, 35.22%; Fig. 23D2) with prolonged inhibition. Cells with no significant change in spiking (black traces) constitute 14.77% of the sample (N=13; Fig. 23E). These data provide insight into the dynamic responses of cortical neurons in the frontal cortex upon aversive stimuli, with distinct patterns of excitation, inhibition, and non-responsiveness.

4.10.2 Firing in perisomatic region-targeting inhibitory neurons upon noxious stimuli

To obtain recordings in the different types of interneurons, we used *in vivo* visually guided juxtacellular recordings in transgenic mice expressing fluorescent proteins in defined GABAergic cells. First, we wanted to understand how the three types of inhibitory cells giving rise to perisomatic inhibition - PVBCs, AACs, and CCKCB1BCs - react to noxious stimulation.

PVBCs were measured in the offspring of Pvalb-IRES-Cre x CAG-LSL-ZsGreen1 mice. We found two populations of PVBCs based on their responses to noxious stimulation. Type 1 PVBCs 60.35 % (N=35, 16 filled with Neurobiotin; Fig. 24A1, B1, C1) showed

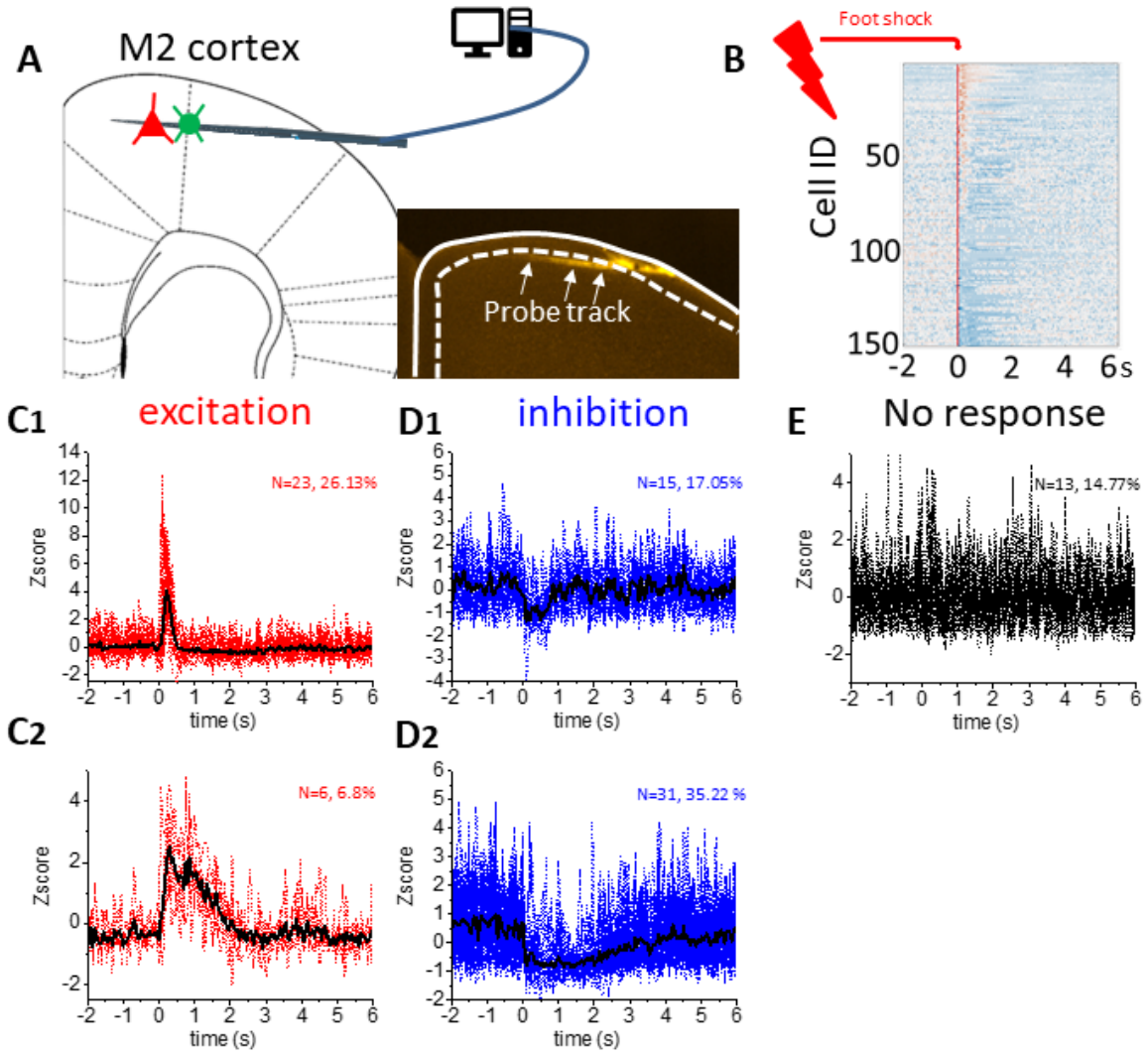

Figure 23. ***Silicon probe recordings in the M2 cortex reveal diverse response patterns in cortical neurons.*** *(**A**) Schematic representation of the experimental setup, with the silicon probe inserted laterally to preserve the integrity of the upper cortical layers during craniotomy. (**B**) Heatmap illustrating pyramidal cell responses, where warmer colors indicate higher activation and cooler colors indicate inhibition. Time 0 marks the foot shock onset. (**C1, C2**) Examples of pyramidal cells exhibiting distinct activation patterns. (**D1, D2**) Pyramidal cells displaying different inhibition durations. (**E**) Non-responsive pyramidal cells (Daniel Magyar's experiments).*

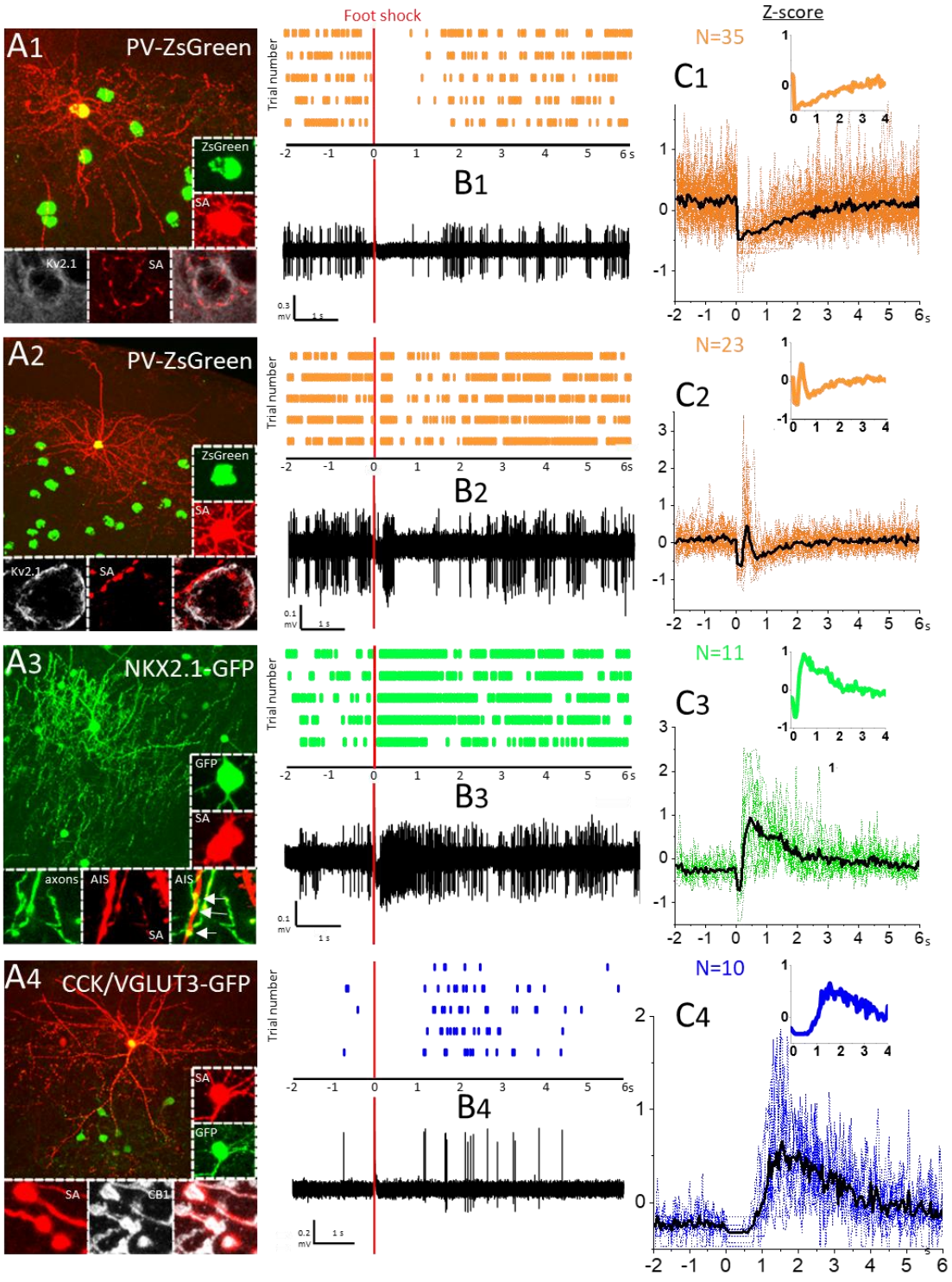

Figure 24. ***Spiking alterations in perisomatic inhibitory interneurons to noxious stimulation.*** *(**A1-4**) Fluorescent images of interneuron types that were juxtacellularly recorded and subsequently labelled followed by visualization with Streptavidin-conjugated fluorescent dyes. From top to bottom: Type 1 PVBCs, Type 2 PVBCs, AACs, and CCKCB1BCs. (**B1-4**) Raster plots displaying the spiking upon delivery of five consecutive shocks and an example trace illustrating the response in each neuron type to noxious stimuli. The red line indicates foot shock onset. (**C1-4**) Z-scored firing rate plots showing the individual (color) and averaged (black) responses in recorded neurons within each group. Inserts show the averaged traces.*

prolonged inhibition, lasting for 2-4 seconds upon electrical stimulation, while Type 2 PVBCs 39.65% (N=23, 10 filled with Neurobiotin; Fig. 24A2, B2, C2) had a more complex response, starting with a fast-short inhibition, then the activity of the cells returned to baseline (302.62 ± 89 ms, N= 507; Fig. 26A, B, D), with a portion of the cells reaching higher activation, followed by a decrease in activity lasting for 1-2 seconds.

AACs were measured in the offspring of Nkx2.1-CreER x LSL-Flpo mice. The Nkx2.1 marker is commonly used to identify certain subtypes of inhibitory interneurons, particularly in the cortex. Nkx2.1 is a transcription factor that is crucial for the development of several cell types, including specific interneurons derived from the medial ganglionic eminence (MGE) during embryonic development (Taniguchi et al., 2013). The genetical construction of Nkx2.1-CreER x LSL-Flpo allowed the tamoxifen inducible expression of Flpo in interneurons in a specific time window (P0), when development/migration of a group of AACs starts (detailed in materials and methods, Fig. 4). In P60, mice were injected with AAV5.EF1a.eYFP.fDIO to the frontal cortex (M2) to trigger Flpo dependent eYFP expression in AACs. These neurons (N=11, 5 filled with Neurobiotin) showed a fast (391.08± 359 ms, N= 155), strong and long-lasting spike increase (2-4 s; Fig. 24A3, B3, C3; Fig. 26A, B, F) upon stimulation.

CCKCB1BCs were sampled in both BAC-CCK-dsRed and the offspring of BAC-VGLUT3-iCre x BAC-CCK/gfp-coIN_sb mice. In the first type of mice there were many dsRed labeled cells, which were not BCs (determined after recordings). Therefore, we changed strategy to target these BCs in double transgenic mice, leading to a higher success rate. Overall, identified CCKBCs were immunopositive for CB1 recorded in both types of mice and these cells showed delayed activation, starting at 1 second after noxious stimulation and lasting for 4-5 seconds (N= 10, 5 filled with Neurobiotin; Fig. 24A4, B4, C4).

4.10.3 Dendrite-targeting and Interneuron selective interneurons

Next, we examined two other groups of interneurons, 1) interneurons which are responsible for dendritic inhibition, and 2) VIP ISIs. In the first group, we measured the activity of NPY-positive NGFCs (NPY/NGFCs) and SST INs. NPY/NGFCs cells were

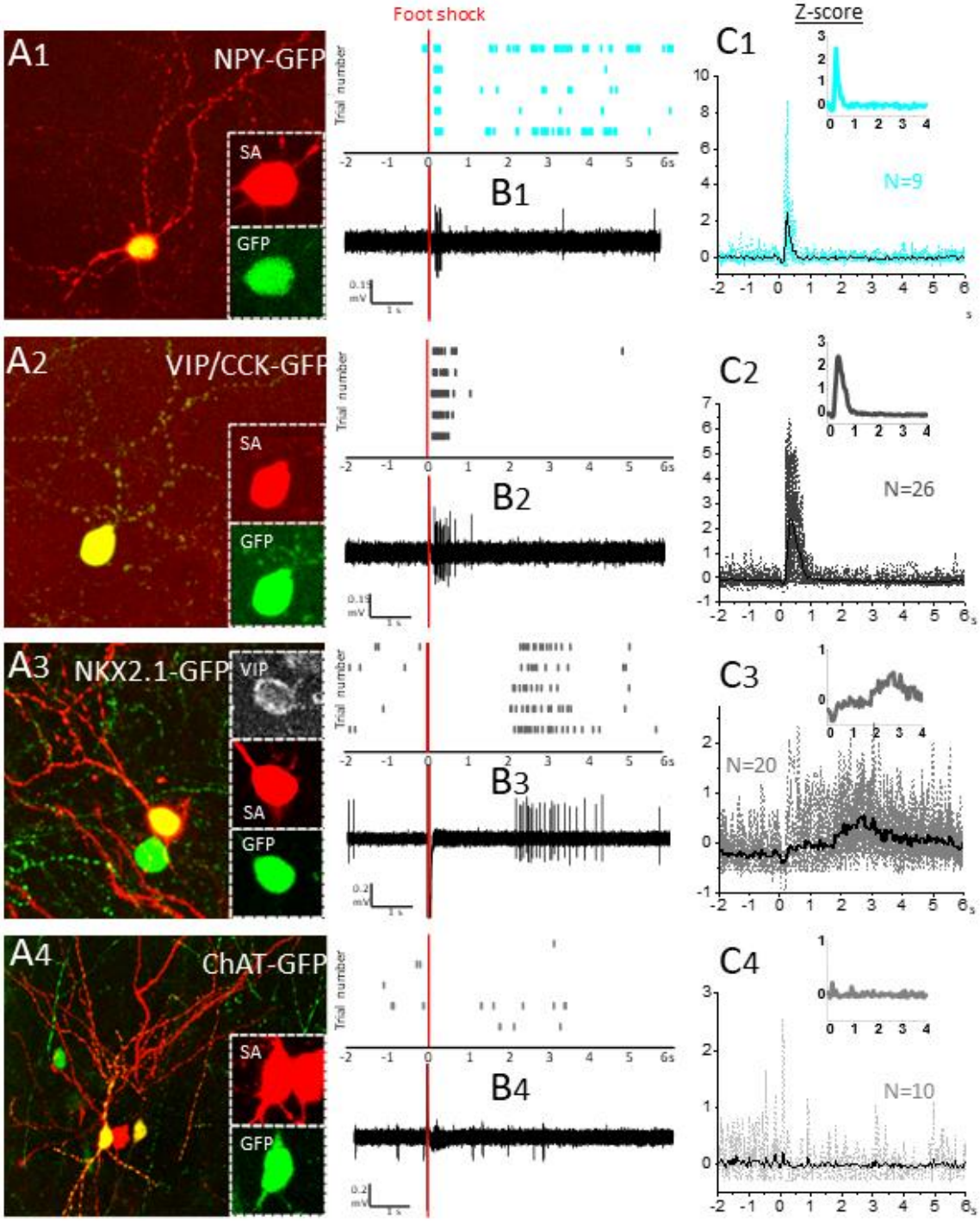

Figure 25. ***The responses of dendrite-targeting and interneuron-selective interneurons to noxious stimulation.***
(A1-4) *Fluorescent images of interneuron types that were juxtacellularly recorded and subsequently revealed with Streptavidin-conjugated fluorescent dyes. From top to bottom: NPY/NGFCs, Type 1 VIP ISIs (VIP/CCK ISIs), Type 2 VIP ISIs (VIP/Nkx2.1 ISIs), Type 3 VIP ISIs (VIP/ChAT ISIs).* ***(B1-4)*** *Raster plots displaying spikes in relation to five consecutive shocks and an example trace illustrating the response of each neuron type to noxious stimuli. The red line indicates foot shock onset.* ***(C1-4)*** *Z-score plots showing the individual (color) and averaged (black) responses of recorded neurons within each group. Inserts show the averaged traces.*

sampled in the offspring of NPY-IRES-Cre x BAC-CCK/gfp-coIN_sb and NPY-IRES-Cre x CAG-LSL-ZsGreen1. Among all the interneurons these cells (N=9; 6 filled with Neurobiotin, Fig. 25A1, B1, C1) fired with the shortest latency upon noxious stimulation (262.42± 97 ms, N= 137) (Fig. 26A, B, E). Interestingly, SST INs recorded in SST-Cre mice injected with AAV5.EF1a.DIO.eGFP were typically silent and discharged no spikes upon electrical stimulation (data not shown).

A subset of ISIs in cortical structures expresses VIP and preferentially inhibits other interneuron types. Here we found three functionally different types of VIP ISIs, showing distinct activation patterns to electrical stimuli. In the offspring of VIP-IRES-Cre x BAC-CCK/gfp-coIN_sb, VIP/CCK ISIs (Type 1 VIP ISIs; N= 26, 15 filled with Neurobiotin; Fig. 25A2, B2, C2) were activated with a short latency but slightly later than NPY/NGFCs (291.02± 105 ms, N= 427; Fig. 26A, B, C). Using Nkx2.1-CreER x LSL-Flpo mouse line, we discovered that if the tamoxifen is administered at P1 or P2, most virus infected cells will be, instead of AACs, VIP ISIs, confirmed by morphological features and immunostaining against VIP. This allowed us to investigate another group of VIP ISIs, VIP/Nkx2.1 ISIs (Type 2 VIP ISIs; N=20, 9 filled with Neurobiotin; Fig. 25A3, B3, C3), which to our surprise exhibited a different activation pattern to stimulation in comparison to VIP/CCK ISIs. All VIP/Nkx2.1 ISIs responded with a long-lasting activation upon electrical shocks, but the start of their activation varied, contrary to other groups. Some of the cells were activated immediately -, while the majority of the cells peaked their spiking at 2 seconds after shocks, reaching an average peak amplitude between 2.5-3 seconds (Fig. 25B3, C3). Lastly, we measured the response of VIP ISIs in ChAT-Cre mice. Based on our immunolabeling at least 80% of ChAT neurons were positive for VIP in the frontal cortex. These VIP/ChAT ISIs (Type 3 VIP ISIs; N=10, 4 filled with Neurobiotin; Fig. 25A4, B4, C4) had a low baseline firing rate and no observable response to noxious stimulation.

4.10.4 Drug application

In the next set of experiments, we investigated the nature of synaptic transmission driving interneuronal firing upon noxious stimulation. There are two subcortical inputs that may account for exciting interneurons: glutamatergic afferents from the thalamus and cholinergic projection from the BF. To block the effects of these subcortical modulatory

inputs, we applied locally the nAChR blocker hexamethonium and the AMPA/kainate receptor antagonist NBQX (2,3-dihydroxy-6-nitro-7-sulfamyl-benz(f)quinoxaline). To achieve effective and specific delivery, we used an additional glass pipette filled with the water-soluble drugs, allowing their controlled application using iontophoresis (Fig. 27 A1-2). Given that Layer 2/3 VIP ISIs are one of the targets of cholinergic afferents in the cortex (Letzkus et

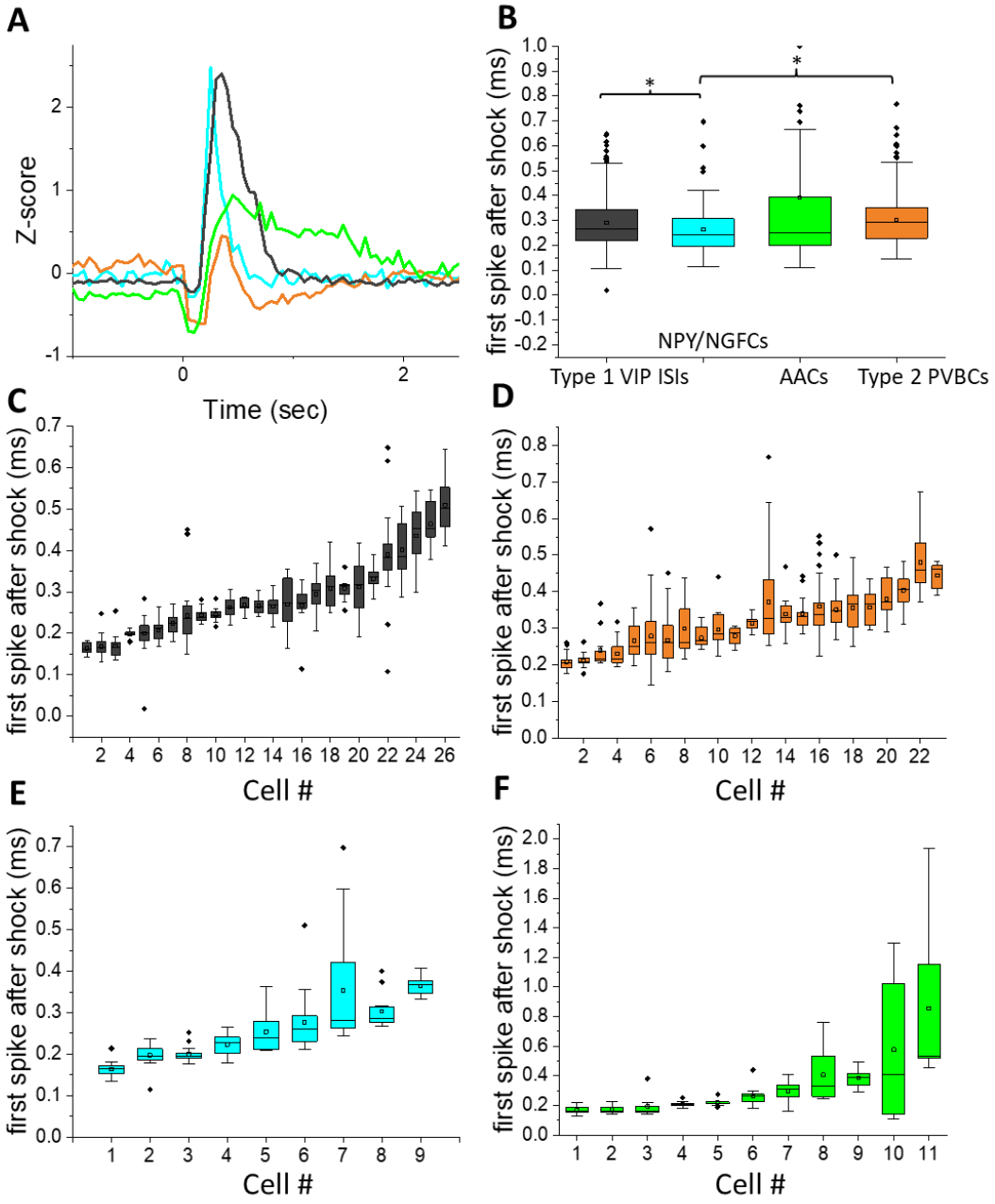

Figure 26. ***First spike latency in interneuron types with the shortest response time***
A*) Z-scored firing rate plot showing the averaged spike responses in four IN types. (****B****) First spike latencies*

*following noxious stimulation showing that NPY/NGFCs respondign significantly faster then Type 1 VIP ISIs and Type 2 PVBCs (K-W ANOVA p=0.0325, NPY/NGFCs vs Type 1 VIP ISIs; p=0.0102, NPY/NGFCs vs Type 2 PVBCs). (**C–F**) First spike latencies in individual neurons within each interneuron type: (**C**) Type 1 VIP ISIs, (**D**) Type 2 PVBCs, (**E**) NPY/NGFCs, and (**F**) AACs.*

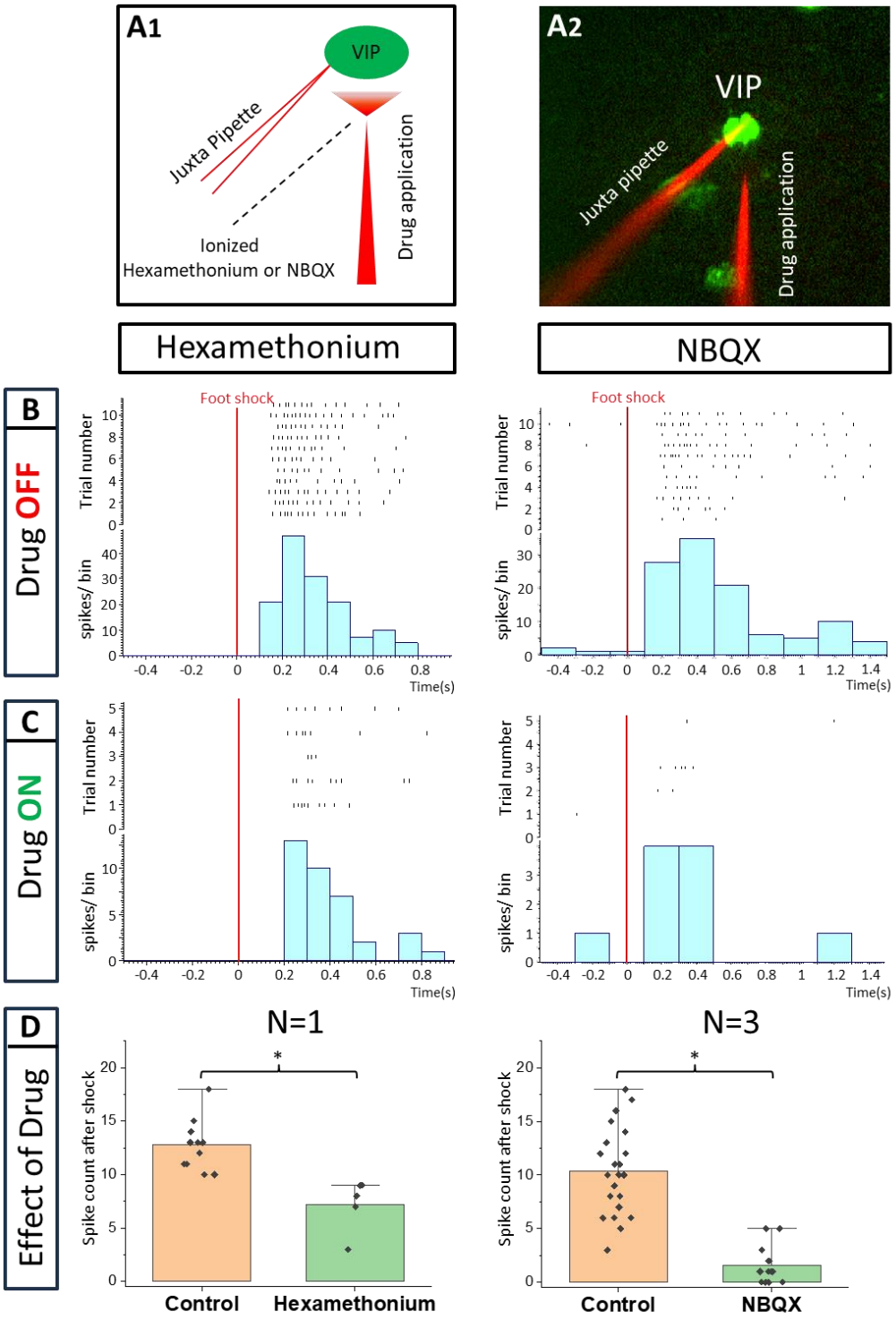

Figure 27. ***Both Hexamethonium and NBQX attenuate the shock response of Type 1 VIP ISIs (VIP/CCK ISIs).***

*(**A1, A2**) Schematic and real representation of the experimental approach. A second pipette, filled with either hexamethonium or NBQX, was positioned within 1–2 soma distances from the recorded neuron. The water-soluble (positively charged) drugs were retained in the pipette using a -20 nA holding current and released by applying a +20 nA current pulse. (**B**) Peristimulus raster plot and histogram depicting the response of an example Type 1 VIP ISIs to foot shock in the absence of drug application. The red line indicates foot shock onset. (**C**) Peristimulus raster plot and histogram showing the response of another Type 1 VIP ISIs to foot shock during Hexamethonium or NBQX application. The red line indicates foot shock onset. (**D**) Effect of drug application on spike count following foot shock (Mann-Whitney Test, p=0.0019 Control vs Hexamethonium; p=0.0001 Control vs NBQX).*

al., 2011), we investigated how hexamethonium and NBQX influence their response to noxious stimulation. Our findings indicate that hexamethonium reduced Type 1 VIP ISIs (VIP/CCK ISIs) activity by approximately 45% (Fig. 27 B, C, D), while NBQX had an even stronger suppressive effect (84.43%, Fig. 27 B, C, D). However, due to the limited sample size, these results should be considered preliminary, offering initial insights into the role of ACh and glutamate in modulating VIP/CCK IN activity triggered by noxious stimulation.

Overall, our data underscore the critical influence of BF cholinergic and potentially thalamic glutamatergic input on frontal cortical function and provide the first insights into the synaptic mechanisms how noxious stimulation alters interneuron activity patterns.

5. Discussion

In the first part of my thesis, we investigated the cholinergic innervation of two reciprocally interconnected cortical structures, the mPFC and BLA. Our main findings are the followings (Fig. 28). 1) Cholinergic cells located in two separate BF areas, the HDB and VP/SI innervate different parts of the BLA in a mutually exclusive manner. Although, they exhibit overlapping projections in the mPFC, the HDB tends to project more to the vPFC, whereas the VP/SI prefers to innervate the dPFC. 2) Importantly, using retrograde-anterograde virus tracing and double-retrograde tracing, we provide evidence that a significant portion of cholinergic cells can simultaneously innervate the BLA and mPFC. 3) Dual-projecting cells are intermingled with single-projecting neurons within the HDB and VP/SI. 4) Cholinergic and VGLUT3-containing BF cells form largely overlapping populations in the VP/SI and exhibit similar projection patterns toward the amygdala region and PFC. Moreover, VGLUT3+ axons originate primarily from the VP/SI and express ChAT in both the mPFC and BA. 5) VGLUT3 is much less typical for cholinergic cells and their axon terminals in the HDB and other amygdala areas. 6) Cholinergic cells in the HDB and VP/SI do not express VGAT in adult mice, thus, they unlikely have GABAergic phenotype (Fig. 28).

Our results are in good agreement with previous observations showing that most BF neurons (61%) located in the VP/SI innervating the BA express ChAT (Carlsen et al., 1985; Poulin et al., 2006). In addition, we provide evidence that the HDB innervates the BMA, yet the ratio of cholinergic neurons in this pathway is considerably lower (25%). The difference in the proportion of cholinergic neurons within the BF afferents terminating in the BA and BMA is also reflected in the abundance of cholinergic fibers in these amygdala nuclei (Fig. 6B-C).

In our study we found striking similarities in the distribution of BF afferents innervating the PFC to that observed earlier (Bloem et al., 2014). However, we substantially expanded these pervious findings by showing that the same BF regions distinctly projected to the amygdala region. Thus, beside the extensively studied nucleus basalis of Meynert (Crouse et al., 2020; Jiang et al., 2016; Kitt et al., 1987; Mallet et al., 1995), the VP/SI gives rise to a significant innervation to the BA, while the HDB provides inputs to additional amygdala areas albeit less intensively. We also observed cholinergic

projection from the VP/SI to the CeM, in agreements with a previous study (Aitta-aho et al., 2018). Based on our tracing experiments,

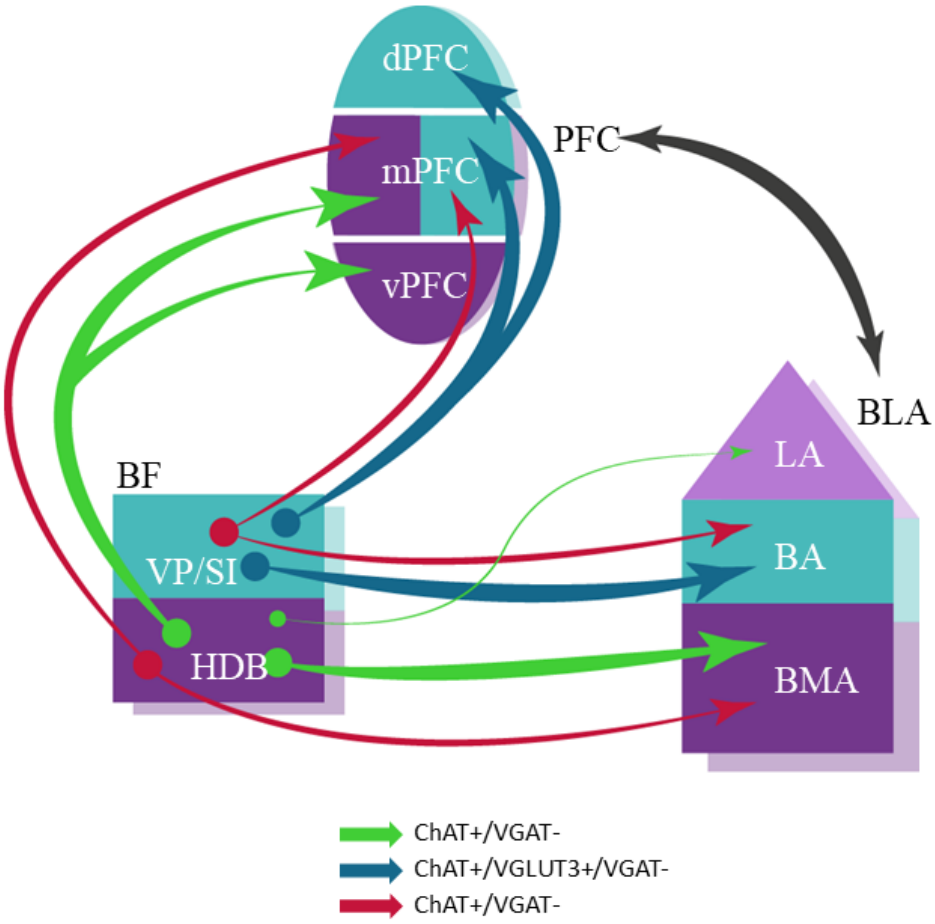

Figure 28. ***Schematic illustration of BF cholinergic inputs to the interconnected PFC-BLA networks in adult brain.***
Both single- and dual-projecting BF cholinergic cells give rise to the innervation of the functionally linked PFC and BLA. This structural arrangement of cholinergic inputs can allow the maximalization of computational support for coordinated functioning of interconnected cortical regions. Anatomical and functional related brain regions are indicated in the same colors. The thickness of the arrows corresponds to the abundance of cholinergic innervation. The color of the arrows represents the neurochemical content of the projecting neurons. BA, basal amygdala; BLA, basolateral amygdala; BMA, basomedial amygdala; dPFC, dorsal part of the PFC; HDB, nucleus of the horizontal limb of the diagonal band; LA, lateral amygdala; mPFC, medial PFC; PFC, prefrontal cortex; VP/SI, ventral pallidum/substantia innominata; vPFC, ventral part of the PFC.

two parallel cholinergic innervation patterns can be outlined: 1) the VP/SI to the dPFC – mPFC and BA and 2) the HDB to the vPFC – mPFC and BMA/LA projections. While these parallel pathways overlap in the mPFC, they may have differential effects on circuit operation in subregions like PL and IL, potentially regulating opposing fear states (Burgos-Robles et al., 2009; Santini et al., 2008; Senn et al., 2014). Collectively, these neuronal circuits may play a crucial role in conveying salient information to the BLA and

mPFC, thereby regulating functions associated with fear and reward processing, as well as social memory and interaction (Jiang et al., 2016; Kim et al., 2016; Lee and Kim, 2019; Okada et al., 2021; Robert et al., 2021). A recent study reported that the HDB is important in 1) predicting whether a perceptual outcome in a behavioral task was hit or miss and 2) encoding the omission of anticipated rewards, while the VP/SI can encode 1) nociceptive inputs and auditory stimuli and 2) learning related plasticity of auditory cues associated with punishment (Robert et al., 2021). These observations highlight the distinct functions for the two parallel cholinergic pathways.

Our retrograde-anterograde tracings not only confirmed the presence of dual-projecting cholinergic cell axons in the mPFC and BLA, but also defined the area in the BF where these neurons were located. To reveal the ratio of double-projecting cells, we used double retrograde tracing between the mPFC and BA. Based on these experiments, we found that ~ 30% of VP/SI cholinergic cells project to both cortical structures. This observation is somewhat contradictory to earlier observations obtained in rats (Carlsen et al., 1985), where the authors barely found any double-labeled neurons between the BA and the neo- or allocortex. In our study, we noticed that different retrograde tracers or viruses had different success in labeling BF cells. For example, when we injected AAVretro.CAG.eGFP or AAVretro.CAG.tdTomato into the mPFC and/or BLA, we found no retrogradely labeled cells in the BF, but there were many retrogradely labeled cells in the other regions, including the thalamus, PFC and BLA. Similarly, using Alexa-conjugated CTB, we only found 1-3 retrogradely labeled BF cells per section, whereas using FG and Fast Blue with the same injection parameters, we observed 10-20 retrogradely labeled BF cells in a section. Carlsen et al. used Fast Blue combined with Nuclear Yellow, an approach that might have different success compared to our method, while they also injected into mostly different cortical regions as we did. Furthermore, injecting a small volume of tracers into brain areas, which have extensive rostro-caudal spread – such as the mPFC and amygdala – might not cover the axonal fields of BF cells in both areas, therefore, the double-projecting cholinergic cells may be missed. Meanwhile, larger injections have the risk to spread into neighboring regions, resulting in unwanted labeling. To overcome this issue, we applied multiple small injections within the mPFC and BA along the anterior-posterior axis. In line with our findings, Li et al., 2017 have shown that single cholinergic cells in the medial septum/ ventral diagonal band

of Broca projected simultaneously to multiple brain areas, such as the mPFC and MeA. Collectively, our and other results indicate that cholinergic cells in the HDB and VP/SI predominantly send axons separately the BLA and mPFC, but a significant portion of ChAT+ neruons have dual projections towards both regions, an innervation strategy, which allows for simultaneous as well as independent control of operation in these cortical areas.

A portion of subcortical neuromodulatory afferents typically express more than one kind of neurotransmitter molecule. For instance, dopaminergic cells can release GABA or glutamate in addition to dopamine (Stuber et al., 2010; Tecuapetla et al., 2010; Tritsch et al., 2012, 2014). Similarly, BF cholinergic cells projecting to the neocortex and hippocampus typically release GABA as well (Saunders et al., 2015; Takács et al., 2018). Here, we showed that 70% of VP/SI cholinergic neurons co-express VGLUT3, while this ratio is ~30% in the HDB. Moreover, VGLUT3-containing neurons and cholinergic cells in the VP/SI share similar projection patterns, innervating mostly to the mPFC and BA. We also found that 60% of cholinergic axon terminals in the BA contain VGLUT3, whereas this ratio is insignificant in other areas surrounding the amygdala. These results are in agreement with data obtained previously in rats (Poulin et al., 2006), showing that one of the two parallel BF projections to the amygdala, the VP/SI to BA pathway expresses significantly more VGLUT3, and therefore, may release both glutamate and acetylcholine.

In addition, our data suggest that cholinergic cells in the HDB and VP/SI transiently express VGAT during development. This conclusion is based on the fact that i) the vast majority of ChAT+ neurons in the HDB and VP/SI also expressed the reporter protein ZsGreen1 under the control of VGAT promoter in offspring of mice crossed by VGAT-Cre and Ai6 and ii) neither the labeling of VGAT+ cell bodies in the BF, nor the VGAT+ axon terminals in the BA showed immunoreactivity for ChAT in adult mice. These results can be explained if VGAT gene is transiently switches on during development, resulting in expression of ZsGreen1, the lifetime of which protein significantly outlasts the VGAT expression in cholinergic cells. Our findings, thus, show that GABAergic phenotype of ChAT+ neurons innervating the BLA is transient in agreement with recent results (Granger et al., 2023).

In summary, our results indicate that there are two parallel cholinergic pathways that are in the position to control simultaneously or independently the mPFC and BLA. This organizational principle of cholinergic projections can allow the maximalization of computational support for coordinated functioning of innervated brain regions. The uncovered structural arrangement sheds light on logic underlying cholinergic control of cortical function and has implications for understanding the neural basis of emotional regulation.

The second part of my thesis examines how noxious stimulation, a well-established teaching signal, activates BF cholinergic neurons and modulates cortical network dynamics. Our main findings are as follows (Fig. 29). 1) Foot shock stimulation robustly activates cholinergic neurons in HDB and the VP/SI. 2) Silicon probe recordings in the frontal cortex revealed that cortical neurons, the majority of which are pyramidal cells, exhibit diverse responses, with approximately 32% showing excitation, 50% inhibition, and 15% remaining unresponsive. 3) Using *in vivo* visually guided juxtacellular recordings, we characterized the spiking features of eight distinct interneuron types, including PTIs, dendrite-targeting interneurons, and ISIs. We observed that NPY/NGFCs, Type 1 VIP ISIs, AACs, and Type 2 PVBCs were the first to fire in response to noxious stimulation, with NPY/NGFCs activating slightly earlier than Type 1 VIP ISIs and Type 2 PVBCs. Additionally, we identified three genetically distinct subtypes of VIP ISIs, all of which responded differentially to noxious stimuli. Interestingly, CCKCB1BCs were the latest to be activated, while SST interneurons showed no activation to noxious stimulation. 4) By applying hexamethonium, an nAChR antagonist, and NBQX, an AMPA/kainate receptor antagonist, via iontophoresis during noxious stimulation, we demonstrated that both cholinergic and glutamatergic signaling are crucial for shock-induced spiking in, Type 1 VIP ISIs. These findings provide new insights into how neuromodulatory systems shape cortical network activity during aversive experiences, highlighting distinct activation patterns across interneuron subtypes.

Our silicon probe recordings align with recent studies (Del Arco et al., 2020), demonstrating that noxious stimulation leads to both activation and inhibition of pyramidal neurons across multiple cortical regions. The most detailed study to date (Letzkus et al., 2011) showed that BF cholinergic projections to the auditory cortex

activate Layer 1 VIP ISIs, which in turn inhibit Layer 2/3 PVBCs via GABAergic transmission. This disinhibition enables pyramidal cells to encode auditory cue-dependent information. While this model explains how some pyramidal neurons become active following noxious stimulation, it does not account for the widespread inhibition observed in many pyramidal cells.

In our study, we confirmed similar activation patterns in VIP ISIs and PVBCs in the M2 cortex as previously reported in the auditory cortex (Letzkus et al., 2011) but expanded these findings by characterizing the shock-evoked spiking in three additional interneuron types: 1) NPY/ NGFCs, 2) AACs, and 3) CCKCB1BCs. Currently, only two studies (Bienvenu et al., 2012; Massi et al., 2012) are in line with our findings that AACs increase their firing rate with a short latency (~400 ms) following noxious stimuli. However, there is no existing data in the literature regarding the response of NPY/NGFCs and CCKCB1BCs under similar conditions. Overall, these interneurons have distinct activation profiles and contribute to the inhibition of pyramidal cells, providing a more complete explanation for why approximately 50% of pyramidal neurons are suppressed in response to aversive stimuli, when VIP-expressing disinhibitory circuits are switched on.

Our study is the first to characterize the activation patterns of three genetically distinct subtypes of VIP ISIs in response to noxious stimulation. The first subtype, VIP/CCK ISIs, exhibited a

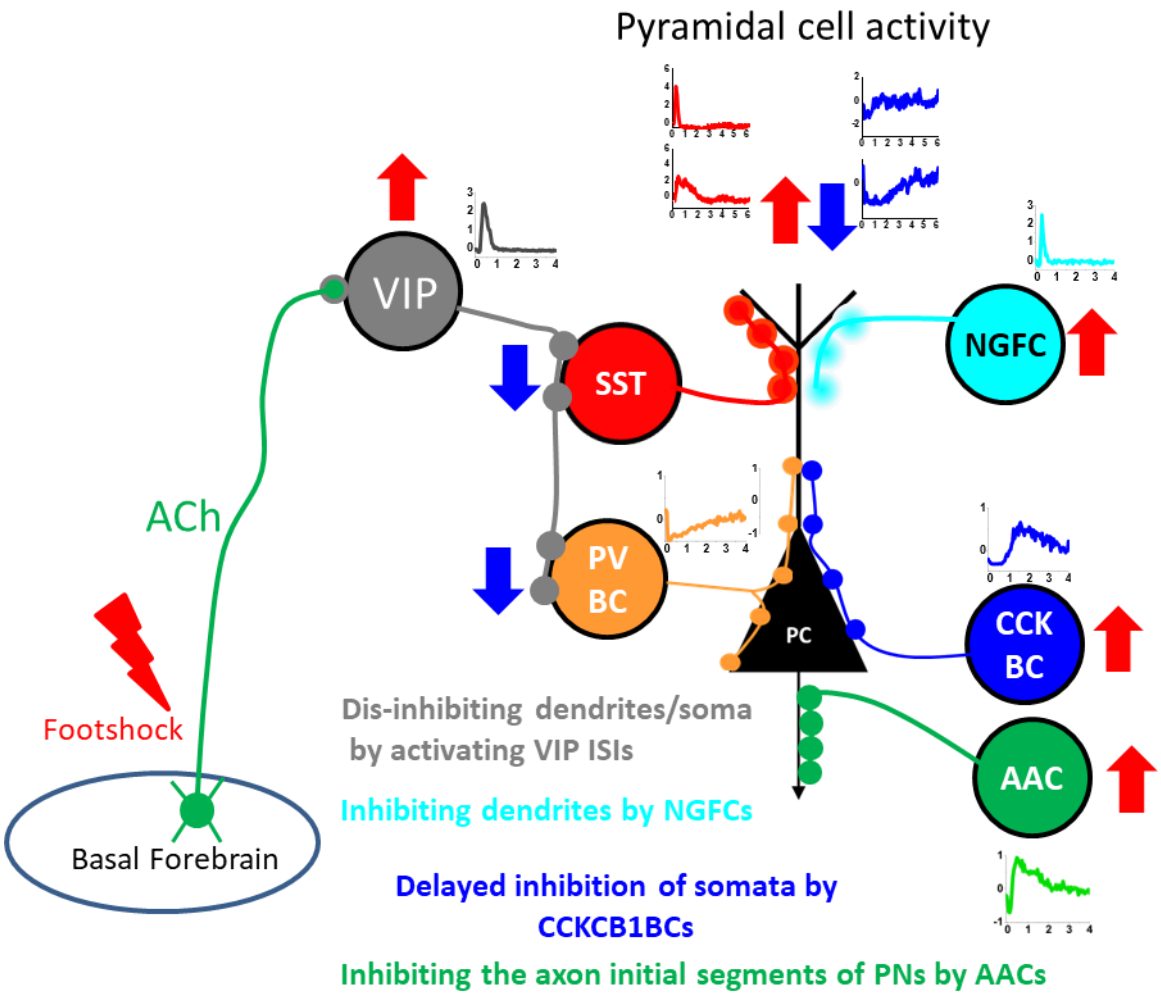

Figure 29. ***Cholinergic modulation of inhibitory interneuron networks and their effects on pyramidal cell activity upon foot shock.***
This schematic illustrates the observed changes in frontal cortical networks, including pyramidal cells and six functionally distinct interneurons upon foot shock (red lightning bolt). The current model implies that in response to the noxious stimulus, the BF cholinergic neurons release acetylcholine (ACh, green), which activates VIP ISIs (gray). These VIP ISIs inhibit SST interneurons (red) and PVBCs (orange), resulting into the disinhibition of the PC's dendrites and soma, thereby increasing their excitability (red upward arrows). Our research extends these results by demonstrating that additional interneuron types inhibit PCs upon noxious stimulation. NGFCs (cyan) provide direct inhibition to the distal dendrites of PCs (blue downward arrows). Additionally, AACs (green) specifically inhibit the axon initial segment of PCs (green downward arrows), directly regulating their action potential generation. CCKCB1BCs (blue) mediate a delayed inhibition of the soma and proximal dendrites of PCs (blue downward arrows), controlling their excitability at a delayed time period.
Together, these inhibitory interactions, shaped by ACh release from the BF, play a crucial role in modulating PC excitability in response to aversive stimuli. The red upward arrows indicate increased neuronal activity, while the blue downward arrows represent inhibition. Averaged Z-scored spike rate plots are also displayed near each neuron type.

fast and short response profile. While previous studies have identified these neurons (Apicella, 2022; Xu et al., 2010), their firing behavior during noxious stimulation had not been revealed using electrophysiological recordings. The second subtype, VIP/Nkx2.1

ISIs has not been recognized so far. Genetic labeling of AACs was first achieved through fate mapping neural progenitors of the medial ganglionic eminence (MGE) at late embryonic stages using the Nkx2.1-CreER mouse line (Taniguchi et al., 2013). To label AACs in our experiments, we applied the genetic fate-mapping technique described by Taniguchi et al. and injected tamoxifen between P0-P2. Interestingly, when tamoxifen was administered at P1-P2, the labeled neurons were not AACs but VIP ISIs with activation patterns distinct from VIP/CCK ISIs. This discovery challenges current knowledge about VIP ISIs, as they are widely believed to originate from the caudal ganglionic eminence (CGE; Miyoshi et al., 2010). The third subtype, VIP/ChAT ISIs, was already found to be distinct in basic electrophysiological properties from ChAT-negative VIP ISIs by previous studies reviewed in Dudai et al., 2020. In our experiments, under urethane anesthesia, these cells, along with SST INs, displayed little to no baseline activity and did not respond to noxious stimulation. The only definitive conclusion we can draw is that under these conditions, VIP/ChAT ISIs and SST INs do not increase their firing rates in response to noxious stimulation. In future experiments, we aim to reveal the firing features of these three VIP interneuron types in awake mice, as they may play a significant role in shaping cortical dynamics under diverse conditions.

Another important question regarding these interneuron activation patterns is to reveal the sources of their feed forward excitation. Previous study showed that the NB cholinergic neurons play a crucial role in dynamically regulating cortical coding of sensory information by reducing redundancy among neurons and increasing individual neuron accuracy (Goard and Dan, 2009). Moreover, thalamocortical inputs are also enhanced by nAChR activation, while excitatory intracortical synaptic activity can be suppressed by stimulating of mAChRs (Hsieh et al., 2000). Our preliminary experiments on VIP/CCK ISIs showed that both hexamethonium and NBQX can suppress their firing to noxious stimulation with different magnitudes, indicating that both thalamic and cholinergic inputs can contribute to shock-evoked responses. It is also a possibility that these subcortical afferents have synergistic effects at VIP ISIs.

While the resolution of local drug spread is inherently limited, the proximity of the iontophoretic pipette—placed within 1–2 soma distances from the recorded neurons—ensured that the applied compounds predominantly affected somatic and proximal dendritic compartments, which are known to contain both nicotinic acetylcholine

receptors (nAChRs) and AMPA/kainate receptors. Previous anatomical and functional studies (Letzkus et al., 2011) have demonstrated the somatic and dendritic expression of nAChRs on VIP-expressing interneurons, supporting the interpretation that iontophoretically applied hexamethonium likely blocked cholinergic excitation at these sites. Similarly, AMPA/kainate receptors, targeted by NBQX, are abundantly expressed along the somatodendritic axis of interneurons, including VIP/CCK-positive ISIs. Although terminal and distal dendritic receptor populations cannot be ruled out entirely, the observed rapid and robust suppression of firing in response to local application suggests a primarily somatic/proximal effect.

6. Conclusion

Our study provides a detailed characterization of cholinergic innervation patterns in the mPFC and BLA, revealing two parallel cholinergic pathways that may allow independent as well as simultaneous regulation of these interconnected cortical structures. The presence of dual-projecting cholinergic neurons suggests a structural arrangement optimized for coordinated neuromodulatory influence over circuits involved in fear, reward processing, and social behaviors. Furthermore, our findings on VGLUT3-expressing cholinergic neurons in the VP/SI emphasize the potential role of glutamatergic co-transmission in shaping cortical and amygdala activity.

In addition, our research sheds light on how noxious stimuli engage cholinergic circuits to influence cortical network dynamics. We identified distinct activation patterns across multiple interneuron types, expanding current models of cortical processing during aversive experiences. Notably, our findings challenge prior assumptions about homogenous VIP interneuron populations by identifying three genetically distinct subtypes with different activation profiles upon noxious stimulation. Pharmacological interventions demonstrated that both cholinergic and glutamatergic transmission can play critical roles in modulating the firing in VIP ISIs, suggesting a complex interplay of subcortical influences on cortical inhibition and excitation.

Overall, our findings advance the understanding of BF cholinergic function, revealing the structural basis of regulating cortical and amygdala circuits involved in emotional and sensory processing. This work provides a foundation for future research into the functional implications of cholinergic co-transmission and its relevance to neuropsychiatric conditions involving altered cholinergic signaling, such as anxiety, depression, and neurodegenerative diseases.

7. Summary

In this thesis, we investigated the cholinergic innervation of the interconnected medial prefrontal cortex (mPFC) and basolateral amygdala (BLA) and examined the impact of noxious stimulation on neuronal spiking in frontal cortical networks. To achieve this, we employed a combination of anatomical tracing, *in vivo* electrophysiology, and pharmacological interventions.

Using viral tracing techniques, we mapped the projections of cholinergic neurons from two basal forebrain (BF) regions, the horizontal limb of the diagonal band (HDB) and the ventral pallidum/substantia innominata (VP/SI), to the BLA and mPFC. Retrograde and anterograde tracing methods allowed us to determine that these BF areas innervate distinct subregions of the BLA while exhibiting overlapping projections in the mPFC. Additionally, dual-labeling approaches revealed that a subset of cholinergic neurons simultaneously target both the mPFC and BLA, suggesting coordinated neuromodulatory control. Immunohistochemical analyses further demonstrated that VGLUT3 is co-expressed in a significant proportion of VP/SI cholinergic neurons, indicating their potential to release both acetylcholine and glutamate, while cholinergic cells in the HDB and VP/SI do not express VGAT in adult mice.

To investigate the functional impact of cholinergic activation in the frontal cortex, we used *in vivo* electrophysiology to record neuronal activity following foot shock stimulation. Our recordings showed that HDB and VP/SI cholinergic neurons were strongly activated by noxious stimuli, while cortical pyramidal neurons were diverse in their responses, with some exhibiting excitation while others were inhibited. To dissect the underlying mechanisms, we classified nine interneuron types based on their spiking properties and neurochemical markers, including axo-axonic cells (AACs), parvalbumin-positive basket cells (PVBCs), cholecystokinin-positive basket cells (CCKCB1BCs), vasoactive intestinal polypeptide and cholecystokinin-positive interneurons (VIP/CCK ISIs), VIP/Nkx2.1 ISIs, VIP and choline acetyltransferase (VIP/ChAT ISIs), Neuropeptide-Y-positive neurogliaform (NPY/NGFCs) and somatostatin interneurons (SST INs). Pharmacological manipulations using cholinergic and glutamatergic antagonists confirmed that both neurotransmitter systems contribute to the shock-evoked firing in VIP/CCK ISIs, highlighting the complex interplay between subcortical afferents during aversive experiences.

8. Összefoglalás

Disszertációmban a mediális prefrontális kéreg (mPFC) és a bazolaterális amigdala (BLA) bazális előagy (BF) általi kolinerg innervációját vizsgáltuk, valamint feltérképeztük az elektromos stimuláció, mint fájdalmi inger hatását a frontalis agykérgi idegsejtek tüzelésére. Ennek megvalósításához anatómiai pályakövetési módszereket, *in vivo* elektrofiziológiát és farmakológiai beavatkozásokat alkalmaztunk.

Vírusos pályakövetési technikák segítségével feltérképeztük a BF két régiójából – a diagonális köteg horizontális ágából (HDB) és a ventrális pallidum/substantia innominatából (VP/SI) – származó kolinerg vetítés eloszlását a BLA-ba és az mPFC-be. Retrográd és anterográd pályakövetési módszerek segítségével kimutattuk, hogy ezek a BF területek eltérő BLA alrégiókat idegeznek be, miközben átfedő projekciókat mutatnak az mPFC-ben. Továbbá kettős retrográd jelöléssel igazoltuk, hogy a kolinerg neuronok egy alcsoportja egyszerre innerválja az mPFC-t és a BLA-t, mely összehangolt modulációt tesz lehetővé a két kortikális struktúra közt. Immunhisztokémiai elemzéseink kimutatták, hogy a VP/SI kolinerg neuronok jelentős hányada VGLUT3-at is kifejez, ami arra utal, hogy ezek a sejtek egyszerre képesek acetilkolint és glutamátot felszabadítani, míg ugyanezen sejtek nem expresszálnak VGAT-ot felnőtt egerekben.

A kolinerg moduláció hatásainak vizsgálatához *in vivo* elektrofiziológiai méréseket végeztünk, mely során áramütés hatását vizsgáltuk először a BF-ban, majd a kérgi hálózatokban. Eredményeink azt mutatták, hogy HDB és VP/SI kolinerg neuronjai aktiválódtak elektromos sokkra, amivel párhuzamosan a kortikális idegsejthálózatokban is jelentősen változott az egyes idegsejttípusok aktivitása. Az elektromos sokk hatására a piramissejtek egy része aktiválódik, másik része gátlódik, míg a kilenc vizsgált interneuron típus - Axon-axonikus sejtek (AAC-k), parvalbumin-pozitív kosársejtek (PVBC-k), kolecisztokinin-pozitív kosársejtek (CCKCB1BC-k), vazoaktív intesztinális polipeptid- és kolecisztokinin-pozitív interneuronok (VIP/CCK ISI-k), VIP/Nkx2.1 ISI-k, VIP- és kolin-acetiltranszferáz-pozitív sejtek (VIP/ChAT ISI-k), neuropeptid Y-pozitív neurogliaform sejtek (NPY/NGFC-k) és szomatosztatin interneuronok (SST-k) - egyedi aktivitási mintázatot mutattak. A kolinerg és glutamáterg antagonistákkal végzett farmakológiai beavatkozások megerősítették, hogy mindkét neurotranszmitter-rendszer hozzájárul a VIP/CCK ISI-k sokk által kiváltott aktivitásához, kiemelve a szubkortikális afferensek közötti összetett kölcsönhatást averzív élmények során.

9. References

Abe K, Kambe Y, Majima K, Hu Z, Ohtake M, Momennezhad A, Izumi H, Tanaka T, Matunis A, Stacy E, Itokazu T, Sato TR, Sato T. Functional diversity of dopamine axons in prefrontal cortex during classical conditioning. Elife. 2024 May 15;12:RP91136. doi: 10.7554/eLife.91136. PMID: 38747563; PMCID: PMC11095940.

Abs E, Poorthuis RB, Apelblat D, Muhammad K, Pardi MB, Enke L, Kushinsky D, Pu DL, Eizinger MF, Conzelmann KK, Spiegel I, Letzkus JJ. Learning-Related Plasticity in Dendrite-Targeting Layer 1 Interneurons. Neuron. 2018 Nov 7;100(3):684-699.e6. doi: 10.1016/j.neuron.2018.09.001. Epub 2018 Sep 27. PMID: 30269988; PMCID: PMC6226614.

Acsády L, Görcs TJ, Freund TF. Different populations of vasoactive intestinal polypeptide-immunoreactive interneurons are specialized to control pyramidal cells or interneurons in the hippocampus. Neuroscience. 1996 Jul;73(2):317-34. doi: 10.1016/0306-4522(95)00609-5. PMID: 8783252.

Adesnik H, Bruns W, Taniguchi H, Huang ZJ, Scanziani M. A neural circuit for spatial summation in visual cortex. Nature. 2012 Oct 11;490(7419):226-31. doi: 10.1038/nature11526. PMID: 23060193; PMCID: PMC3621107.

Adhikari A, Lerner TN, Finkelstein J, Pak S, Jennings JH, Davidson TJ, Ferenczi E, Gunaydin LA, Mirzabekov JJ, Ye L, Kim SY, Lei A, Deisseroth K. Basomedial amygdala mediates top-down control of anxiety and fear. Nature. 2015 Nov 12;527(7577):179-85. doi: 10.1038/nature15698. Epub 2015 Nov 4. PMID: 26536109; PMCID: PMC4780260.

Aitta-Aho T, Hay YA, Phillips BU, Saksida LM, Bussey TJ, Paulsen O, Apergis-Schoute J. Basal Forebrain and Brainstem Cholinergic Neurons Differentially Impact Amygdala Circuits and Learning-Related Behavior. Curr Biol. 2018 Aug 20;28(16):2557-2569.e4. doi: 10.1016/j.cub.2018.06.064. Epub 2018 Aug 9. PMID: 30100338.

Andrási T, Veres JM, Rovira-Esteban L, Kozma R, Vikór A, Gregori E, Hájos N. Differential excitatory control of 2 parallel basket cell networks in amygdala microcircuits. PLoS Biol. 2017 May 24;15(5):e2001421. doi: 10.1371/journal.pbio.2001421. PMID: 28542195; PMCID: PMC5443504.

Apicella AJ, Marchionni I. VIP-Expressing GABAergic Neurons: Disinhibitory vs. Inhibitory Motif and Its Role in Communication Across Neocortical Areas. Front Cell Neurosci. 2022 Feb 10;16:811484. doi: 10.3389/fncel.2022.811484. PMID: 35221922; PMCID:

PMC8867699.

Aransay A, Rodríguez-López C, García-Amado M, Clascá F, Prensa L. Long-range projection neurons of the mouse ventral tegmental area: a single-cell axon tracing analysis. Front Neuroanat. 2015 May 19;9:59. doi: 10.3389/fnana.2015.00059. PMID: 26042000; PMCID: PMC4436899.

Armstrong C, Soltesz I. Basket cell dichotomy in microcircuit function. J Physiol. 2012 Feb 15;590(4):683-94. doi: 10.1113/jphysiol.2011.223669. Epub 2011 Dec 23. PMID: 22199164; PMCID: PMC3381302.

Arnsten AF. Stress signalling pathways that impair prefrontal cortex structure and function. Nat Rev Neurosci. 2009 Jun;10(6):410-22. doi: 10.1038/nrn2648. PMID: 19455173; PMCID: PMC2907136.

Arroyo S, Bennett C, Aziz D, Brown SP, Hestrin S. Prolonged disynaptic inhibition in the cortex mediated by slow, non-α7 nicotinic excitation of a specific subset of cortical interneurons. J Neurosci. 2012 Mar 14;32(11):3859-64. doi: 10.1523/JNEUROSCI.0115-12.2012. PMID: 22423106; PMCID: PMC3320796.

Arruda-Carvalho M, Clem RL. Prefrontal-amygdala fear networks come into focus. Front Syst Neurosci. 2015 Oct 30;9:145. doi: 10.3389/fnsys.2015.00145. PMID: 26578902; PMCID: PMC4626554.

Bartos M, Vida I, Jonas P. Synaptic mechanisms of synchronized gamma oscillations in inhibitory interneuron networks. Nat Rev Neurosci. 2007 Jan;8(1):45-56. doi: 10.1038/nrn2044. PMID: 17180162.

Betterton RT, Broad LM, Tsaneva-Atanasova K, Mellor JR. Acetylcholine modulates gamma frequency oscillations in the hippocampus by activation of muscarinic M1 receptors. Eur J Neurosci. 2017 Jun;45(12):1570-1585. doi: 10.1111/ejn.13582. Epub 2017 May 8. PMID: 28406538; PMCID: PMC5518221.

Bienvenu TC, Busti D, Magill PJ, Ferraguti F, Capogna M. Cell-type-specific recruitment of amygdala interneurons to hippocampal theta rhythm and noxious stimuli *in vivo*. Neuron. 2012 Jun 21;74(6):1059-74. doi: 10.1016/j.neuron.2012.04.022. PMID: 22726836; PMCID: PMC3391683.

Bloem B, Schoppink L, Rotaru DC, Faiz A, Hendriks P, Mansvelder HD, van de Berg WD, Wouterlood FG. Topographic mapping between basal forebrain cholinergic neurons and the medial prefrontal cortex in mice. J Neurosci. 2014 Dec 3;34(49):16234-46. doi: 10.1523/JNEUROSCI.3011-14.2014. PMID: 25471564; PMCID: PMC6608490.

Bloodgood, D. W., Sugam, J. A., Holmes, A., and Kash, T. L. (2018). Fear extinction requires

infralimbic cortex projections to the basolateral amygdala. Transl. Psychiatry 8:60. doi: 10.1038/s41398-018-0106-x

Brodmann, K., translated by Garey, L.J. (1909/1994) Brodmann's Localisation in the Cerebral Cortex, Smith-Gordon

Brombas A, Fletcher LN, Williams SR. Activity-dependent modulation of layer 1 inhibitory neocortical circuits by acetylcholine. J Neurosci. 2014 Jan 29;34(5):1932-41. doi: 10.1523/JNEUROSCI.4470-13.2014. PMID: 24478372; PMCID: PMC6827591.

Brown RE, Basheer R, McKenna JT, Strecker RE, McCarley RW. Control of sleep and wakefulness. Physiol Rev. 2012 Jul;92(3):1087-187. doi: 10.1152/physrev.00032.2011. PMID: 22811426; PMCID: PMC3621793.

Bukalo O, Pinard CR, Silverstein S, Brehm C, Hartley ND, Whittle N, Colacicco G, Busch E, Patel S, Singewald N, Holmes A. Prefrontal inputs to the amygdala instruct fear extinction memory formation. Sci Adv. 2015 Jul;1(6):e1500251. doi: 10.1126/sciadv.1500251. Epub 2015 Jul 31. PMID: 26504902; PMCID: PMC4618669.

Burgos-Robles, A., Vidal-Gonzalez, I., and Quirk, G. J. (2009). Sustained conditioned responses in prelimbic prefrontal neurons are correlated with fear expression and extinction failure. J. Neurosci. 29, 8474–8482. doi: 10.1523/JNEUROSCI.0378-09.2009

Cardin JA, Carlén M, Meletis K, Knoblich U, Zhang F, Deisseroth K, Tsai LH, Moore CI. Driving fast-spiking cells induces gamma rhythm and controls sensory responses. Nature. 2009 Jun 4;459(7247):663-7. doi: 10.1038/nature08002. Epub 2009 Apr 26. PMID: 19396156; PMCID: PMC3655711.

Carlsen, J., Záborszky, L., and Heimer, L. (1985). Cholinergic projections from the basal forebrain to the basolateral amygdaloid complex: a combined retrograde fluorescent and immunohistochemical study. J. Comp. Neurol. 234, 155–167. doi: 10.1002/cne.902340203

Cassell, M. D., and Wright, D. J. (1986). Topography of projections from the medial prefrontal cortex to the amygdala in the rat. Brain Res. Bull. 17, 321–333. doi: 10.1016/0361-9230(86)90237-6

Cauli B, Audinat E, Lambolez B, Angulo MC, Ropert N, Tsuzuki K, Hestrin S, Rossier J. Molecular and physiological diversity of cortical nonpyramidal cells. J Neurosci. 1997 May 15;17(10):3894-906. doi: 10.1523/JNEUROSCI.17-10-03894.1997. PMID: 9133407; PMCID: PMC6573690.

Chandler DJ. Evidence for a specialized role of the locus coeruleus noradrenergic system in cortical circuitries and behavioral operations. Brain Res. 2016 Jun 15;1641(Pt B):197-

206. doi: 10.1016/j.brainres.2015.11.022. Epub 2015 Nov 25. PMID: 26607255; PMCID: PMC4879003.

Chang, C. H., and Maren, S. (2010). Strain difference in the effect of infralimbic cortex lesions on fear extinction in rats. Behav. Neurosci. 124, 391–397. doi: 10. 1037/a0019479

Chevaleyre V, Castillo PE. Endocannabinoid-mediated metaplasticity in the hippocampus. Neuron. 2004 Sep 16;43(6):871-81. doi: 10.1016/j.neuron.2004.08.036. PMID: 15363397.

Christophe E, Roebuck A, Staiger JF, Lavery DJ, Charpak S, Audinat E. Two types of nicotinic receptors mediate an excitation of neocortical layer I interneurons. J Neurophysiol. 2002 Sep;88(3):1318-27. doi: 10.1152/jn.2002.88.3.1318. PMID: 12205153.

Ciocchi S, Herry C, Grenier F, Wolff SB, Letzkus JJ, Vlachos I, Ehrlich I, Sprengel R, Deisseroth K, Stadler MB, Müller C, Lüthi A. Encoding of conditioned fear in central amygdala inhibitory circuits. Nature. 2010 Nov 11;468(7321):277-82. doi: 10.1038/nature09559. PMID: 21068837.

Connors BW, Gutnick MJ. Intrinsic firing patterns of diverse neocortical neurons. Trends Neurosci. 1990 Mar;13(3):99-104. doi: 10.1016/0166-2236(90)90185-d. PMID: 1691879.

Costanzi M, Cannas S, Saraulli D, Rossi-Arnaud C, Cestari V. Extinction after retrieval: effects on the associative and nonassociative components of remote contextual fear memory. Learn Mem. 2011 Jul 15;18(8):508-18. doi: 10.1101/lm.2175811. PMID: 21764847.

Courtin J, Chaudun F, Rozeske RR, Karalis N, Gonzalez-Campo C, Wurtz H, Abdi A, Baufreton J, Bienvenu TC, Herry C. Prefrontal parvalbumin interneurons shape neuronal activity to drive fear expression. Nature. 2014 Jan 2;505(7481):92-6. doi: 10.1038/nature12755. Epub 2013 Nov 20. PMID: 24256726.

Crimmins, B. E., Lingawi, N. W., Chieng, B. C., Leung, B. K., Maren, S., and Laurent, V. (2023). Basal forebrain cholinergic signaling in the basolateral amygdala promotes strength and durability of fear memories. Neuropsychopharmacology 48, 605–614. doi: 10.1038/s41386-022-01427-w

Crouse RB, Kim K, Batchelor HM, Girardi EM, Kamaletdinova R, Chan J, Rajebhosale P, Pittenger ST, Role LW, Talmage DA, Jing M, Li Y, Gao XB, Mineur YS, Picciotto MR. Acetylcholine is released in the basolateral amygdala in response to predictors of reward and enhances the learning of cue-reward contingency. Elife. 2020 Sep 18;9:e57335. doi: 10.7554/eLife.57335. PMID: 32945260; PMCID: PMC7529459.

Cruikshank SJ, Lewis TJ, Connors BW. Synaptic basis for intense thalamocortical activation of

feedforward inhibitory cells in neocortex. Nat Neurosci. 2007 Apr;10(4):462-8. doi: 10.1038/nn1861. Epub 2007 Mar 4. PMID: 17334362.

Davis, M. (1997). Neurobiology of fear responses: the role of the amygdala. J. Neuropsychiatr. Clin. Neurosci. 9, 382–402. doi: 10.1176/jnp.9.3.382

DeFelipe, J., and Fariñas, I. (1992). The pyramidal neuron of the cerebral cortex: morphological and chemical characteristics of the synaptic inputs. Prog. Neurobiol. 39, 563–607. doi: 10.1016/0301-0082(92)90015-7

Del Arco A, Park J, Moghaddam B. Unanticipated Stressful and Rewarding Experiences Engage the Same Prefrontal Cortex and Ventral Tegmental Area Neuronal Populations. eNeuro. 2020 Jun 11;7(3):ENEURO.0029-20.2020. doi: 10.1523/ENEURO.0029-20.2020. PMID: 32385042; PMCID: PMC7294461.ű

Del Cid-Pellitero E, Garzón M. Medial prefrontal cortex receives input from dorsal raphe nucleus neurons targeted by hypocretin1/orexinA-containing axons. Neuroscience. 2011 Jan 13;172:30-43. doi: 10.1016/j.neuroscience.2010.10.058. Epub 2010 Oct 29. PMID: 21036204.

Do JP, Xu M, Lee SH, Chang WC, Zhang S, Chung S, Yung TJ, Fan JL, Miyamichi K, Luo L, Dan Y. Cell type-specific long-range connections of basal forebrain circuit. Elife. 2016 Sep 19;5:e13214. doi: 10.7554/eLife.13214. Erratum in: Elife. 2016 Oct 24;5:e22475. doi: 10.7554/eLife.22475. PMID: 27642784; PMCID: PMC5095704.

Donoghue JP, Wise SP (1982) The motor cortex of the rat: cytoarchitecture and microstimulation mapping. J Comp Neurol 212: 76–88.

Dudai A, Yayon N, Soreq H, London M. Cortical VIP+ /ChAT+ interneurons: From genetics to function. J Neurochem. 2021 Sep;158(6):1320-1333. doi: 10.1111/jnc.15263. Epub 2021 Jan 20. PMID: 33301603.

Dudok B, Klein PM, Hwaun E, Lee BR, Yao Z, Fong O, Bowler JC, Terada S, Sparks FT, Szabo GG, Farrell JS, Berg J, Daigle TL, Tasic B, Dimidschstein J, Fishell G, Losonczy A, Zeng H, Soltesz I. Alternating sources of perisomatic inhibition during behavior. Neuron. 2021 Mar 17;109(6):997-1012.e9. doi: 10.1016/j.neuron.2021.01.003. Epub 2021 Feb 1. PMID: 33529646; PMCID: PMC7979482.

Duvarci S, Pare D. Amygdala microcircuits controlling learned fear. Neuron. 2014 Jun 4;82(5):966-80. doi: 10.1016/j.neuron.2014.04.042. PMID: 24908482; PMCID: PMC4103014.

Farr, S. A., Uezu, K., Flood, J. F., and Morley, J. E. (1999). Septo-hippocampal drug interactions in post-trial memory processing. Brain Res. 847, 221–230. doi: 10.1016/s0006-

8993(99)02049-1

Fekete Z, Weisz F, Karlócai MR, Veres JM, Andrási T, Hájos N. Synaptic communication within the microcircuits of pyramidal neurons and basket cells in the mouse prefrontal cortex. J Physiol. 2024 Oct 17. doi: 10.1113/JP286284. Epub ahead of print. PMID: 39418315.

Felix-Ortiz AC, Beyeler A, Seo C, Leppla CA, Wildes CP, Tye KM. BLA to vHPC inputs modulate anxiety-related behaviors. Neuron. 2013 Aug 21;79(4):658-64. doi: 10.1016/j.neuron.2013.06.016. PMID: 23972595; PMCID: PMC4205569.

Fino E, Yuste R. Dense inhibitory connectivity in neocortex. Neuron. 2011 Mar 24;69(6):1188-203. doi: 10.1016/j.neuron.2011.02.025. PMID: 21435562; PMCID: PMC3086675.

Fontanez-Nuin, D. E., Santini, E., Quirk, G. J., and Porter, J. T. (2011). Memory for fear extinction requires mGluR5-mediated activation of infralimbic neurons. Cereb. Cortex 21, 727–735. doi: 10.1093/cercor/bhq147

Francavilla R, Villette V, Luo X, Chamberland S, Muñoz-Pino E, Camiré O, Wagner K, Kis V, Somogyi P, Topolnik L. Connectivity and network state-dependent recruitment of long-range VIP-GABAergic neurons in the mouse hippocampus. Nat Commun. 2018 Nov 28;9(1):5043. doi: 10.1038/s41467-018-07162-5. PMID: 30487571; PMCID: PMC6261953.

Freund TF, Antal M. GABA-containing neurons in the septum control inhibitory interneurons in the hippocampus. Nature. 1988 Nov 10;336(6195):170-3. doi: 10.1038/336170a0. PMID: 3185735.

Freund TF, Katona I. Perisomatic inhibition. Neuron. 2007 Oct 4;56(1):33-42. doi: 10.1016/j.neuron.2007.09.012. PMID: 17920013.

Freund TF, Meskenaite V. gamma-Aminobutyric acid-containing basal forebrain neurons innervate inhibitory interneurons in the neocortex. Proc Natl Acad Sci U S A. 1992 Jan 15;89(2):738-42. doi: 10.1073/pnas.89.2.738. PMID: 1731348; PMCID: PMC48314.

Freund TF. Interneuron Diversity series: Rhythm and mood in perisomatic inhibition. Trends Neurosci. 2003 Sep;26(9):489-95. doi: 10.1016/S0166-2236(03)00227-3. PMID: 12948660.

Fuhrmann F, Justus D, Sosulina L, Kaneko H, Beutel T, Friedrichs D, Schoch S, Schwarz MK, Fuhrmann M, Remy S. Locomotion, Theta Oscillations, and the Speed-Correlated Firing of Hippocampal Neurons Are Controlled by a Medial Septal Glutamatergic Circuit. Neuron. 2015 Jun 3;86(5):1253-64. doi: 10.1016/j.neuron.2015.05.001. Epub 2015 May 14. PMID: 25982367.

Gabbott, P. L. A., Warner, T. A., Jays, P. R. L., Salway, P., and Busby, S. J. (2005). Prefrontal

cortex in the rat: projections to subcortical autonomic, motor, and limbic centers. J. Comp. Neurol. 492, 145–177. doi: 10.1002/cne.20738

Gabernet L, Jadhav SP, Feldman DE, Carandini M, Scanziani M. Somatosensory integration controlled by dynamic thalamocortical feed-forward inhibition. Neuron. 2005 Oct 20;48(2):315-27. doi: 10.1016/j.neuron.2005.09.022. PMID: 16242411.

Galarreta M, Erdélyi F, Szabó G, Hestrin S. Electrical coupling among irregular-spiking GABAergic interneurons expressing cannabinoid receptors. J Neurosci. 2004 Nov 3;24(44):9770-8. doi: 10.1523/JNEUROSCI.3027-04.2004. PMID: 15525762; PMCID: PMC6730255.

Gielow MR, Zaborszky L. The Input-Output Relationship of the Cholinergic Basal Forebrain. Cell Rep. 2017 Feb 14;18(7):1817-1830. doi: 10.1016/j.celrep.2017.01.060. PMID: 28199851; PMCID: PMC5725195.

Giustino TF, Maren S. The Role of the Medial Prefrontal Cortex in the Conditioning and Extinction of Fear. Front Behav Neurosci. 2015 Nov 9;9:298. doi: 10.3389/fnbeh.2015.00298. PMID: 26617500; PMCID: PMC4637424.

Goard M, Dan Y. Basal forebrain activation enhances cortical coding of natural scenes. Nat Neurosci. 2009 Nov;12(11):1444-9. doi: 10.1038/nn.2402. Epub 2009 Oct 4. PMID: 19801988; PMCID: PMC3576925.

Goldbach, R., Allgaier, C., Heimrich, B., and Jackisch, R. (1998). Postnatal development ofmuscarinic autoreceptors modulating acetylcholine release in the septohippocampal cholinergic system I. Axon terminal region: hippocampus. Develop. BrainRes. 108, 23–30. doi: 10.1016/s0165-3806(98)00026-1

Gombkoto, P., Gielow, M., Varsanyi, P., Chavez, C., and Zaborszky, L. (2021). Contribution of the basal forebrain to corticocortical network interactions. Brain Struct. Funct. 226, 1803–1821. doi: 10.1007/s00429-021-02290-z

Granger AJ, Mulder N, Saunders A, Sabatini BL. Cotransmission of acetylcholine and GABA. Neuropharmacology. 2016 Jan;100:40-6. doi: 10.1016/j.neuropharm.2015.07.031. Epub 2015 Jul 26. PMID: 26220313; PMCID: PMC4584188.

Granger, A. J., Mao, K., Saulnier, J. L., Hines, M. E., and Sabatini, B. L. (2023). Developmental regulation of GABAergic gene expression in forebrain cholinergic neurons. Front. Neural Circuits 17. doi: 10.3389/fncir.2023.1125071

Gulyás AI, Szabó GG, Ulbert I, Holderith N, Monyer H, Erdélyi F, Szabó G, Freund TF, Hájos N. Parvalbumin-containing fast-spiking basket cells generate the field potential oscillations induced by cholinergic receptor activation in the hippocampus. J Neurosci.

2010 Nov 10;30(45):15134-45. doi: 10.1523/JNEUROSCI.4104-10.2010. PMID: 21068319; PMCID: PMC3044880.

Guo W, Wang X, Zhou Z, Li Y, Hou Y, Wang K, Wei R, Ma X, Zhang H. Advances in fear memory erasure and its neural mechanisms. Front Neurol. 2025 Jan 6;15:1481450. doi: 10.3389/fneur.2024.1481450. PMID: 39835153; PMCID: PMC11743187.

Hajos N, Acsady L, Freund TF. Target selectivity and neurochemical characteristics of VIP-immunoreactive interneurons in the rat dentate gyrus. Eur J Neurosci. 1996 Jul;8(7):1415-31. doi: 10.1111/j.1460-9568.1996.tb01604.x. PMID: 8758949.

Hangya B, Ranade SP, Lorenc M, Kepecs A. Central Cholinergic Neurons Are Rapidly Recruited by Reinforcement Feedback. Cell. 2015 Aug 27;162(5):1155-68. doi: 10.1016/j.cell.2015.07.057. PMID: 26317475; PMCID: PMC4833212.

Hasselmo ME, Sarter M. Modes and models of forebrain cholinergic neuromodulation of cognition. Neuropsychopharmacology. 2011 Jan;36(1):52-73. doi: 10.1038/npp.2010.104. Epub 2010 Jul 28. PMID: 20668433; PMCID: PMC2992803.

Hasselmo ME. The role of acetylcholine in learning and memory. Curr Opin Neurobiol. 2006 Dec;16(6):710-5. doi: 10.1016/j.conb.2006.09.002. Epub 2006 Sep 29. PMID: 17011181; PMCID: PMC2659740.

Haubensak W, Kunwar PS, Cai H, Ciocchi S, Wall NR, Ponnusamy R, Biag J, Dong HW, Deisseroth K, Callaway EM, Fanselow MS, Lüthi A, Anderson DJ. Genetic dissection of an amygdala microcircuit that gates conditioned fear. Nature. 2010 Nov 11;468(7321):270-6. doi: 10.1038/nature09553. PMID: 21068836; PMCID: PMC3597095.

Hegedüs P, Király B, Schlingloff D, Lyakhova V, Velencei A, Szabó Í, Mayer MI, Zelenak Z, Nyiri G, Hangya B. Parvalbumin-expressing basal forebrain neurons mediate learning from negative experience. Nat Commun. 2024 Jun 7;15(1):4768. doi: 10.1038/s41467-024-48755-7. PMID: 38849336; PMCID: PMC11161511.

Herry, C., Ciocchi, S., Senn, V., Demmou, L., Müller, C., and Lüthi, A. (2008). Switching on and off fear by distinct neuronal circuits. Nature 454, 600–606. doi: 10.1038/nature07166

Hogg RC, Raggenbass M, Bertrand D. Nicotinic acetylcholine receptors: from structure to brain function. Rev Physiol Biochem Pharmacol. 2003;147:1-46. doi: 10.1007/s10254-003-0005-1. Epub 2003 Mar 20. PMID: 12783266.

Hsieh CY, Cruikshank SJ, Metherate R. Differential modulation of auditory thalamocortical and intracortical synaptic transmission by cholinergic agonist. Brain Res. 2000 Oct 13;880(1-2):51-64. doi: 10.1016/s0006-8993(00)02766-9. PMID: 1103

Hu R, Jin S, He X, Xu F, Hu J. Whole-Brain Monosynaptic Afferent Inputs to Basal Forebrain Cholinergic System. Front Neuroanat. 2016 Oct 10;10:98. doi: 10.3389/fnana.2016.00098. PMID: 27777554; PMCID: PMC5056182.

Hur EE, Zaborszky L. Vglut2 afferents to the medial prefrontal and primary somatosensory cortices: a combined retrograde tracing in situ hybridization study [corrected]. J Comp Neurol. 2005 Mar 14;483(3):351-73. doi: 10.1002/cne.20444. Erratum in: J Comp Neurol. 2005 May 23;486(1):98-9. PMID: 15682395.

Hurley, K. M., Herbert, H., Moga, M. M., and Saper, C. B. (1991). Efferent projections of the infralimbic cortex of the rat. J. Comp. Neurol. 308, 249–276. doi: 10.1002/cne.903080210

Ibrahim LA, Mesik L, Ji XY, Fang Q, Li HF, Li YT, Zingg B, Zhang LI, Tao HW. Cross-Modality Sharpening of Visual Cortical Processing through Layer-1-Mediated Inhibition and Disinhibition. Neuron. 2016 Mar 2;89(5):1031-45. doi: 10.1016/j.neuron.2016.01.027. Epub 2016 Feb 18. PMID: 26898778; PMCID: PMC4874809.

Izquierdo I, Furini CR, Myskiw JC. Fear Memory. Physiol Rev. 2016 Apr;96(2):695-750. doi: 10.1152/physrev.00018.2015. PMID: 26983799.

Janak PH, Tye KM. From circuits to behaviour in the amygdala. Nature. 2015 Jan 15;517(7534):284-92. doi: 10.1038/nature14188. PMID: 25592533; PMCID: PMC4565157.

Jiang L, Kundu S, Lederman JD, López-Hernández GY, Ballinger EC, Wang S, Talmage DA, Role LW. Cholinergic Signaling Controls Conditioned Fear Behaviors and Enhances Plasticity of Cortical-Amygdala Circuits. Neuron. 2016 Jun 1;90(5):1057-70. doi: 10.1016/j.neuron.2016.04.028. Epub 2016 May 5. PMID: 27161525; PMCID: PMC4891303.

Jope, R. S. (1979). High affinity choline transport and acetylCoA production in brain and their roles in the regulation of acetylcholine synthesis. Brain Res. 1, 313–344. doi: 10.1016/0165-0173(79)90009-2

Karnani MM, Jackson J, Ayzenshtat I, Hamzehei Sichani A, Manoocheri K, Kim S, Yuste R. Opening Holes in the Blanket of Inhibition: Localized Lateral Disinhibition by VIP Interneurons. J Neurosci. 2016 Mar 23;36(12):3471-80. doi: 10.1523/JNEUROSCI.3646-15.2016. PMID: 27013676; PMCID: PMC4804006.

Karube F, Kubota Y, Kawaguchi Y. Axon branching and synaptic bouton phenotypes in GABAergic nonpyramidal cell subtypes. J Neurosci. 2004 Mar 24;24(12):2853-65. doi:

10.1523/JNEUROSCI.4814-03.2004. PMID: 15044524; PMCID: PMC6729850.

Kawaguchi Y, Katsumaru H, Kosaka T, Heizmann CW, Hama K. Fast spiking cells in rat hippocampus (CA1 region) contain the calcium-binding protein parvalbumin. Brain Res. 1987 Jul 28;416(2):369-74. doi: 10.1016/0006-8993(87)90921-8. PMID: 3304536.

Kawaguchi Y, Kubota Y. GABAergic cell subtypes and their synaptic connections in rat frontal cortex. Cereb Cortex. 1997 Sep;7(6):476-86. doi: 10.1093/cercor/7.6.476. PMID: 9276173.

Kemper TLB, Galaburda AM (1984) Principles of cytoarchitectonics. In: Cerebral cortex (Peters A, Jones EG, eds), Vol 1, pp. 35–57. New York: Plenum Press

Kim T, Thankachan S, McKenna JT, McNally JM, Yang C, Choi JH, Chen L, Kocsis B, Deisseroth K, Strecker RE, Basheer R, Brown RE, McCarley RW. Cortically projecting basal forebrain parvalbumin neurons regulate cortical gamma band oscillations. Proc Natl Acad Sci U S A. 2015 Mar 17;112(11):3535-40. doi: 10.1073/pnas.1413625112. Epub 2015 Mar 2. Erratum in: Proc Natl Acad Sci U S A. 2015 May 26;112(21):E2848. doi: 10.1073/pnas.1507465112. PMID: 25733878; PMCID: PMC4371918.

Kim, J., Pignatelli, M., Xu, S., Itohara, S., and Tonegawa, S. (2016). Antagonistic negative and positive neurons of the basolateral amygdala. Nat. Neurosci. 19, 1636–1646. doi: 10.1038/nn.4414

Kitt, C. A., Mitchell, S. J., Delong, M. R., Wainer, B. H., and Price, D. L. (1987). Fiber pathways of basal forebrain cholinergic neurons in monkeys. Brain Res. 406, 192–206. doi: 10.1016/0006-8993(87)90783-9

Knox, D. (2016). "The role of basal forebrain cholinergic neurons in fear and extinction memory" in Neurobiology of learning and memory, vol. 133 (Academic Press Inc.), 39–52. doi: 10.1016/j.nlm.2016.06.001

Kozlowska K, Walker P, McLean L, Carrive P. Fear and the Defense Cascade: Clinical Implications and Management. Harv Rev Psychiatry. 2015 Jul-Aug;23(4):263-87. doi: 10.1097/HRP.0000000000000065. PMID: 26062169; PMCID: PMC4495877.

Krabbe S, Paradiso E, d'Aquin S, Bitterman Y, Courtin J, Xu C, Yonehara K, Markovic M, Müller C, Eichlisberger T, Gründemann J, Ferraguti F, Lüthi A. Adaptive disinhibitory gating by VIP interneurons permits associative learning. Nat Neurosci. 2019 Nov;22(11):1834-1843. doi: 10.1038/s41593-019-0508-y. Epub 2019 Oct 21. PMID: 31636447.

Krimer LS, Zaitsev AV, Czanner G, Kröner S, González-Burgos G, Povysheva NV, Iyengar S, Barrionuevo G, Lewis DA. Cluster analysis-based physiological classification and

morphological properties of inhibitory neurons in layers 2-3 of monkey dorsolateral prefrontal cortex. J Neurophysiol. 2005 Nov;94(5):3009-22. doi: 10.1152/jn.00156.2005. Epub 2005 Jun 29. PMID: 15987765.

Kuchibhotla KV, Gill JV, Lindsay GW, Papadoyannis ES, Field RE, Sten TA, Miller KD, Froemke RC. Parallel processing by cortical inhibition enables context-dependent behavior. Nat Neurosci. 2017 Jan;20(1):62-71. doi: 10.1038/nn.4436. Epub 2016 Oct 31. PMID: 27798631; PMCID: PMC5191967.

Lacroix, L., Spinelli, S., Heidbreder, C. A., and Feldon, J. (2000). Differential Role of the medial and lateral prefrontal cortices in fear and anxiety. Behav. Neurosci. 114, 1119–1130. doi: 10.1037/0735-7044.114.6.1119

LeDoux J. Rethinking the emotional brain. Neuron. 2012 Feb 23;73(4):653-76. doi: 10.1016/j.neuron.2012.02.004. Erratum in: Neuron. 2012 Mar 8;73(5):1052. PMID: 22365542; PMCID: PMC3625946.

LeDoux, J. E. (2000). Emotion circuits in the brain. Annu. Rev. Neurosci. 23, 155–184. doi: 10.1146/annurev.neuro.23.1.155

Lee MG, Chrobak JJ, Sik A, Wiley RG, Buzsáki G. Hippocampal theta activity following selective lesion of the septal cholinergic system. Neuroscience. 1994 Oct;62(4):1033-47. doi: 10.1016/0306-4522(94)90341-7. PMID: 7845584.

Lee, S., and Kim, J. H. (2019). Basal forebrain cholinergic-induced activation of cholecystokinin inhibitory neurons in the basolateral amygdala. Experiment. Neurobiol. 28, 320–328. doi: 10.5607/en.2019.28.3.320

Lewis WB (1878) On the comparative structure of the cortex cerebri. Brain 1:79–86

Li X, Yu B, Sun Q, Zhang Y, Ren M, Zhang X, Li A, Yuan J, Madisen L, Luo Q, Zeng H, Gong H, Qiu Z. Generation of a whole-brain atlas for the cholinergic system and mesoscopic projectome analysis of basal forebrain cholinergic neurons. Proc Natl Acad Sci U S A. 2018 Jan 9;115(2):415-420. doi: 10.1073/pnas.1703601115. Epub 2017 Dec 19. PMID: 29259118; PMCID: PMC5777024.

Lin SC, Brown RE, Hussain Shuler MG, Petersen CC, Kepecs A. Optogenetic Dissection of the Basal Forebrain Neuromodulatory Control of Cortical Activation, Plasticity, and Cognition. J Neurosci. 2015 Oct 14;35(41):13896-903. doi: 10.1523/JNEUROSCI.2590-15.2015. PMID: 26468190; PMCID: PMC4604228.

Lingawi, N. W., Laurent, V., Westbrook, R. F., and Holmes, N. M. (2019). “The role of the basolateral amygdala and infralimbic cortex in (re)learning extinction” in Psychopharmacology, vol. 236 (Springer Verlag), 303–312. doi: 10.1007/s00213-018-

4957-x

Little, J. P., and Carter, A. G. (2013). Synaptic mechanisms underlying strong reciprocal connectivity between the medial prefrontal cortex and basolateral amygdala. J. Neurosci. 33, 15333–15342. doi: 10.1523/JNEUROSCI.2385-13.2013

Lozovaya N, Eftekhari S, Cloarec R, Gouty-Colomer LA, Dufour A, Riffault B, Billon-Grand M, Pons-Bennaceur A, Oumar N, Burnashev N, Ben-Ari Y, Hammond C. GABAergic inhibition in dual-transmission cholinergic and GABAergic striatal interneurons is abolished in Parkinson disease. Nat Commun. 2018 Apr 12;9(1):1422. doi: 10.1038/s41467-018-03802-y. PMID: 29651049; PMCID: PMC5897332.

Luchicchi A, Bloem B, Viaña JN, Mansvelder HD, Role LW. Illuminating the role of cholinergic signaling in circuits of attention and emotionally salient behaviors. Front Synaptic Neurosci. 2014 Oct 27;6:24. doi: 10.3389/fnsyn.2014.00024. PMID: 25386136; PMCID: PMC4209819.

Mallet, P. E., Beninger, R. J., Flesher, S. N., Jhamandas, K., and Boegman, R. J. (1995). Nucleus basalis lesions: implication of Basoamygdaloid cholinergic pathways in memory. Brain Res. Bull. 36, 51–56. doi: 10.1016/0361-9230(94)00162-t

Maness EB, Burk JA, McKenna JT, Schiffino FL, Strecker RE, McCoy JG. Role of the locus coeruleus and basal forebrain in arousal and attention. Brain Res Bull. 2022 Oct 1;188:47-58. doi: 10.1016/j.brainresbull.2022.07.014. Epub 2022 Jul 22. PMID: 35878679; PMCID: PMC9514025.

Marek R, Strobel C, Bredy TW, Sah P. The amygdala and medial prefrontal cortex: partners in the fear circuit. J Physiol. 2013 May 15;591(10):2381-91. doi: 10.1113/jphysiol.2012.248575. Epub 2013 Feb 18. PMID: 23420655; PMCID: PMC3678031.

Maren S, Phan KL, Liberzon I. The contextual brain: implications for fear conditioning, extinction and psychopathology. Nat Rev Neurosci. 2013 Jun;14(6):417-28. doi: 10.1038/nrn3492. Epub 2013 May 2. PMID: 23635870; PMCID: PMC5072129.

Maren, S., Aharonov, G., Stote, D. L., and Fanselow, M. S. (1996). 7v-methyl-d-aspartate receptors in the basolateral amygdala are required for both acquisition and expression of conditional fear in rats. Behav. Neurosci. 110, 1365–1374. doi: 10.1037/0735-7044.110.6.1365

Markram H, Toledo-Rodriguez M, Wang Y, Gupta A, Silberberg G, Wu C. Interneurons of the neocortical inhibitory system. Nat Rev Neurosci. 2004 Oct;5(10):793-807. doi: 10.1038/nrn1519. PMID: 15378039.

Martinotti C (1889). "Contributo allo studio della corteccia cerebrale, ed all'origine centrale dei nervi". Ann. Freniatr. Sci. Affini. 1: 14–381.

Massi L, Lagler M, Hartwich K, Borhegyi Z, Somogyi P, Klausberger T. Temporal dynamics of parvalbumin-expressing axo-axonic and basket cells in the rat medial prefrontal cortex in vivo. J Neurosci. 2012 Nov 14;32(46):16496-16502. doi: 10.1523/JNEUROSCI.3475-12.2012. PMID: 23152631; PMCID: PMC4487822.

Mayo W, Dubois B, Ploska A, Javoy-Agid F, Agid Y, Le Moal M, Simon H. Cortical cholinergic projections from the basal forebrain of the rat, with special reference to the prefrontal cortex innervation. Neurosci Lett. 1984 Jun 15;47(2):149-54. doi: 10.1016/0304-3940(84)90421-x. PMID: 6462538.

McDonald AJ, Muller JF, Mascagni F. Postsynaptic targets of GABAergic basal forebrain projections to the basolateral amygdala. Neuroscience. 2011 Jun 2;183:144-59. doi: 10.1016/j.neuroscience.2011.03.027. Epub 2011 Mar 22. PMID: 21435381; PMCID: PMC4586026.

McDonald AJ. Is there an amygdala and how far does it extend? An anatomical perspective. Ann N Y Acad Sci. 2003 Apr;985:1-21. doi: 10.1111/j.1749-6632.2003.tb07067.x. PMID: 12724144.

Mcdonald, A. J., Mascagni, F., and Guo, L. (1996). Projections of the medial and lateral prefrontal cortices to the amygdala: a Phaseolus vulgaris leucoagglutinin study in the rat. Neuroscience 71, 55–75. doi: 10.1016/0306-4522(95)00417-3

McGarry LM, Packer AM, Fino E, Nikolenko V, Sippy T, Yuste R. Quantitative classification of somatostatin-positive neocortical interneurons identifies three interneuron subtypes. Front Neural Circuits. 2010 May 14;4:12. doi: 10.3389/fncir.2010.00012. PMID: 20617186; PMCID: PMC2896209.

McKenna JT, Yang C, Bellio T, Anderson-Chernishof MB, Gamble MC, Hulverson A, McCoy JG, Winston S, Hodges E, Katsuki F, McNally JM, Basheer R, Brown RE. Characterization of basal forebrain glutamate neurons suggests a role in control of arousal and avoidance behavior. Brain Struct Funct. 2021 Jul;226(6):1755-1778. doi: 10.1007/s00429-021-02288-7. Epub 2021 May 16. PMID: 33997911; PMCID: PMC8340131.

McKlveen JM, Myers B, Herman JP. The medial prefrontal cortex: coordinator of autonomic, neuroendocrine and behavioural responses to stress. J Neuroendocrinol. 2015 Jun;27(6):446-56. doi: 10.1111/jne.12272. PMID: 25737097; PMCID: PMC4580281.

Mesik L, Ma WP, Li LY, Ibrahim LA, Huang ZJ, Zhang LI, Tao HW. Functional response

properties of VIP-expressing inhibitory neurons in mouse visual and auditory cortex. Front Neural Circuits. 2015 May 22;9:22. doi: 10.3389/fncir.2015.00022. PMID: 26106301; PMCID: PMC4460767.

Mesulam MM, Mufson EJ, Levey AI, Wainer BH. Cholinergic innervation of cortex by the basal forebrain: cytochemistry and cortical connections of the septal area, diagonal band nuclei, nucleus basalis (substantia innominata), and hypothalamus in the rhesus monkey. J Comp Neurol. 1983 Feb 20;214(2):170-97. doi: 10.1002/cne.902140206. PMID: 6841683.

Miles R, Tóth K, Gulyás AI, Hájos N, Freund TF. Differences between somatic and dendritic inhibition in the hippocampus. Neuron. 1996 Apr;16(4):815-23. doi: 10.1016/s0896-6273(00)80101-4. PMID: 8607999

Mineur YS, Mose TN, Maibom KL, Pittenger ST, Soares AR, Wu H, Taylor SR, Huang Y, Picciotto MR. ACh signaling modulates activity of the GABAergic signaling network in the basolateral amygdala and behavior in stress-relevant paradigms. Mol Psychiatry. 2022 Dec;27(12):4918-4927. doi: 10.1038/s41380-022-01749-7. Epub 2022 Sep 1. PMID: 36050437; PMCID: PMC10718266.

Miyoshi G, Hjerling-Leffler J, Karayannis T, Sousa VH, Butt SJ, Battiste J, Johnson JE, Machold RP, Fishell G. Genetic fate mapping reveals that the caudal ganglionic eminence produces a large and diverse population of superficial cortical interneurons. J Neurosci. 2010 Feb 3;30(5):1582-94. doi: 10.1523/JNEUROSCI.4515-09.2010. PMID: 20130169; PMCID: PMC2826846.

Murayama M, Pérez-Garci E, Nevian T, Bock T, Senn W, Larkum ME. Dendritic encoding of sensory stimuli controlled by deep cortical interneurons. Nature. 2009 Feb 26;457(7233):1137-41. doi: 10.1038/nature07663. Epub 2009 Jan 18. PMID: 19151696.

Nagai, T., Kimura, H., Maeda, T., Mcgeer, P. L., Peng, F., and Mcgeer, E. G. (1982). “Cholinergic projections from the basal forebrain of rat to the amygdala” in Society for Neuroscience printed in U.S.a, vol. 2. doi: 10.1523/JNEUROSCI.02-04-00513.1982

Nagy-Pál P, Veres JM, Fekete Z, Karlócai MR, Weisz F, Barabás B, Reéb Z, Hájos N. Structural Organization of Perisomatic Inhibition in the Mouse Medial Prefrontal Cortex. J Neurosci. 2023 Oct 18;43(42):6972-6987. doi: 10.1523/JNEUROSCI.0432-23.2023. Epub 2023 Aug 28. PMID: 37640552; PMCID: PMC10586541.

Naka A, Adesnik H. Inhibitory Circuits in Cortical Layer 5. Front Neural Circuits. 2016 May 6;10:35. doi: 10.3389/fncir.2016.00035. PMID: 27199675; PMCID: PMC4859073.

Okada, K., Nishizawa, K., Kobayashi, T., Sakata, S., Hashimoto, K., and Kobayashi, K. (2021). Different cholinergic cell groups in the basal forebrain regulate social interaction and

social recognition memory. Sci. Rep. 11:13589. doi: 10.1038/s41598-021-93045-7

Oláh S, Füle M, Komlósi G, Varga C, Báldi R, Barzó P, Tamás G. Regulation of cortical microcircuits by unitary GABA-mediated volume transmission. Nature. 2009 Oct 29;461(7268):1278-81. doi: 10.1038/nature08503. PMID: 19865171; PMCID: PMC2771344.

Overstreet-Wadiche L, McBain CJ. Neurogliaform cells in cortical circuits. Nat Rev Neurosci. 2015 Aug;16(8):458-68. doi: 10.1038/nrn3969. PMID: 26189693; PMCID: PMC5207343.

Padilla-Coreano N, Bolkan SS, Pierce GM, Blackman DR, Hardin WD, Garcia-Garcia AL, Spellman TJ, Gordon JA. Direct Ventral Hippocampal-Prefrontal Input Is Required for Anxiety-Related Neural Activity and Behavior. Neuron. 2016 Feb 17;89(4):857-66. doi: 10.1016/j.neuron.2016.01.011. Epub 2016 Feb 4. PMID: 26853301; PMCID: PMC4760847.

Pan-Vazquez A, Wefelmeyer W, Gonzalez Sabater V, Neves G, Burrone J. Activity-Dependent Plasticity of Axo-axonic Synapses at the Axon Initial Segment. Neuron. 2020 Apr 22;106(2):265-276.e6. doi: 10.1016/j.neuron.2020.01.037. Epub 2020 Feb 27. PMID: 32109363; PMCID: PMC7181187.

Pascual, M., Pérez-Sust, P., and Soriano, E. (2004). The GABAergic septohippocampal pathway in control and reeler mice: target specificity and termination onto reelin-expressing interneurons. Mol. Cell. Neurosci. 25, 679–691. doi: 10.1016/j.mcn.2003.12.009

Paxinos, G., and Franklin, K. B. J. (2004). Mouse brain in stereotaxic coordinates, 2nd Edn. (Deluxe) by G. Paxinos and K. B. J. Franklin, vol. 2. New York: Academic Press.

Petrovich, G. D., Risold, P. Y., and Swanson, L. W. (1996). Organization of projections from the basomedial nucleus of the amygdala: a PHAL study in the rat. J. Comp. Neurol. 374, 387–420. doi:

Pfeffer CK, Xue M, He M, Huang ZJ, Scanziani M. Inhibition of inhibition in visual cortex: the logic of connections between molecularly distinct interneurons. Nat Neurosci. 2013 Aug;16(8):1068-76. doi: 10.1038/nn.3446. Epub 2013 Jun 30. PMID: 23817549; PMCID: PMC3729586.

Phelps EA, LeDoux JE. Contributions of the amygdala to emotion processing: from animal models to human behavior. Neuron. 2005 Oct 20;48(2):175-87. doi: 10.1016/j.neuron.2005.09.025. PMID: 16242399.

Pi HJ, Hangya B, Kvitsiani D, Sanders JI, Huang ZJ, Kepecs A. Cortical interneurons that specialize in disinhibitory control. Nature. 2013 Nov 28;503(7477):521-4. doi:

10.1038/nature12676. Epub 2013 Oct 6. PMID: 24097352; PMCID: PMC4017628.

Picciotto MR, Higley MJ, Mineur YS. Acetylcholine as a neuromodulator: cholinergic signaling shapes nervous system function and behavior. Neuron. 2012 Oct 4;76(1):116-29. doi: 10.1016/j.neuron.2012.08.036. PMID: 23040810; PMCID: PMC3466476.

Pinard CR, Mascagni F, McDonald AJ. Medial prefrontal cortical innervation of the intercalated nuclear region of the amygdala. Neuroscience. 2012 Mar 15;205:112-24. doi: 10.1016/j.neuroscience.2011.12.036. Epub 2012 Jan 5. PMID: 22249157; PMCID: PMC4586033.

Poorthuis RB, Bloem B, Schak B, Wester J, de Kock CP, Mansvelder HD. Layer-specific modulation of the prefrontal cortex by nicotinic acetylcholine receptors. Cereb Cortex. 2013 Jan;23(1):148-61. doi: 10.1093/cercor/bhr390. Epub 2012 Jan 30. PMID: 22291029; PMCID: PMC3513956.

Porter JT, Cauli B, Staiger JF, Lambolez B, Rossier J, Audinat E. Properties of bipolar VIPergic interneurons and their excitation by pyramidal neurons in the rat neocortex. Eur J Neurosci. 1998 Dec;10(12):3617-28. doi: 10.1046/j.1460-9568.1998.00367.x. PMID: 9875341.

Poulin, A. N., Guerci, A., Mestikawy, S., and Semba, K. (2006). Vesicular glutamate transporter 3 immunoreactivity is present in cholinergic basal forebrain neurons projecting to the basolateral amygdala in rat. J. Comp. Neurol. 498, 690–711. doi: 10.1002/cne.21081

Power, A. E., Vazdarjanova, A., and McGaugh, J. L. (2003). Muscarinic cholinergic influences in memory consolidation. Neurobiol. Learn. Mem. 80, 178–193. doi: 10.1016/S1074-7427(03)00086-8

Quirk GJ, Paré D, Richardson R, Herry C, Monfils MH, Schiller D, Vicentic A. Erasing fear memories with extinction training. J Neurosci. 2010 Nov 10;30(45):14993-7. doi: 10.1523/JNEUROSCI.4268-10.2010. PMID: 21068303; PMCID: PMC3380534.

Quirk, G. J., Russo, G. K., Barron, J. L., and Lebron, K. (2000). The role of ventromedial prefrontal cortex in the recovery of extinguished fear. J. Neurosci. 20, 6225–6231.

Raver SM, Lin SC. Basal forebrain motivational salience signal enhances cortical processing and decision speed. Front Behav Neurosci. 2015 Oct 12;9:277. doi: 10.3389/fnbeh.2015.00277. PMID: 26528157; PMCID: PMC4600917.

Reyes A, Lujan R, Rozov A, Burnashev N, Somogyi P, Sakmann B. Target-cell-specific facilitation and depression in neocortical circuits. Nat Neurosci. 1998 Aug;1(4):279-85. doi: 10.1038/1092. PMID: 10195160.

Rhomberg T, Rovira-Esteban L, Vikór A, Paradiso E, Kremser C, Nagy-Pál P, Papp OI, Tasan

R, Erdélyi F, Szabó G, Ferraguti F, Hájos N. Vasoactive Intestinal Polypeptide-Immunoreactive Interneurons within Circuits of the Mouse Basolateral Amygdala. J Neurosci. 2018 Aug 1;38(31):6983-7003. doi: 10.1523/JNEUROSCI.2063-17.2018. Epub 2018 Jun 28. PMID: 29954847; PMCID: PMC6070667.

Richardson RT, DeLong MR. Electrophysiological studies of the functions of the nucleus basalis in primates. Adv Exp Med Biol. 1991;295:233-52. doi: 10.1007/978-1-4757-0145-6_12. PMID: 1776570.

Robert B, Kimchi EY, Watanabe Y, Chakoma T, Jing M, Li Y, Polley DB. A functional topography within the cholinergic basal forebrain for encoding sensory cues and behavioral reinforcement outcomes. Elife. 2021 Nov 25;10:e69514. doi: 10.7554/eLife.69514. PMID: 34821218; PMCID: PMC8654357.

Rose JE, Woolsey CN. The orbitofrontal cortex and its connections with the mediodorsal nucleus in rabbit, sheep and cat. Res Publ Assoc Res Nerv Ment Dis. 1948;27 (1 vol.):210-32. PMID: 18106857.

Rovira-Esteban L, Péterfi Z, Vikór A, Máté Z, Szabó G, Hájos N. Morphological and physiological properties of CCK/CB1R-expressing interneurons in the basal amygdala. Brain Struct Funct. 2017 Nov;222(8):3543-3565. doi: 10.1007/s00429-017-1417-z. Epub 2017 Apr 8. PMID: 28391401.

Rozeske RR, Valerio S, Chaudun F, Herry C. Prefrontal neuronal circuits of contextual fear conditioning. Genes Brain Behav. 2015 Jan;14(1):22-36. doi: 10.1111/gbb.12181. Epub 2014 Oct 27. PMID: 25287656.

Rudy B, Fishell G, Lee S, Hjerling-Leffler J. Three groups of interneurons account for nearly 100% of neocortical GABAergic neurons. Dev Neurobiol. 2011 Jan 1;71(1):45-61. doi: 10.1002/dneu.20853. PMID: 21154909; PMCID: PMC3556905.

Sah P, Faber ES, Lopez De Armentia M, Power J. The amygdaloid complex: anatomy and physiology. Physiol Rev. 2003 Jul;83(3):803-34. doi: 10.1152/physrev.00002.2003. PMID: 12843409.

Santini E, Quirk GJ, Porter JT. Fear conditioning and extinction differentially modify the intrinsic excitability of infralimbic neurons. J Neurosci. 2008 Apr 9;28(15):4028-36. doi: 10.1523/JNEUROSCI.2623-07.2008. PMID: 18400902; PMCID: PMC3844823.

Santini, E., Sepulveda-Orengo, M., and Porter, J. T. (2012). Muscarinic receptors modulate the intrinsic excitability of infralimbic neurons and consolidation of fear extinction. Neuropsychopharmacology 37, 2047–2056. doi: 10.1038/npp. 2012.52

Sarter M, Bruno JP. The neglected constituent of the basal forebrain corticopetal projection

system: GABAergic projections. Eur J Neurosci. 2002 Jun;15(12):1867-73. doi: 10.1046/j.1460-9568.2002.02004.x. PMID: 12099892.

Sarter M, Lustig C, Howe WM, Gritton H, Berry AS. Deterministic functions of cortical acetylcholine. Eur J Neurosci. 2014 Jun;39(11):1912-20. doi: 10.1111/ejn.12515. Epub 2014 Mar 4. PMID: 24593677; PMCID: PMC4371531.

Sarter M, Parikh V, Howe WM. Phasic acetylcholine release and the volume transmission hypothesis: time to move on. Nat Rev Neurosci. 2009 May;10(5):383-90. doi: 10.1038/nrn2635. PMID: 19377503; PMCID: PMC2699581.

Sarter M. The substantia innominata remains incognita: pressing research themes on basal forebrain neuroanatomy. Brain Struct Funct. 2008 Sep;213(1-2):11-5. doi: 10.1007/s00429-007-0165-x. Epub 2008 Jan 9. PMID: 18183419.

Saunders, A., Granger, A. J., and Sabatini, B. L. (2015). Corelease of acetylcholine and GABA from cholinergic forebrain neurons. eLife 4:e06412. doi: 10.7554/eLife.06412

Schliebs R, Arendt T. The cholinergic system in aging and neuronal degeneration. Behav Brain Res. 2011 Aug 10;221(2):555-63. doi: 10.1016/j.bbr.2010.11.058. Epub 2010 Dec 9. PMID: 21145918.

Schneider-Mizell CM, Bodor AL, Collman F, Brittain D, Bleckert A, Dorkenwald S, Turner NL, Macrina T, Lee K, Lu R, Wu J, Zhuang J, Nandi A, Hu B, Buchanan J, Takeno MM, Torres R, Mahalingam G, Bumbarger DJ, Li Y, Chartrand T, Kemnitz N, Silversmith WM, Ih D, Zung J, Zlateski A, Tartavull I, Popovych S, Wong W, Castro M, Jordan CS, Froudarakis E, Becker L, Suckow S, Reimer J, Tolias AS, Anastassiou CA, Seung HS, Reid RC, Costa NMD. Structure and function of axo-axonic inhibition. Elife. 2021 Dec 1;10:e73783. doi: 10.7554/eLife.73783. PMID: 34851292; PMCID: PMC8758143.

Seki T, Namba T, Mochizuki H, Onodera M. Clustering, migration, and neurite formation of neural precursor cells in the adult rat hippocampus. J Comp Neurol. 2007 May 10;502(2):275-90. doi: 10.1002/cne.21301. PMID: 17348003.

Semba K. Multiple output pathways of the basal forebrain: organization, chemical heterogeneity, and roles in vigilance. Behav Brain Res. 2000 Nov;115(2):117-41. doi: 10.1016/s0166-4328(00)00254-0. PMID: 11000416.

Senn V, Wolff SB, Herry C, Grenier F, Ehrlich I, Gründemann J, Fadok JP, Müller C, Letzkus JJ, Lüthi A. Long-range connectivity defines behavioral specificity of amygdala neurons. Neuron. 2014 Jan 22;81(2):428-37. doi: 10.1016/j.neuron.2013.11.006. PMID: 24462103.

Shipp S, Adams RA, Friston KJ. Reflections on agranular architecture: predictive coding in the

motor cortex. Trends Neurosci. 2013 Dec;36(12):706-16. doi: 10.1016/j.tins.2013.09.004. Epub 2013 Oct 22. PMID: 24157198; PMCID: PMC3858810.

Shipp S. The importance of being agranular: a comparative account of visual and motor cortex. Philos Trans R Soc Lond B Biol Sci. 2005 Apr 29;360(1456):797-814. doi: 10.1098/rstb.2005.1630. PMID: 15937013; PMCID: PMC1569485.

Shnitko TA, Robinson DL. Anatomical and pharmacological characterization of catecholamine transients in the medial prefrontal cortex evoked by ventral tegmental area stimulation. Synapse. 2014 Apr;68(4):131-43. doi: 10.1002/syn.21723. Epub 2013 Nov 28. PMID: 24285555; PMCID: PMC4060446.

Sierra-Mercado, D., Padilla-Coreano, N., and Quirk, G. J. (2011). Dissociable roles of prelimbic and infralimbic cortices, ventral hippocampus and basolateral amygdala in the expression and extinction of conditioned fear. Neuropsychopharmacology 36, 529–538. doi: 10.1038/npp.2010.184

Silberberg G, Markram H. Disynaptic inhibition between neocortical pyramidal cells mediated by Martinotti cells. Neuron. 2007 Mar 1;53(5):735-46. doi: 10.1016/j.neuron.2007.02.012. PMID: 17329212.

Simon A, Oláh S, Molnár G, Szabadics J, Tamás G. Gap-junctional coupling between neurogliaform cells and various interneuron types in the neocortex. J Neurosci. 2005 Jul 6;25(27):6278-85. doi: 10.1523/JNEUROSCI.1431-05.2005. PMID: 16000617; PMCID: PMC6725286.

Simons DJ, Woolsey TA. Functional organization in mouse barrel cortex. Brain Res. 1979 Apr 13;165(2):327-32. doi: 10.1016/0006-8993(79)90564-x. PMID: 421142.

Solari, N., and Hangya, B. (2018). Cholinergic modulation of spatial learning, memory and navigation. Eur. J. Neurosci. 48, 2199–2230. doi: 10.1111/ejn.14089

Soma S, Shimegi S, Suematsu N, Tamura H, Sato H. Modulation-specific and laminar-dependent effects of acetylcholine on visual responses in the rat primary visual cortex. PLoS One. 2013 Jul 2;8(7):e68430. doi: 10.1371/journal.pone.0068430. PMID: 23844199; PMCID: PMC3699542.

Somogyi J, Baude A, Omori Y, Shimizu H, El Mestikawy S, Fukaya M, Shigemoto R, Watanabe M, Somogyi P. GABAergic basket cells expressing cholecystokinin contain vesicular glutamate transporter type 3 (VGLUT3) in their synaptic terminals in hippocampus and isocortex of the rat. Eur J Neurosci. 2004 Feb;19(3):552-69. doi: 10.1111/j.0953-816x.2003.03091.x. PMID: 14984406.

Somogyi P. A specific 'axo-axonal' interneuron in the visual cortex of the rat. Brain Res. 1977 Nov 11;136(2):345-50. doi: 10.1016/0006-8993(77)90808-3. PMID: 922488.

Sotres-Bayon, F., Sierra-Mercado, D., Pardilla-Delgado, E., and Quirk, G. J. (2012). Gating of fear in prelimbic cortex by hippocampal and amygdala inputs. Neuron 76, 804–812. doi: 10.1016/j.neuron.2012. 09.028

Stuber, G. D., Hnasko, T. S., Britt, J. P., Edwards, R. H., and Bonci, A. (2010). Dopaminergic terminals in the nucleus accumbens but not the dorsal striatum corelease glutamate. J. Neurosci. 30, 8229–8233. doi: 10.1523/JNEUROSCI.1754-10.2010

Sugino K, Hempel CM, Miller MN, Hattox AM, Shapiro P, Wu C, Huang ZJ, Nelson SB. Molecular taxonomy of major neuronal classes in the adult mouse forebrain. Nat Neurosci. 2006 Jan;9(1):99-107. doi: 10.1038/nn1618. Epub 2005 Dec 20. Erratum in: Nat Neurosci. 2006 Feb;9(2):292. PMID: 16369481.

Suzuki N, Bekkers JM. Distinctive classes of GABAergic interneurons provide layer-specific phasic inhibition in the anterior piriform cortex. Cereb Cortex. 2010 Dec;20(12):2971-84. doi: 10.1093/cercor/bhq046. Epub 2010 May 10. PMID: 20457693; PMCID: PMC2978245.

Szabadics J, Varga C, Molnár G, Oláh S, Barzó P, Tamás G. Excitatory effect of GABAergic axo-axonic cells in cortical microcircuits. Science. 2006 Jan 13;311(5758):233-5. doi: 10.1126/science.1121325. PMID: 16410524.

Szentágothai J. The 'module-concept' in cerebral cortex architecture. Brain Res. 1975 Sep 23;95(2-3):475-96. doi: 10.1016/0006-8993(75)90122-5. PMID: 808252.

Szocs S, Henn-Mike N, Agocs-Laboda A, Szabo-Meleg E, Varga C. Neurogliaform cells mediate feedback inhibition in the medial entorhinal cortex. Front Neuroanat. 2022 Aug 8;16:779390. doi: 10.3389/fnana.2022.779390. PMID: 36003850; PMCID: PMC9393258.

Takács VT, Cserép C, Schlingloff D, Pósfai B, Szőnyi A, Sos KE, Környei Z, Dénes Á, Gulyás AI, Freund TF, Nyiri G. Co-transmission of acetylcholine and GABA regulates hippocampal states. Nat Commun. 2018 Jul 20;9(1):2848. doi: 10.1038/s41467-018-05136-1. PMID: 30030438; PMCID: PMC6054650.

Tamás G, Lorincz A, Simon A, Szabadics J. Identified sources and targets of slow inhibition in the neocortex. Science. 2003 Mar 21;299(5614):1902-5. doi: 10.1126/science.1082053. PMID: 12649485.

Taniguchi H, Lu J, Huang ZJ. The spatial and temporal origin of chandelier cells in mouse neocortex. Science. 2013 Jan 4;339(6115):70-4. doi: 10.1126/science.1227622. Epub

2012 Nov 22. PMID: 23180771; PMCID: PMC4017638.

Tasic B, Yao Z, Graybuck LT, Smith KA, Nguyen TN, Bertagnolli D, Goldy J, Garren E, Economo MN, Viswanathan S, Penn O, Bakken T, Menon V, Miller J, Fong O, Hirokawa KE, Lathia K, Rimorin C, Tieu M, Larsen R, Casper T, Barkan E, Kroll M, Parry S, Shapovalova NV, Hirschstein D, Pendergraft J, Sullivan HA, Kim TK, Szafer A, Dee N, Groblewski P, Wickersham I, Cetin A, Harris JA, Levi BP, Sunkin SM, Madisen L, Daigle TL, Looger L, Bernard A, Phillips J, Lein E, Hawrylycz M, Svoboda K, Jones AR, Koch C, Zeng H. Shared and distinct transcriptomic cell types across neocortical areas. Nature. 2018 Nov;563(7729):72-78. doi: 10.1038/s41586-018-0654-5. Epub 2018 Oct 31. PMID: 30382198; PMCID: PMC6456269.

Tecuapetla F, Patel JC, Xenias H, English D, Tadros I, Shah F, Berlin J, Deisseroth K, Rice ME, Tepper JM, Koos T. Glutamatergic signaling by mesolimbic dopamine neurons in the nucleus accumbens. J Neurosci. 2010 May 19;30(20):7105-10. doi: 10.1523/JNEUROSCI.0265-10.2010. PMID: 20484653; PMCID: PMC3842465.

Thierry AM, Stinus L, Blanc G, Glowinski J. Some evidence for the existence of dopaminergic neurons in the rat cortex. Brain Res. 1973 Feb 14;50(1):230-4. doi: 10.1016/0006-8993(73)90614-8. PMID: 4347847.

Tóth K, Freund TF, Miles R. Disinhibition of rat hippocampal pyramidal cells by GABAergic afferents from the septum. J Physiol. 1997 Apr 15;500 (Pt 2)(Pt 2):463-74. doi: 10.1113/jphysiol.1997.sp022033. PMID: 9147330; PMCID: PMC1159396.

Tovote P, Fadok JP, Lüthi A. Neuronal circuits for fear and anxiety. Nat Rev Neurosci. 2015 Jun;16(6):317-31. doi: 10.1038/nrn3945. Erratum in: Nat Rev Neurosci. 2015 Jul;16(7):439. PMID: 25991441.

Traub RD, Bibbig A, LeBeau FE, Buhl EH, Whittington MA. Cellular mechanisms of neuronal population oscillations in the hippocampus in vitro. Annu Rev Neurosci. 2004;27:247-78. doi: 10.1146/annurev.neuro.27.070203.144303. PMID: 15217333.

Tritsch, N. X., Ding, J. B., and Sabatini, B. L. (2012). Dopaminergic neurons inhibit striatal output through non-canonical release of GABA. Nature 490, 262–266. doi: 10.1038/nature11466

Tritsch, N. X., Oh, W. J., Gu, C., and Sabatini, B. L. (2014). Midbrain dopamine neurons sustain inhibitory transmission using plasma membrane uptake of GABA, not synthesis. eLife 3:e01936. doi: 10.7554/eLife.01936

Tyan L, Chamberland S, Magnin E, Camiré O, Francavilla R, David LS, Deisseroth K, Topolnik L. Dendritic inhibition provided by interneuron-specific cells controls the firing rate and

timing of the hippocampal feedback inhibitory circuitry. J Neurosci. 2014 Mar 26;34(13):4534-47. doi: 10.1523/JNEUROSCI.3813-13.2014. PMID: 24671999; PMCID: PMC6608127.

Tye KM, Prakash R, Kim SY, Fenno LE, Grosenick L, Zarabi H, Thompson KR, Gradinaru V, Ramakrishnan C, Deisseroth K. Amygdala circuitry mediating reversible and bidirectional control of anxiety. Nature. 2011 Mar 17;471(7338):358-62. doi: 10.1038/nature09820. Epub 2011 Mar 9. PMID: 21389985; PMCID: PMC3154022.

Uematsu A, Tan BZ, Johansen JP. Projection specificity in heterogeneous locus coeruleus cell populations: implications for learning and memory. Learn Mem. 2015 Sep 1;22(9):444-51. doi: 10.1101/lm.037283.114. PMID: 26330494; PMCID: PMC4561410.

Unal CT, Pare D, Zaborszky L. Impact of basal forebrain cholinergic inputs on basolateral amygdala neurons. J Neurosci. 2015 Jan 14;35(2):853-63. doi: 10.1523/JNEUROSCI.2706-14.2015. PMID: 25589777; PMCID: PMC4293427.

Van De Werd HJ, Rajkowska G, Evers P, Uylings HB. Cytoarchitectonic and chemoarchitectonic characterization of the prefrontal cortical areas in the mouse. Brain Struct Funct. 2010 May;214(4):339-53. doi: 10.1007/s00429-010-0247-z. Epub 2010 Mar 12. PMID: 20221886; PMCID: PMC2862954.

Vandecasteele M, Varga V, Berényi A, Papp E, Barthó P, Venance L, Freund TF, Buzsáki G. Optogenetic activation of septal cholinergic neurons suppresses sharp wave ripples and enhances theta oscillations in the hippocampus. Proc Natl Acad Sci U S A. 2014 Sep 16;111(37):13535-40. doi: 10.1073/pnas.1411233111. Epub 2014 Sep 2. PMID: 25197052; PMCID: PMC4169920.

Vereczki VK, Müller K, Krizsán É, Máté Z, Fekete Z, Rovira-Esteban L, Veres JM, Erdélyi F, Hájos N. Total Number and Ratio of GABAergic Neuron Types in the Mouse Lateral and Basal Amygdala. J Neurosci. 2021 May 26;41(21):4575-4595. doi: 10.1523/JNEUROSCI.2700-20.2021. Epub 2021 Apr 9. PMID: 33837051; PMCID: PMC8260245.

Veres JM, Fekete Z, Müller K, Andrasi T, Rovira-Esteban L, Barabas B, Papp OI, Hajos N. Fear learning and aversive stimuli differentially change excitatory synaptic transmission in perisomatic inhibitory cells of the basal amygdala. Front Cell Neurosci. 2023 Sep 5;17:1120338. doi: 10.3389/fncel.2023.1120338. PMID: 37731462; PMCID: PMC10507864.

Veres JM, Nagy GA, Hájos N. Perisomatic GABAergic synapses of basket cells effectively control principal neuron activity in amygdala networks. Elife. 2017 Jan 6;6:e20721. doi:

10.7554/eLife.20721. PMID: 28060701; PMCID: PMC5218536.

Vertes RP. Differential projections of the infralimbic and prelimbic cortex in the rat. Synapse. 2004 Jan;51(1):32-58. doi: 10.1002/syn.10279. PMID: 14579424.

Wallis JD. Cross-species studies of orbitofrontal cortex and value-based decision-making. Nat Neurosci. 2011 Nov 20;15(1):13-9. doi: 10.1038/nn.2956. PMID: 22101646; PMCID: PMC3549638.

Wang Y, Toledo-Rodriguez M, Gupta A, Wu C, Silberberg G, Luo J, Markram H. Anatomical, physiological and molecular properties of Martinotti cells in the somatosensory cortex of the juvenile rat. J Physiol. 2004 Nov 15;561(Pt 1):65-90. doi: 10.1113/jphysiol.2004.073353. Epub 2004 Aug 26. PMID: 15331670; PMCID: PMC1665344.

Weiskrantz, L. (1956). Behavioral changes associated with ablation of the amygdaloid complex in monkeys. J. Comp. Physiol. Psychol. 49, 381–391. doi: 10.1037/h0088009

Wilson FA, Rolls ET. Neuronal responses related to the novelty and familarity of visual stimuli in the substantia innominata, diagonal band of Broca and periventricular region of the primate basal forebrain. Exp Brain Res. 1990;80(1):104-20. doi: 10.1007/BF00228852. PMID: 2358021.

Wilson MA, Fadel JR. Cholinergic regulation of fear learning and extinction. J Neurosci Res. 2017 Mar;95(3):836-852. doi: 10.1002/jnr.23840. Epub 2016 Oct 5. PMID: 27704595; PMCID: PMC5241223.

Wilson RI, Nicoll RA. Endogenous cannabinoids mediate retrograde signalling at hippocampal synapses. Nature. 2001 Mar 29;410(6828):588-92. doi: 10.1038/35069076. Erratum in: Nature 2001 Jun 21;411(6840):974. PMID: 11279497.

Wolff SB, Gründemann J, Tovote P, Krabbe S, Jacobson GA, Müller C, Herry C, Ehrlich I, Friedrich RW, Letzkus JJ, Lüthi A. Amygdala interneuron subtypes control fear learning through disinhibition. Nature. 2014 May 22;509(7501):453-8. doi: 10.1038/nature13258. Epub 2014 May 11. PMID: 24814341.

Woodruff A, Xu Q, Anderson SA, Yuste R. Depolarizing effect of neocortical chandelier neurons. Front Neural Circuits. 2009 Oct 20;3:15. doi: 10.3389/neuro.04.015.2009. PMID: 19876404; PMCID: PMC2769545.

Xu X, Roby KD, Callaway EM. Mouse cortical inhibitory neuron type that coexpresses somatostatin and calretinin. J Comp Neurol. 2006 Nov 1;499(1):144-60. doi: 10.1002/cne.21101. PMID: 16958092.

Xu, X., Roby, K. D., and Callaway, E. M. (2010). Immunochemical characterization of inhibitory

mouse cortical neurons: three chemically distinct classes of inhibitory cells. J. Comp. Neurol. 518, 389–404. doi: 10.1002/cne.22229

Yavorska I, Wehr M. Somatostatin-Expressing Inhibitory Interneurons in Cortical Circuits. Front Neural Circuits. 2016 Sep 29;10:76. doi: 10.3389/fncir.2016.00076. PMID: 27746722; PMCID: PMC5040712.

Yu AJ, Dayan P. Uncertainty, neuromodulation, and attention. Neuron. 2005 May 19;46(4):681-92. doi: 10.1016/j.neuron.2005.04.026. PMID: 15944135.

Zaborszky L, Pang K, Somogyi J, Nadasdy Z, Kallo I. The basal forebrain corticopetal system revisited. Ann N Y Acad Sci. 1999 Jun 29;877:339-67. doi: 10.1111/j.1749-6632.1999.tb09276.x. PMID: 10415658.

Zaborszky, L. (2002). The modular organization of brain systems. Basal forebrain: the last frontier. Prog. Brain Res. 136, 359–372. doi: 10.1016/S0079-6123(02)36030-8

Zaborszky L, Csordas A, Mosca K, Kim J, Gielow MR, Vadasz C, Nadasdy Z. Neurons in the basal forebrain project to the cortex in a complex topographic organization that reflects corticocortical connectivity patterns: an experimental study based on retrograde tracing and 3D reconstruction. Cereb Cortex. 2015 Jan;25(1):118-37. doi: 10.1093/cercor/bht210. Epub 2013 Aug 19. PMID: 23964066; PMCID: PMC4259277.

Zaborszky, L., Gaykema, R. P., Swanson, D. J., and Cullinan, W. E. (1997). Cortical input to the basal forebrain. Neuroscience 79, 1051–1078. doi: 10.1016/s0306-4522(97)00049-3

Zhang K, Chen CD, Monosov IE. Novelty, Salience, and Surprise Timing Are Signaled by Neurons in the Basal Forebrain. Curr Biol. 2019 Jan 7;29(1):134-142.e3. doi: 10.1016/j.cub.2018.11.012. Epub 2018 Dec 20. PMID: 30581022; PMCID: PMC6901356.

Zhang K, Ren BH, Tai YL, Lyu JT. Distinct recruitment dynamics of chandelier cells and basket cells by thalamocortical inputs. Sheng Li Xue Bao. 2022 Oct 25;74(5):697-704. PMID: 36319093.

10. Bibliography of the candidate's publications

Publications related to this thesis

Barabás B, Reéb Z, Papp OI, Hájos N. Functionally linked amygdala and prefrontal cortical regions are innervated by both single and double projecting cholinergic neurons. Front Cell Neurosci. 2024 Jul 10;18:1426153. doi: 10.3389/fncel.2024.1426153. PMID: 39049824; PMCID: PMC11266109.

Veres JM, Fekete Z, Müller K, Andrasi T, Rovira-Esteban L, Barabas B, Papp OI, Hajos N. Fear learning and aversive stimuli differentially change excitatory synaptic transmission in perisomatic inhibitory cells of the basal amygdala. Front Cell Neurosci. 2023 Sep 5;17:1120338. doi: 10.3389/fncel.2023.1120338. PMID: 37731462; PMCID: PMC10507864.

Other publication

Nagy-Pál P, Veres JM, Fekete Z, Karlócai MR, Weisz F, Barabás B, Reéb Z, Hájos N. Structural Organization of Perisomatic Inhibition in the Mouse Medial Prefrontal Cortex. J Neurosci. 2023 Oct 18;43(42):6972-6987. doi: 10.1523/JNEUROSCI.0432-23.2023. Epub 2023 Aug 28. PMID: 37640552; PMCID: PMC10586541.

11. Acknowledgments

First and foremost, I would like to express my deepest gratitude to my supervisor, **Dr Norbert Hájos**, for his invaluable supervision, guidance, and unwavering support throughout my PhD journey. His expertise, patience, and insightful discussions have been instrumental in shaping my scientific thinking and research skills.

I am also grateful to **Dr Tibor Andrási** for introducing me to and teaching me the intricacies of the juxtacellular technique. His expertise and willingness to share knowledge have been essential to my experimental work. Likewise, I sincerely appreciate **Dániel Magyar** for his continuous help in data analysis and Matlab programming. His problem-solving skills and dedication have significantly contributed to the success of my work.

A heartfelt thanks to **Petra Nagy-Pál, Zsófi Reéb, Dr Orsoly Papp and Dr Judit Veres**, whose expertise and constant support in anatomical studies, including immunohistochemistry, virus injections, and analysis, have been indispensable. Their collaboration and commitment have played a crucial role in the completion of my research.

I would also like to express my gratitude to **Bálint Király, Anna Velencei, and Vivien Pillar** for teaching me the fiber photometry technique and its analysis. Their patience and expertise in guiding me through this complex methodology have been invaluable to my research, and I am deeply appreciative of their support.

A very special thank you to my **girlfriend, Dominika Darabos**, for her incredible support, not only emotionally but also scientifically. Her help in writing custom Python scripts for in vivo analysis has been invaluable, and her encouragement has been a constant source of motivation.

I would also like to acknowledge the **SE Doctoral School** for their guidance and for providing the academic environment necessary for my development as a researcher.

Finally, I am deeply grateful to my **family** for their unwavering support, love, and patience throughout this journey. Their encouragement and belief in me have been the foundation upon which I have built my academic pursuits.

Thank you all for your invaluable contributions to my research and personal growth.